Trinity College Dublin
Coláiste na Tríonóide, Baile Átha Cliath
The University of Dublin

Dept. of Mechanical, Manufacturing and Biomedical Engineering

Air Curtain Design for Landing Gear Noise Reduction

Daniel Carroll - 18320802

Supervisor: Prof. Gareth J. Bennett

14 April, 2023

A Thesis report submitted in partial fulfilment
of the requirements for the degree of
MAI (Engineering with Management)

Declaration

I hereby declare that this Thesis report is entirely my own work and that it has not been submitted as an exercise for a degree at this or any other university.

I have read and I understand the plagiarism provisions in the General Regulations of the University Calendar for the current year, found at `http://www.tcd.ie/calendar`.

I have completed the Online Tutorial on avoiding plagiarism 'Ready Steady Write', located at `http://tcd-ie.libguides.com/plagiarism/ready-steady-write`.

I consent / do not consent to the examiner retaining a copy of the thesis beyond the examining period, should they so wish (EU GDPR May 2018).

I agree that this thesis will not be publicly available, but will be available to TCD staff and students in the University's open access institutional repository on the Trinity domain only, subject to Irish Copyright Legislation and Trinity College Library conditions of use and acknowledgement.

Signed:  Date: 14.04.2023

Abstract

This project examined experimentally the use of air curtains as a possible noise reduction technology on aircraft landing gear. Such a concept sought to utilise an upstream planar jet of air to deflect oncoming flow away from the landing gear, hence reducing aerodynamic noise. A thorough design study was first undertaken in the Trinity College fluids lab in which the flow deflection and acoustic performance of various air nozzle concepts and designs were analysed. An open jet wind tunnel was used to generate cross flow, hot wire anemometry was used to characterise flow deflection, and a sound level meter provided acoustic readings. The primary result of this design study was the development of a fundamental nozzle design philosophy, which featured the use of pressurised air to generate choked flow at an outlet consisting of a large number of micro outlet holes. Such a design achieved a uniform planar jet of air with low levels of noise in the audible hearing range, and also achieved high levels of flow deflection compared to alternative designs. Further optimisation of the design through oblique blowing and the use of dual and triple jet configurations improved performance further. This design philosophy was used to develop a series of air curtain nozzles which were tested on a scaled model of the Lagoon nose landing gear in the aeroacoustic wind tunnel at the German Aerospace Centre in Braunschweig, as part of the H2020 collaborative European research project, INVENTOR. Microphone arrays were used to generate frequency spectra and beamforming plots with various orientations relative to the landing gear. While different nozzle configurations showed highly varying degrees of success, noise reductions were observed in the 1-8kHz range, with 10-12dB reductions recorded in some frequency bands. While high frequency noise generated by the nozzles dominated above 10kHz, adding significant noise to the system, the importance of such high frequency noise is unknown as atmospheric attenuation is thought to be substantial for such frequencies, and should therefore be the focus of future work.

This work has merited the publication of its findings, and hence a paper titled "Aerodynamic noise reduction of aircraft landing gear using air curtain technology" was being drafted at the time of submission, with the intent to publish in the Aerospace Science and Technology journal.

Acknowledgements

I would like to express my sincere gratitude to my supervisor, Professor Gareth Bennett, for his invaluable guidance, patience, and support throughout my research journey. His expertise and encouragement have been instrumental in shaping my ideas and refining my work.

I am also grateful to Michael Reilly and his team of technicians in the workshop for their technical knowledge and assistance in the manufacturing of parts used in my research. Much of the work conducted during this research was only possible due to their contribution and attention to detail.

I would like to extend my thanks to Michael Pott-Pollenske of the German Aerospace Centre for his valuable assistance during the wind tunnel testing component of this research. His experience and insights were much appreciated and contributed to the shaping of my research outcomes.

I am deeply indebted to my parents for their constant support, encouragement and inspiration throughout my academic journey. I am greatly appreciative of the opportunities they have granted me, and without their support, my education would not have been possible.

Finally, I would like to express my gratitude to my friends in Trinity College, whose camaraderie and positive attitude have made the long days and late nights spent in the Parsons Building a genuinely enjoyable experience.

Thank you all for your support and encouragement, without which this research would not have been possible.

Contents

List of Figures

List of Tables

Nomenclature

AB Air Blade

ALLEGRA Advanced Low Noise Landing Gear for Regional Aircraft

AT Air Tube

AWB Aeroacoustic Wind Tunnel Braunschweig

CNC Computer Numerical Control

DAS Data Acquisition System

DLR German Aerospace Centre

EPNL Effective Perceived Noise Level

FFT Fast Fourier Transform

HWA Hot Wire Anemometer

LHD Local High Density

LLD Local Low Density

LNT Low Noise Technology

ML Main Leg Placement

NLG Nose Landing Gear

OASPL Overall Sound Pressure Level

PIV Particle Image Velocimetry

SILENCER Significantly Lower Community Exposure to Aircraft Noise

SLM Sound Level Meter

SLPM Standard Litres Per Minute

SPL Sound Pressure Level

SPLA A-weighted Sound Pressure Level

TIMPAN Technology to IMProve Airframe Noise

TRL Test Readiness Level

1 Introduction

1.1 Context and Research Motivation

The aviation industry has grown consistently over the past number of decades into its modern role as a pillar of the global economy. Between 1980 and 2015, demand for air transport grew by 5.4% annually, with total passenger ticket sales reaching 4.54 billion in 2019 [1]. This expansion has positively impacted society in numerous ways, contributing to economic growth and globalisation [2, 3]. However, the substantial increases in air traffic volume have also faced scrutiny, with studies linking the industry to negative impacts upon biodiversity [4], health [5] and the environment [6]. One such issue is the acoustic noise emission which is particularly problematic in close proximity to airports, where there is a large volume of aircraft regularly taking off and landing. Such acoustic noise has been linked to a range of health issues such as sleep deprivation and cardiovascular diseases [7].

Considering these impacts, the reduction of aircraft noise is a topic with strong research interest, with the Advisory Council for Aeronautics Research in Europe setting a target of 65% reduction in perceived noise emissions by 2050 [8]. Since the transition from turbojet to turbofan engine technology in the 1970's, the engines have become a less significant contributor to overall aircraft noise [9], particularly during landing when the engine thrust is low. Therefore, during the landing phase, the airframe is a primary source of noise, with the landing gear contributing largely to this, representing as much as 30% of the total aircraft noise during landing [10]. This is mainly due to the highly unaerodynamic shape of the landing gear, which is left exposed to the high velocity crossflow to allow for ease of inspection on the ground, a necessary feature considering the landing gear is critical to the safety of the aircraft.

While various Low Noise Technologies (LNT's) are currently the focus of much research interest with the goal of reducing landing gear noise, such as meshes [11] and fairings [12], this project focuses on the development of the low Test Readiness Level (TRL) air curtain technology to reduce landing gear noise as a high risk-high gain solution. An air curtain is an upstream planar jet of air which is intended to deflect the high velocity oncoming flow away from the non aerodynamic surfaces of the landing gear, and hence reduce the associated aerodynamic acoustic noise which scales with velocity to the sixth power, i.e. V^6.

A number of studies have been conducted which have validated the potential for crossflow deflection by a planar jet of air, see the book chapter by Bennett and Zhao [13] for example, but this project will focus specifically on the further development of air curtains as a LNT for aircraft landing gear.

This thesis supports the EU H2020 collaborative research project, INVENTOR [14], in which Trinity College is a partner. Work to date has been documented by Bennett et al. [15] and in the MSc thesis of Meuly [16]. These works developed preliminary nozzle designs which were tested on a scaled model of the Lagoon Nose Landing Gear (NLG) in the Aeroacoustic Wind Tunnel in Braunschweig (AWB) at the German Aerospace Centre (DLR), with a view to reaching a proof of concept for landing gear noise reduction. The wind tunnel tests revealed that the air curtain deflected the crossflow sufficiently such that a tone produced by the flow passing a rod, open at one end, was suppressed. However, the nozzles tested possessed multiple significant flaws which limited the success of the test campaign to just this validation. In brief, the most significant of these flaws was the high self noise of the air curtain nozzle, and the production of a non-uniform planar jet.

1.2 Scope and Research Objectives

The primary objective of Trinity Colleges contribution to the INVENTOR project is to develop a range of nozzles capable of producing air curtains which will effectively shield a scaled landing gear model from a crossflow, and in doing so reduce the aerodynamic noise produced. Within INVENTOR, in the previously mentioned test campaign in the AWB wind tunnel (February 20220), preliminary air curtain nozzles were tested which were unsuccessful in that they generated noise which was louder than the noise source they were to shield. The overall objective of the current thesis work is to redesign the air curtain nozzles in preparation for a second wind tunnel test campaign to take place in AWB in March 2023.

1.2.1 Objectives

The following goals were set out with a view to achieving the aforementioned primary objective:

- Develop a detailed understanding of the sources of noise in the reference system. For example, a strong body of research exists on this topic which indicates that the main sources of noise are likely the lip noise at the outlet, which scales with the 5^{th} power of jet velocity, and the high frequency jet mixing noise, which scales with the 8^{th} power of jet velocity [17].
- Assess if a lower noise outlet could be developed, such as through the implementation of meshes or micro nozzle outlets as seen in some industrial applications, which will be discussed in the literature review section of this report.
- Explore methods to allow reduction of the jet velocity, while achieving similar shielding. The dual jet air curtain was thought to be particularly promising in this regard [18].
- Assess the potential for using a higher pressure air supply, as it was theorised that this could better produce a more uniform jet.
- Analyse existing products on the market such as air knives for cleaning and drying, and attempt to mimic their design philosophy if acoustic and jet uniformity performance is desirable.

Ultimately, the above goals were intended as a pathway to the overarching objective of the establishment of a design philosophy which would act as the foundation for a range of air curtain nozzles.

With this design philosophy established, the research could shift focus towards the implementation of the air nozzles in landing gear scale models, which would involve:

- Recognition of suitable nozzle placements on landing gear.
- Design and manufacture bespoke air curtain nozzles according to their intended placement.
- Design a means of attachment for the nozzle to the landing gear or landing gear bay, such that wind tunnel testing of the components is possible.

2 Literature Review

2.1 Background

2.1.1 Aircraft Noise Pollution

With 38.9 million airline flights taking off in 2019 [19], the relevance of the aviation industry in the modern world is significant. However, while the industry presents many opportunities to society such as stimulating economic activity and promoting globalisation, its rapid growth in recent decades has exceeded the rate of technological development. This has led to criticism of the industry in various areas such as carbon emissions and noise pollution. Focusing on noise pollution, while it is often highlighted as a general source of annoyance and frustration [20], its wider societal implications are more concerning.

Aircraft noise has been linked to impairing the learning capabilities of children, affecting their ability to read, concentrate and memorise [21], while it has also been linked to sleep deprivation. Sleep deprivation is a wide scale problem, with the World Health Organisation publishing a systematic review examining the existing body of evidence relating night time noise exposure to sleep deprivation [22]. This review found aircraft related noise pollution was a contributor to sleep disturbance, and that such disturbances can be linked to a variety of health issues such as high blood pressure. Further studies have examined the relationship between noise and high blood pressure. One such study [7] highlights that transport related noise at night leads to elevated stress hormone levels and oxidative stress, which in turn promotes vascular dysfunction and an elevated risk of cardiovascular disease.

2.1.2 Sources of Aircraft Noise

Engine Noise

The original significant source of noise pollution from aircraft was the engine. Early studies on aircraft noise emissions were conducted in the 1960's when turbojet turbines were used as the propulsion system. The high velocity exhaust flow of a turbojet engine exited the nozzle directly into the surrounding air. A significant velocity gradient between ambient air and exhaust flow created a highly turbulent shear layer which was a significant source of noise. However, since the 1970's, turbofan engines have been adopted which emit significantly less noise [9]. They do this by adopting a high bypass ratio whereby some of the inlet air flow is accelerated around the jet engine core, and is rejected at the nozzle outlet as a lower velocity layer between the ambient air and the high velocity jet of exhaust air. The result is a reduction in the shearing effect caused by the turbojet [23],

and hence a substantial reduction in noise. At the time this technology was implemented on a wide scale in the aviation industry, turbofan engines led to a 10-16dB reduction in noise emissions during ground-run up tests, and since then the technology has been further improved through the use of higher bypass ratios and other technologies such as chevron nozzles [24]. Figure 2.1 illustrates the impact of various turbofan engine generations on aircraft noise [25].

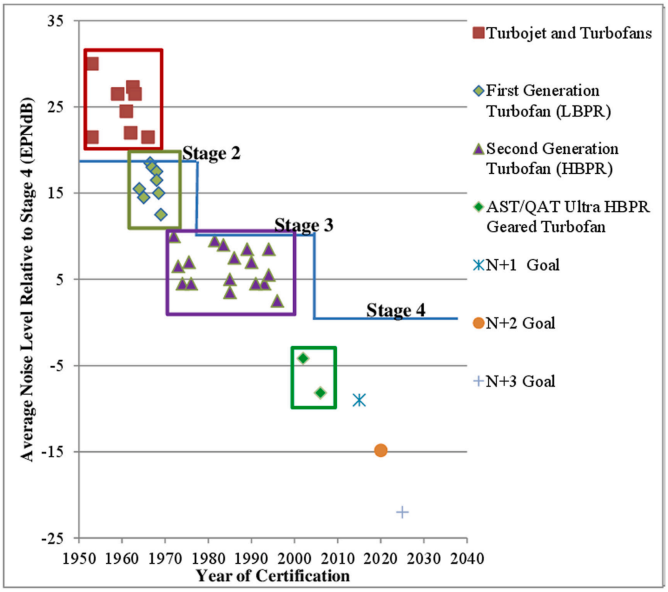

Figure 2.1: Reduction in aircraft noise levels since the 1950's.

Airframe Noise

Turbofan engine bypass ratios have increased significantly from 6 in the 1970's to as high as 12 today, and in doing so drastically reducing their noise emission. Therefore, engine noise is no longer the primary contributor to aircraft noise it once was. In modern aircraft, the airframe noise represents a significant contribution to the overall noise, particularly during the landing phase when engine thrust is low. Figure 2.2 [8] outlines the noise sources on a long range aircraft during the approach to landing phase. These results, originally created by Airbus, clearly indicate that the airframe noise is a more significant contributor than engine noise during the landing phase on modern aircraft. The airframe consists of High Lift Devices such as flaps and slats, and the landing gear. Airframe noise is mainly caused by flow separation, such as occurs at the trailing edges of flaps, the interaction of turbulent flow with solid bodies and tonal noise due to resonating cavities and holes. While the noise generated by high lift devices is not insignificant, the landing gear is the largest contributor to airframe noise, particularly for larger planes where the landing gear is larger in order to sustain the significant loads experienced during use.

The specific noise sources of landing gear consist of tonal noise originating from pins in the joints of the landing gear structure, broadband noise generated by turbulent flow separation and its interaction with downstream landing gear elements [26], and vortex shedding. Such tonal noise is created when the oncoming flow passes the orifice of a hollow pin, hole or cavity, leading to resonance and tonal noise radiation.

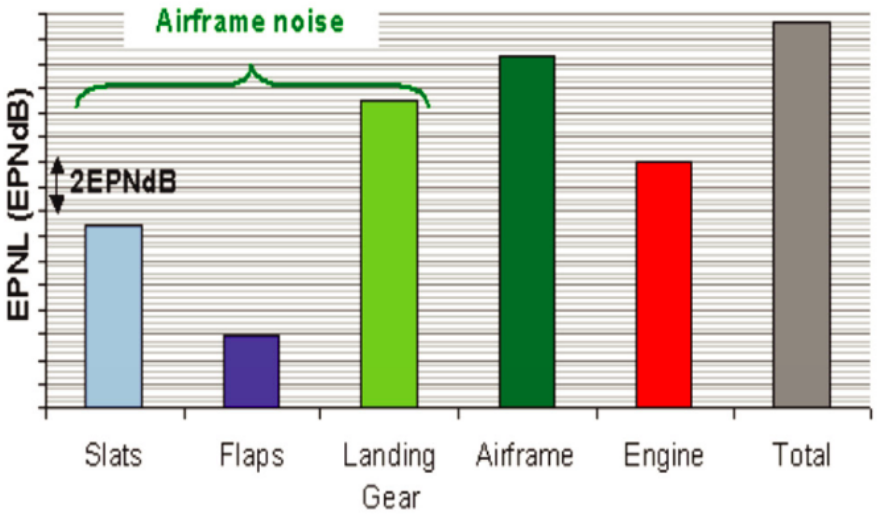

Figure 2.2: Contributing factors to overall aircraft noise during approach to landing for long range aircraft.

2.1.3 Landing Gear Noise Reduction Technology

A variety of noise reduction technologies have been investigated in recent years, many of which through European co-funded projects such as TIMPAN (Technology to IMProve Airframe Noise) [27] and SILENCER (Significantly Lower Community Exposure to Aircraft Noise) [28]. The product of such work is a series of different technologies, at a range of TRL's, which have the potential to be implemented in commercial aircraft in the future. However, due to the stringent safety protocols, regulations and complex design requirements, the technologies discussed in this section have largely not yet reached the wider market. Low Noise Technologies (LNT's) which have reached somewhat advanced TRL's include solid fairings, spoilers, hub caps and perforated fairings and meshes [29], and have been compared and assessed recently as part of the ALLEGRA (Advanced Low Noise Landing (Main and Nose) Gear for Regional Aircraft) project.

Solid Fairings

The implementation of solid fairings in areas such as the wheel axle of the landing gear are one of the LNT's at the highest TRL, and flight tests have been performed in some cases [30]. The role of such fairings is to shield the highly non aerodynamic components around the landing gear bogie, including the axle and brakes, and in doing so reduce the turbulent flow separation that occurs when the flow impinges on such components [12].

An example of such fairings is shown in Figure 2.3 [31]. In this study, full scale flight tests were performed with the Boeing 777-300ER, in which the aircraft was flown over a track layout consisting of microphone arrays. A total of 614 microphones were used with arrays of varying sizes to permit the measurement of a range of frequencies. This was a rather significant study as the high cost and resource requirements generally obstruct the ability to conduct full scale flight tests. The highly complex nature of the test environment, such as variations in wind conditions and aircraft yaw, led to a series of inconclusive results in which the noise reduction potential of the toboggan could not

be validated. However, other full scale flight tests on the landing gear of an Airbus A340 have indicated the use of fairings can reduce landing gear Effective Perceived Noise Levels (EPNL) by 1.8 EPNdB.

Figure 2.3: 'Toboggan' fairings attached to the main landing gear of the Boeing 777-300ER

In the more controlled environment of a wind tunnel, the ALLEGRA project investigated wheel axle fairings on a full scale nose landing gear model. Once again a series of microphone arrays were employed to measure the noise sources from a number of different directions. This study found that the use of a solid fairing was the most effective of all the noise reduction technologies when implemented in isolation in the system, offering noise reductions of between 2dB and 6dB.

Porous Fairings and Meshes

Ultimately, while solid wheel axle fairings have shown high potential for noise reduction, a primary issue with this technology is the reduction of brake cooling. This is particularly problematic for main landing gear which serve a critical role in slowing the aircraft following landing. Furthermore, solid fairings also serve to potentially impair visual inspection in the area around the bogie, and vortex shedding from large fairings and deflection of flow onto other components have also been cited as potential drawbacks to this technology [32]. Therefore, the use of porous meshes and fairings have also been studied.

While porous fairings do not completely prevent air flow around the unaerodynamic components of the landing gear bogie, they aim to reduce noise by slowing down the air impinging on the various landing gear components while also minimising the flow deflected onto downstream components. A study on the impact of solid and perforated fairings on the low, medium and high frequency domains indicates that while solid fairings lead to an increase in low frequency noise, this is not the case for perforated fairings, which show similar levels of medium frequency noise [33]. These measurements were recorded using a series of on-surface microphones on a 0.25 scale model of a generic landing gear in a wind tunnel. Perforated fairings were found in some cases to produce more noise in the high frequency domain than solid fairings, however there is the possibility to tailor the porosity, using an orifice diameter of 2-3mm, such that this high frequency noise is pushed above the upper limit of audible frequency.

While challenges associated with the complexity of porous dimensions have been experienced, such as in the ALLEGRA project, such technology has been validated as a meaningful noise reduction

measure. One such study on the implementation of low noise technologies on a 0.5 scale model of a regional turbo prop aircraft found a noise reduction of 5dB for some frequency ranges with a mesh fairing [34].

Other Technologies

While fairings and meshes have perhaps received the majority of recent research interest, other technologies have also shown promise for noise reduction of landing gear. Wheel hub caps for example have shown noise reductions between 2 and 4 dB, while the implementation of a ramp door spoiler, shown in Figure 2.4, achieved large noise reductions of 6 dB in the low frequency range [29]. In addition, Air Curtain technology has been proposed as a potential noise reduction technology for landing gear and will be the the focus of the remainder of this review.

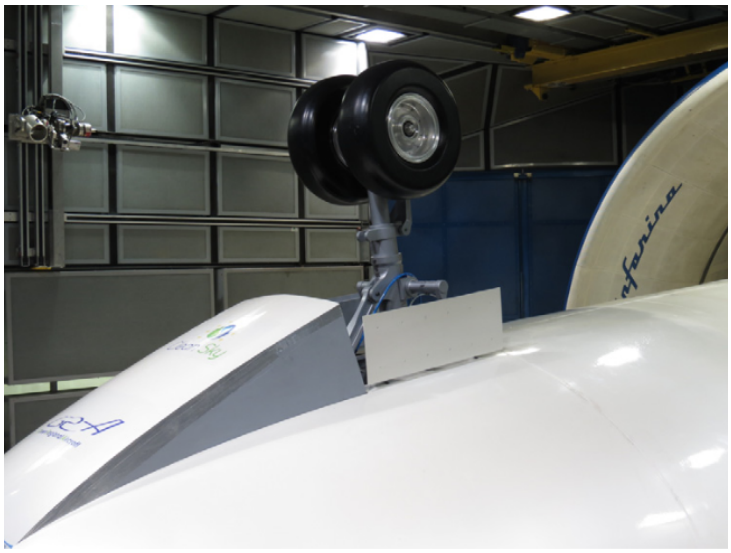

Figure 2.4: Ramp door noise reduction technology used in the ALLEGRA project.

2.2 Air Curtain Technology

An air curtain can be defined as a planar jet in a crossflow, and has found applications in a range of fields, such as reducing flow induced cavity noise [35]. In an application to reduce landing gear noise, it is intended to deflect high velocity incoming air away from the unaerodynamic components of the landing gear structure, hence reducing the aerodynamic noise generated. The original reference to implementing an air curtain for this use case was a patent by by Sijpkes and Wickerhof [36], which presented a number of different possible configurations, all consisting of at least one upstream planar jet of air which would serve to deflect crossflow away from the landing gear. The associated drawings are shown in Figure 2.5.

While this patent was never utilised in a commercial sense, early stage research indicated noise reduction potential for the technology. An initial proof of concept study related to the TIMPAN project [37] explored the ability of a planar jet of air to reduce the acoustic noise generated by a bluff body in a crossflow. Tests were conducted in an anechoic wind tunnel, utilising 2D Particle Image Velocimetry (PIV) to characterise the airflow, and a microphone array to locate the noise

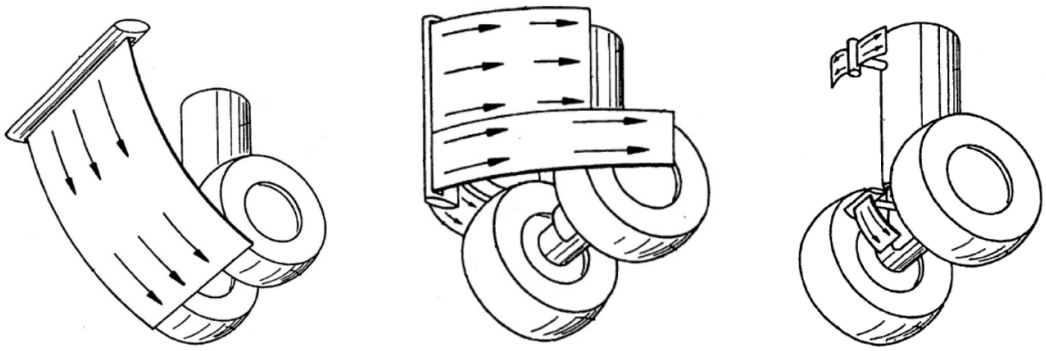

Figure 2.5: Original patent drawings showing a fuselage mounted horizontal air curtain (left), a fuselage mounted vertical air curtain (middle) and landing gear mounted air curtains (right).

source. A 3-5dB broadband noise reduction was observed for certain flow conditions, while higher noise reductions were deemed likely for full scale landing gear structures.

This study drew a strong relation between noise reduction and the jet velocity, with lower jet velocities advantageous if the same shielding could be achieved. Considering this, the use of oblique blowing, that is angling the planar jet upstream, and the use of quarter circle deflectors at the upstream edge of the jet enabled lower jet velocities to be used which led to noise reductions of 5-10dB.

A further proof of concept study was conducted in which a planar jet of air was used to deflect a crossflow away from two tandem rods, and in doing so reduce the associated aerodynamic noise [38]. The main goal of this was to first create a tone using the tandem rods in crossflow, due to vortex shedding, and then to attempt to suppress this tone using a planar jet of air. Similar to the previously mentioned study, a microphone array was used for sound source localisation while PIV was used for flow characterisation. While the planar jet did increase the noise in the system for some frequency ranges, the main tone produced by the tandem rods was successfully suppressed, demonstrating the shielding effect of the planar jet. Sound source localisation indicated that for frequency bands centred at 2kHz and 16kHz, the main source of noise in the system was at the jet nozzle outlet, indicating that the jet was the main noise contributor for these frequencies.

The noise generated at the outlet of a jet has been studied extensively [39] and is known to scale with the fifth power of the jet velocity. While the air curtain jet is intended as a noise reduction device, prior work within the previously mentioned INVENTOR project has revealed that this self noise of a jet has the potential to exceed the aerodynamic noise of the landing gear in crossflow [16]. A microphone array was once again used in an anechoic wind tunnel in order to locate the source of noise when a simple air curtain nozzle was implemented on a lagoon landing gear model. The nozzle consisted of a high aspect ratio slit as the outlet of an air chamber, with a low pressure air supply. The results of the wind tunnel tests indicated that the noise level increased significantly with the use of the air curtain, while the noise source also shifted to the outlet of the nozzle, as shown in Figure 2.6. The increase in noise level was attributed to a range of factors including jet noise as well as aerodynamically inefficient connections, and it was proposed that noise could be reduced by geometric optimisation of these connections.

In order to achieve some concept validation, a hollow tube, open at one end, was retrofitted to the

landing gear with the intention of generating a tone due to the cross flow. The air curtain successfully suppressed this tone, as shown in Figure 2.7a, which validated that the cross flow was deflected to a sufficient extent such that a potentially useful shielding effect was generated.

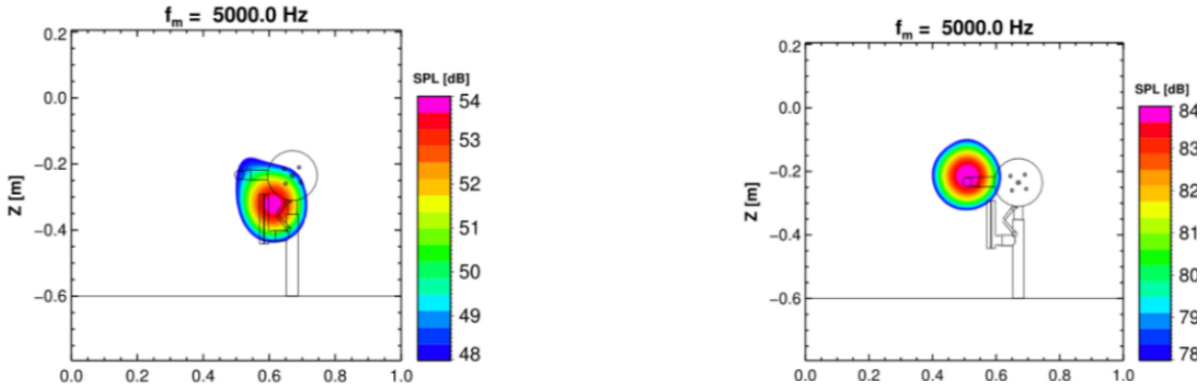

(a) Crossflow with no air curtain

(b) Crossflow with air curtain

Figure 2.6: The sound levels and localisation of wind tunnel tests of an air curtain nozzle prototype

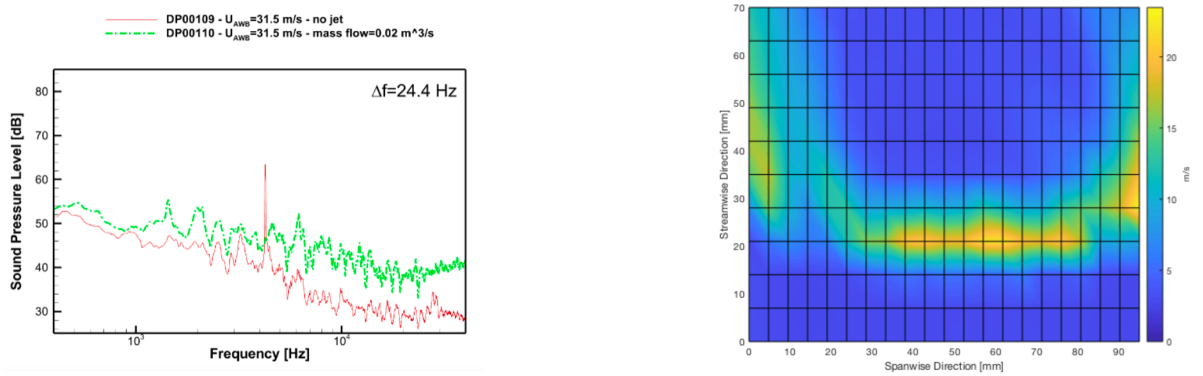

(a) Frequency spectra showing the successful suppression of a tone.

(b) Outlet flow velocity profile of optimised nozzle, when subjected to a cross flow.

Figure 2.7: Air curtain basic concept validation and outlet flow uniformity measurement.

In addition, it was found that a non uniform planar jet was produced by the nozzles in question. A hot wire anemometer placed on a 3D moving stage was used to take velocity measurements, and a velocity contour plot was generated through linear interpolation of velocity values. The non-uniformity of the jet was considered an impairment to the shielding ability of the system, and an improved design was created featuring a series of baffles intended to distribute flow evenly across the outlet, which is shown in Figure 2.8. While this design did improve the uniformity of the jet, achieving an outlet flow profile as shown in Figure 2.7b, it was still sub-optimal and in need of further work. In summary, while these tests offered some validation of the working principle, the high self noise of the nozzle and the issues with generating a uniform planar jet did not permit a true proof of concept for the implementation of air curtain technology on a scaled model of aircraft landing gear.

2.2.1 Air Curtain Trajectory Characterisation

With the potential for noise reduction using air curtain technology comes the need to accurately describe the jet trajectory in a crossflow, as this can enable the optimal positioning and input pa-

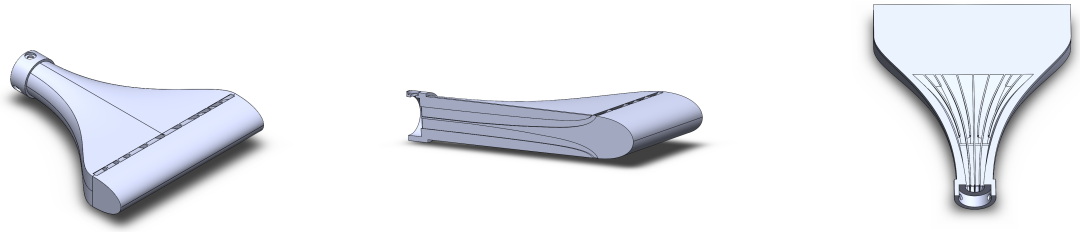

(a) Isometric View

(b) Section View

(c) Section view showing baffle geometry

Figure 2.8: Air curtain nozzle design featuring baffle geometry for flow distribution.

rameters to be chosen. Ramaprian and Haniu [40] developed a series of equations to describe such a trajectory, using a momentum based equation, whereby the assumption was made that the behaviour of the jet solely depends on its initial momentum flux and the crossflow velocity. A parabola was used to describe the centre line height of the jet in crossflow for the non-buoyant case:

$$y = c_j R\sqrt{hx} \tag{2.1}$$

where c_j is a constant of proportionality, generally set as 1.2, R is equal to the ratio of jet velocity to crossflow velocity and h is the width of the planar jet slot.

While linear jets issuing into quiescent air spread with a half width of $b_{\frac{1}{2}} = 0.11s$, where s is the distance along the centre line of the jet from the exit slot, planar jets in cross flow experience different flow conditions due to the presence of a re-circulation zone, co-flowing ambient velocity and curvature along the edge trajectories. Ramaprian and Haniu found planar jets in a cross flow to have a higher jet spreading rate for these reasons, and described it by Equation 2.2

$$b_{\frac{1}{2}} = c_b s \tag{2.2}$$

where s is the curved trajectory and c_b is a proportionality constant with a value between 0.12 and 0.15.

The previously mentioned TIMPAN study of Oerlemans and De Bruin used these equations to determine the point of maximum jet centre line height, y_t, maximum shielding height, y_e, and the downstream position of the maximum point, x_t:

$$y_t = 4.8hR^2, \quad y_e = 1.9hR^2, \quad x_t = 16hR^2$$

A number of studies have utilised these equations or similar for the calculation of maximum shielding height and for analysis of jet spreading [41, 42], and found they are effective at capturing the curvature of the jet close to the outlet. However, due to their quadratic nature, the re-circulation of the jet was not adequately captured far downstream.

2.2.2 Dual Jet Air Curtain

As an improvement on the single jet air curtain concept, the implementation of a dual jet configuration has been proposed [43]. This involves the use of two parallel planar jets, with one upstream of the other. The aim of this configuration is to either increase shielding height while not increasing the jet velocity, or to achieve the same shielding height but with lower velocity jets. As the self noise of the jet has been strongly linked to jet velocity, it was initially theorised that this could enable the reduction of noise with no penalty in terms of shielding effect. The increase in shielding height is depicted by the flow visualisation in Figure 2.9 [44]. Superimposed on the visualisations are the jet trajectories based on a set of equations similar to those described in the previous section. What is clear is that the jet trajectory of the dual jet configuration is more favourable from a perspective of aerodynamic shielding than the calculated trajectory.

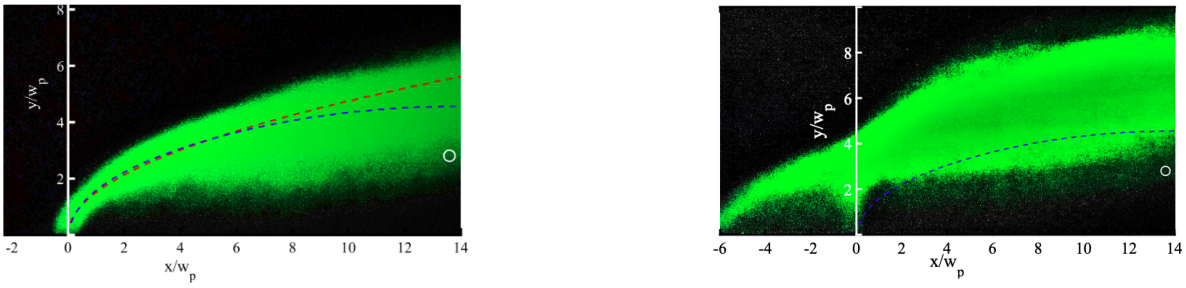

(a) Single jet in crossflow

(b) Dual jets in crossflow

Figure 2.9: Flow visualisation for single and dual jets in crossflow.

In order to validate this configuration, tests were performed on a pair of tandem rods in a crossflow, similar to the experiments described previously. A CFD study was performed to determine the optimal placement of the single jet relative to the rods, and a number of different dual jet configurations were tested. These configurations varied between two jets with velocity equal to that of the single jet, and lower velocity jets. In general, the downstream jet velocity was higher than that of the upstream jet, as it was thought the upstream jet would act as a shield to the downstream, primary, jet.

In each case of the dual jet configuration, a reduction in noise was observed, with the lower velocity jets in particular showing promise with a reduction of 2.9dB compared to the single jet configuration. It was also noted that the placement of the rods was optimised according to the single jet configuration, and minimal optimisation was performed relating to distance between the dual jets, and so further noise reductions are possible.

2.3 Low Noise Air Nozzles

While the crossflow deflection potential of air curtain technology has been well studied and validated, the self noise of the air curtain nozzle is the primary barrier to its implementation as a noise reduction measure. While some studies discussed have shown the noise at the jet outlet is dominant only for some frequencies, the work of Meuly [16] was the only study conducted on a landing gear model, and showed the self noise of the air nozzle far outweighed that of the aerodynamic noise of the landing gear in crossflow. While the implementation of a dual jet configuration has shown potential

in preliminary studies, this literature review will now examine a number of studies which have sought to develop low noise air nozzles, primarily for industrial applications.

2.3.1 Multiple Jet Nozzles

The most frequently studied method for noise control of an industrial air jet is the the use of multiple jet or micro nozzles. Such a nozzle consists of a number of small outlets rather than one large outlet, and is based on the theory that the peak frequency is inversely proportional to the length scale, as explained by Sheen, 2011 [45]. Hence, by reducing the outlet diameter, the sound waves are pushed to frequencies above the audible hearing range. In particular, it has been found that the peak frequency, F_{peak}, can generally be represented by the following:

$$F_{peak} > 0.2\frac{V_{exit}}{D} \tag{2.3}$$

where V_{exit} and D represent the exit velocity of the jet and the jet exit diameter respectively.

Therefore, it can be calculated that the peak frequency of a jet which is choked and flowing through a 1mm diameter nozzle is approximately greater than 70kHz, well above the typical 20kHz upper limit of human hearing. It is important to clarify that this method of noise control generally does not lead to a reduction in the sound power, but rather shifts the majority of the sound power to high frequencies. If total outlet areas are constant, a multi jet nozzle will produce approximately the same sound power and thrust as a single jet.

As nozzle exit noise is pushed to the ultrasound range, the dominant source of audible noise is expected further downstream of the exit. Generally, it is expected that individual jets will entrain ambient air, and at a certain point downstream the jets will merge to form a single jet. This merging of the jets leads to lower frequency noise, due to the larger length scales, and hence is attributed to the majority of the audible noise.

While this method of noise control does not eliminate the sound power, higher frequency noise is generally believed to be less harmful to the human ear. This is reflected in workplace noise exposure regulations. Poland is a good example of this, where regulations permit a higher equivalent continuous Sound Pressure Level for higher frequency noise ($L_{f,eq,8h,adm}$ of 110 dB in 31.5Hz and 40Hz 1/3 octave band frequency, compared to 80dB in the 10, 12.5, and 16Hz bands) [46].

An additional study conducted by Sheen [47], explored the impact of various outlet parameters, most notably the number, size and spacing of exit holes. Nozzles with equal total outlet area were compared, with variations including a single outlet hole, multiple outlet holes, and variable spacing between the multiple outlets. Noise measurements were performed with a microphone, placed 30cm from the nozzle outlet, and with measurements taken at 45°, 90° and 135° to the nozzle axis, where 0° would represent a position whereby the microphone was directly upstream of the nozzle exit, facing downstream. As slight variations in the total outlet area existed due to manufacturing constraints, a load cell placed 15cm downstream of the nozzle was used to measure the thrust of each nozzle, with the flow rate adjusted for each such that thrust was constant across all tests.

The results of this study definitively indicate that noise levels in the audible frequency range are

inversely proportional to outlet size, with smaller outlets shifting a larger proportion of the noise to higher frequencies, as shown in Figure 2.10a. Furthermore, this study found the outlet spacing to be a significant factor in the audible noise produced by the nozzle. Figure 2.10b shows the sound spectra for three different nozzle configurations, a single outlet, 12 1mm outlets arranged in an 8mm diameter circle, and 12 1mm outlets arranged in a 12mm circle. Clearly the arrangement in a 12mm circle leads to larger outlet spacing, and the result is a reduction in low frequency noise compared to the other arrangements. The reason for this effect is attributed to the the mixing of the jets occurring further upstream and closer to the nozzle exit when the hole spacing is reduced. Sheen therefore suggests at least 2-3 hole diameters between outlet edges to ensure adequate acoustic performance of the multi jet nozzle.

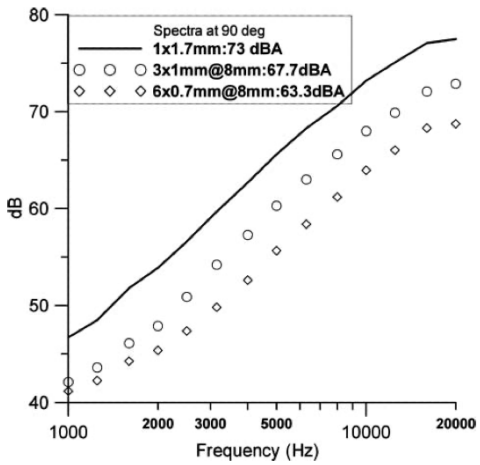

(a) Variable outlet size

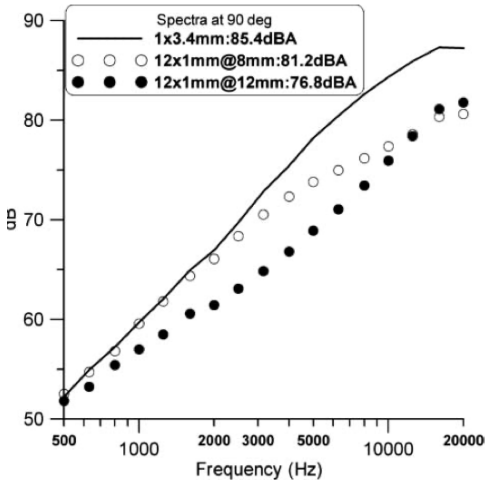

(b) Variable outlet spacing

Figure 2.10: Sound spectra for nozzles with constant thrust, with microphone placed 30cm from outlet and at 90°.

A more recent study on factors affecting the noise produced by multi jet nozzles [48] explored the relationship between upstream pressure, thrust and the A-weighted Sound Pressure Level (SPLA) in the audible range. Similar to Sheen, this study produced a range of micro nozzles with various geometries, and performed acoustic measurements at 30cm from the nozzle and at angles of 45°, 90° and 135°. A sound level meter was used to measure the A weighted sound pressure level produced. Similarly to the previously discussed study, it was found that smaller, more plentiful outlets led to reductions in SPLA, while there was no noticeable difference when the outlet geometry was varied from circular to rectangular. Interestingly, increasing the upstream pressure increased the thrust produced. This is logical as the flow at the nozzle exit is choked, so therefore increasing the upstream pressure will increase the upstream air density, hence increasing mass flow rate. This is particularly relevant as this increase in thrust corresponded with an increase in SPLA in the audible hearing range, as shown in Figure 2.11.

2.3.2 Coanda Effect Nozzles

As air flows over a curved surface, it shows a tendency to adhere to that surface under certain conditions, due to the existence of a low pressure zone which will be discussed. This effect was

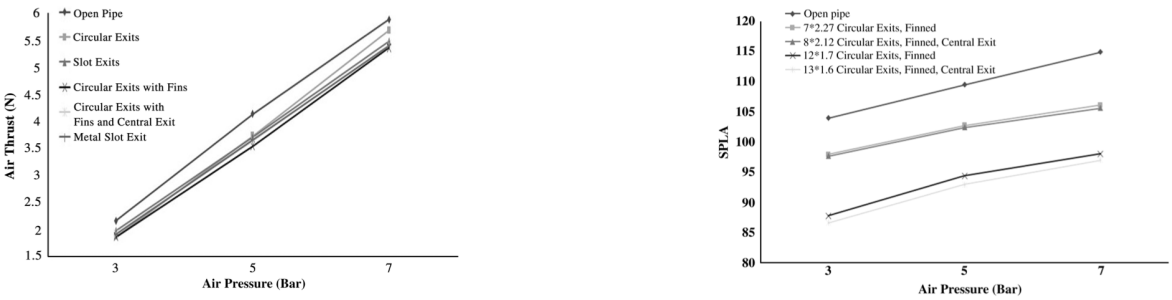

Figure 2.11: Variation of thrust and A-weighted sound pressure level with upstream pressure

first formally studied in the early 1900's, and is named the 'Coanda Effect' after Henri Coanda, who patented the first device utilising this effect in 1936 [49]. The Coanda Effect is in fact the combination of multiple effects [50], which include the tendency of a fluid jet to remain attached to a curved surface, and the tendency of jet flows over a curved surface to attract ambient fluid, which is referred to as entrainment.

Figure 2.12a illustrates the basic principle of the Coanda Effect. As the jet exits the nozzle, a low pressure zone exists between the jet and the curved surface due to the boundary layer development, as the fluid has non zero viscosity, and this is the main cause of the adhesion of the jet to the wall. Downstream, the pressure at the wall gradually rises to reach ambient pressure, as which point the jet detaches from the wall.

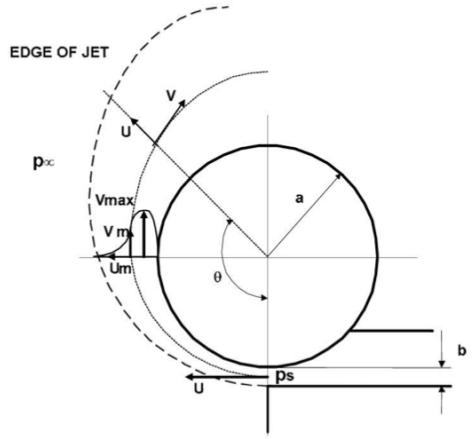

(a) Coanda Effect principle, illustrating the angle of separation θ, slot width b, and radius of curvature a.

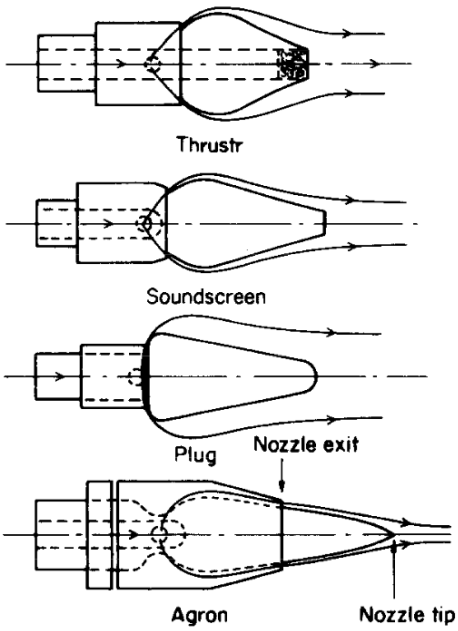

(b) The Coanda Effect air nozzle geometries studied by Li & Halliwell

Figure 2.12: Coanda effect principle and nozzle designs

Li & Halliwell [51] sought to quantify the performance of a range of commercially available Coanda Effect nozzles, with respect to acoustic emissions and thrust. Nozzle performance was compared to to that of an open pipe type nozzle, and the various nozzles studied are shown in Figure 2.12b.

The authors highlight that in a typical open pipe nozzle, the two main sources of noise include turbulent mixing noise and shock cell associated noise. A Schlieren study was performed which revealed the absence of shock cell structures for the Coanda nozzles, while it was clearly present for the the open pipe nozzle, hence providing an initial indication of their superior acoustic performance. This is consistent with the previously discussed micro jet nozzles, as shock cell associated noise is proportional to the length scales, and as the outlets of the Coanda nozzle are also of a small scale, any shock cell noise would be outside the audible hearing range.

For this study, a sound level meter was placed 1m away from the nozzle exit, and at 90°, while a pitot tube was used to measure stagnation pressure at a series of downstream points, and from which the thrust was calculated. While the performance of the nozzles in question was found to vary due to design geometry, the study concludes that a well designed Coanda Effect nozzle has the ability to reduce noise levels by 2-10dB while achieving similar or better thrust efficiency.

2.4 High Frequency Aircraft Noise

While this review has focused on the reduction of noise, the shifting of noise from low frequencies to high frequencies which are out of the audible hearing range has been discussed in the previous section. As this strategy was not commonly discussed in the literature specifically relating to aircraft noise reduction, it was considered necessary to investigate its potential implications for aircraft noise. Figure 2.13 presents the measured frequency spectrum of an Airbus A380 aircraft, as measured during a flyover test with aircraft height and velocity of 67m and 75 ms^{-1} respectively [52]. While the upper limit of the frequency range is 11,200Hz, it is clear that the noise drops off significantly at high frequencies. In the Federal Aviation Administrations 'Guidelines for Adjustment of Aircraft Noise Levels for the Effects of Background Noise' [53], this drop off is assumed to be primarily due to the effects of atmospheric absorption.

Atmospheric absorption involves the conversion of sound energy to heat as it propagates through the air. Attenborough [54] explains how for a plane wave, the pressure p at a distance x from a source pressure, p_0, is given by Equation 2.4:

$$p = p_0 e^{-\frac{\alpha x}{2}} \tag{2.4}$$

where α is the attenuation/absorption coefficient, with units of $\frac{NP}{matm}$, which is calculated according to Equation 2.5:

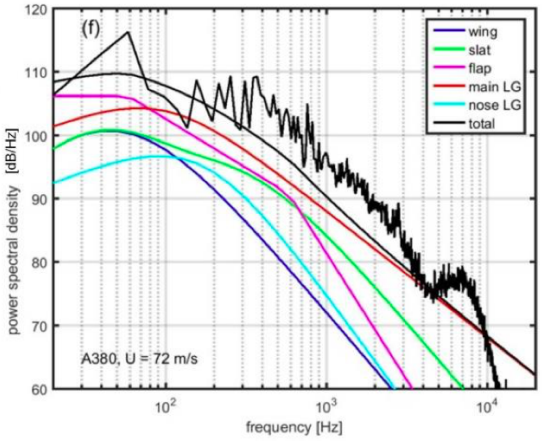

Figure 2.13: Frequency spectrum of Airbus A380, measured during a flyover test.

$$\alpha = f^2 \left[\left(\frac{1.84x10^{-11}}{\left(\frac{T_0}{T}\right)^{\frac{1}{2}} \frac{p_s}{P_0}} \right) + \left(\frac{T_0}{T}\right)^{2.5} x \left(\frac{0.10680e^{-3352/T} f_{r,N}}{f^2 + f_{r,N}^2} + \frac{0.01278^{-2239.1/T} f_{r,O}}{f^2 + f_{r,O}^2} \right) \right] \quad (2.5)$$

where f is the acoustic frequency in Hz, p_s is the atmospheric pressure, p_0 is the reference atmospheric pressure of 1 atm, T is the atmospheric temperature, T_0 is the reference temperature, equal to 293.15K, and $f_{r,N}$ and $f_{r,O}$ are the molecular relaxation frequencies of nitrogen and oxygen respectively.

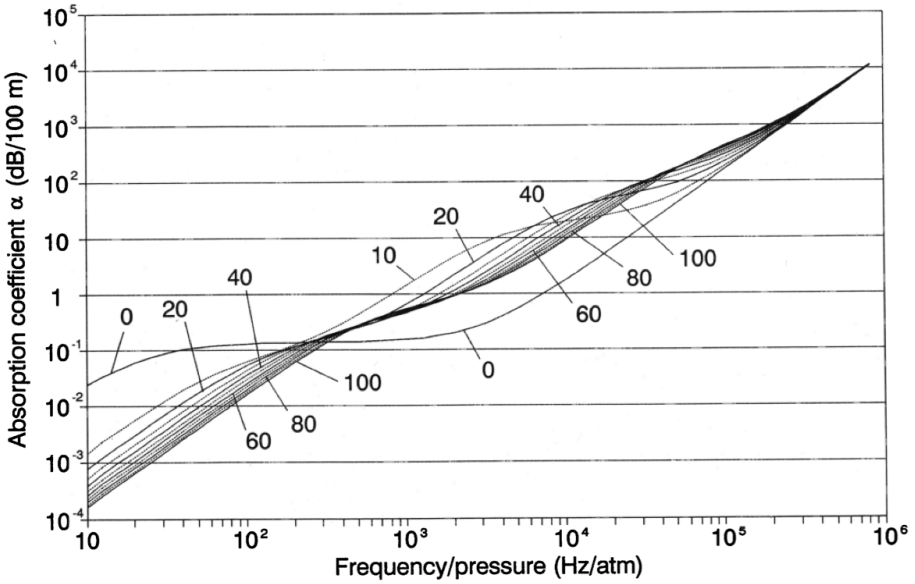

Figure 2.14: Sound absorption coefficient for various percent relative humidities at 20°C

While this is a rather complex formula, the absorption coefficient is positively correlated with acoustic frequency, and is shown in Figure 2.14 with units of dB/100m [55]. These fundamentals of atmospheric sound absorption partly explain the drop off in high frequency noise in the aircraft frequency spectra shown in Figure 2.13. Therefore, while high frequency noise generation cannot be ignored, it is logical to consider acoustic frequencies below 10kHz as most significant.

2.5 Summary

Research has shown that the significant noise pollution caused by the aviation industry has wide ranging and significant societal implications. The landing gear has been identified as a leading source of noise on modern aircraft, particularly during the landing phase when the engine thrust is low. Therefore, a range of LNT's have been proposed and researched over the last two decades, with varying degrees of success, practical feasibility and technology readiness levels, with some technologies reaching the stage of full scale flight tests. One LNT that is currently at a low TRL but shows promising noise reduction potential is the air curtain. Implementation of an air curtain in a landing gear system can serve to deflect high velocity oncoming air away from the unaerodynamic surfaces of the landing gear, and reduce the associated aerodynamic noise. While the primary challenge faced

with this technology to date has been the production of self noise, optimisations such as the dual jet air curtain present opportunities to overcome such a challenge. Furthermore, a body of research exists to suggest that with the implementation of design philosophies such as multi jet and Coanda Effect nozzles, the self noise of air nozzles can be meaningfully reduced, or partly shifted to higher frequencies which are both more readily dissipated in the atmosphere and may also be above the audible hearing range and hence have minimal influence on A-weighted sound levels.

3 Experimental Facilities

This section outlines the test procedures which were undertaken during this research project. The tests performed were primarily experimental, with a component of mathematical modelling which was used to choose suitable air nozzle design parameters. As discussed in Section 1.2, the overarching goal of the project was to test newly designed air curtain nozzles in the AWB wind tunnel at the DLR in Braunschweig, Germany. The conditions in the AWB wind tunnel are highly controlled and favourable for acoustic measurements, and could not be feasibly replicated in the Trinity College fluids lab for the purpose of preliminary tests. However, a small open jet wind tunnel was utilised in order to perform a series of flow deflection tests, such that the main working principle of the air curtains could be achieved, which was to deflect flow around aircraft landing gear. Such tests relied on the use of hot wire anemometry to perform flow velocity measurements, and the test setup will be described in detail in this section. Preliminary acoustic tests were performed separately to flow deflection tests, due to the high noise levels from the open jet wind tunnel, and these will also be described. This section will conclude with a detailed overview of the AWB wind tunnel setup and experimental techniques utilised at the DLR.

3.1 Trinity College Dublin Tests

3.1.1 Open Jet Wind Tunnel

The open jet facility comprises a 5.5kW centrifugal blower operating at 2860rpm, connected to a diffuser and plenum which comprises a series of honeycombs and screens to promote low turbulence intensity. Connected to the plenum is a plywood exit nozzle which was developed through the work of Moreno [56] to achieve a maximum outlet velocity of $70ms^{-1}$ across its 7.5cm x 7.5cm outlet area. A schematic of the open jet is shown in Figure 3.1.

3.1.2 Hot Wire Anemometry

The working principle of the Hot Wire Anemometer (HWA) is based upon the concept that a heated length of wire placed into a flow field will experience heat transfer to the flow by forced convection, and a resulting proportional change in electrical resistance of the wire can be observed. The HWA is connected to a Wheatstone Bridge which measures changes in resistance of the wire. Two main working principles exist; constant current, and constant temperature HWA's. The method used in this research was the constant temperature method, and so this shall be discussed in greater detail.

The wire is initially heated up to a certain temperature, which is dictated by various parameters

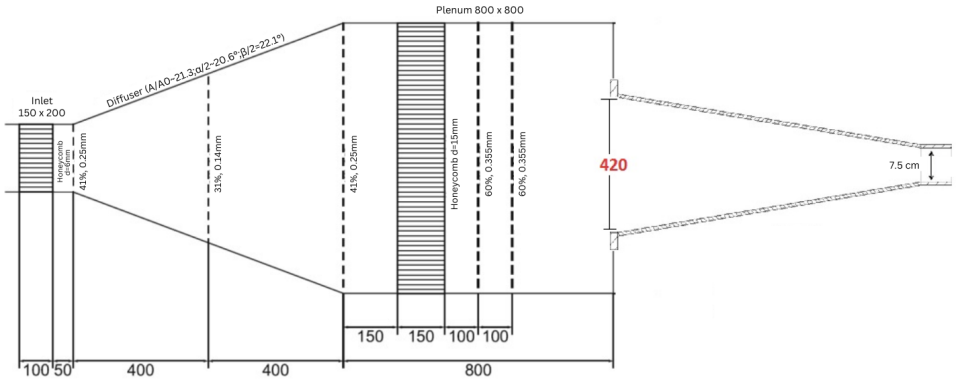

Figure 3.1: Open jet configuration.

including the chosen Overheat Ratio, R_w/R_a, and the properties of the probe in question [57]. Note that some thermal conduction will occur at the ends of the wire due to the connection to the unheated probe arms, hence the wire temperature typically refers to the mean temperature, T_m. As the fluid flow induces forced convection at the wire, the temperature is reduced, resulting in a resistance change. In order to maintain a constant temperature, the current in the circuit increases, and a voltmeter connected across the Wheatstone Bridge provides the signal output which is used as a measurement of flow rate.

Wire material can be platinum, its alloys or tungsten. Tungsten is usually used for air and gas flows with temperatures of less that 150°C, as it has a higher tensile strength than platinum and is therefore more resilient. However, tungsten has an oxidisation temperature of approximately 350°C, and therefore the operating temperature of the sensor must lie below this value to ensure accuracy and prevent damage.

Hot Wire Parameters

The Dantec Dynamics 55P11 HWA probe was primarily used in this study, and consists of a platinum plated tungsten wire, with a maximum rated operating temperature of 300°C. It is advantageous to calculate the mean temperature, T_m, prior to calibration to ensure the system is set up in a way which will not cause damage. Equation 3.1 can be used to calculate operating resistance, where R_{20} is the resistance at 20^0C and α_{20} is the temperature coefficient of resistance. Both values are specified by the manufacturer and are equal to 3.5Ω and $0.36\%/^0C$ respectively. It is typically recommended that the overheat ratio is equal to a value less than 2, and is set to the recommended value of 1.8, with Equation 3.2 outlining the relationship between this ratio, the operating resistance, R_w, and the reference resistance, R_a. For the purpose of this simple analysis, it is sufficient to assume R_a is approximately equal to R_{20}

$$R_w = R_{20}[1 + \alpha_{20}(T_m - T_{20})] \tag{3.1}$$

$$OverheatRatio = \frac{R_w}{R_a} \tag{3.2}$$

Based on these equations, the mean temperature in the wire is calculated to be 230°C, and is sufficiently below the rated maximum operating temperature.

System Setup

The HWA is connected to a Data Acquisition System (DAS) consisting of a StreamLine 90N10 frame and a National Instruments PXI-1033 controller. This system acts to control the temperature of the probe while also outputting the voltage signal which is used in the Dantec Dynamics StreamWare Pro software to calculate flow velocity. Images of the setup and software configurations used are available in Appendix A1.1.

Calibration

The calibration setup consists of the HWA system as previously described, with the HWA placed at the outlet of a high velocity nozzle, which itself is attached to an air supply with a flow rate meter installed. The full system is shown in Figure 3.2, and further images are available in Appendix A1.2. The flow rate meter records the flow rate, Q, in Standard Litres Per Minute (SLPM), and as the outlet area, A, of the high velocity nozzle is known to be $9.156e^{-5}m^2$, the flow velocity at the nozzle outlet can be easily calculated using Equation 3.3. Having configured the setup in the StreamWare Pro software, a two point calibration is performed where the voltage corresponding to the minimum and maximum flow velocities are recorded, allowing the gain and offset of the system to be adjusted within the software. This enables the full use of the 1V to 10V voltage output range, and hence maximum accuracy and sensitivity of the results.

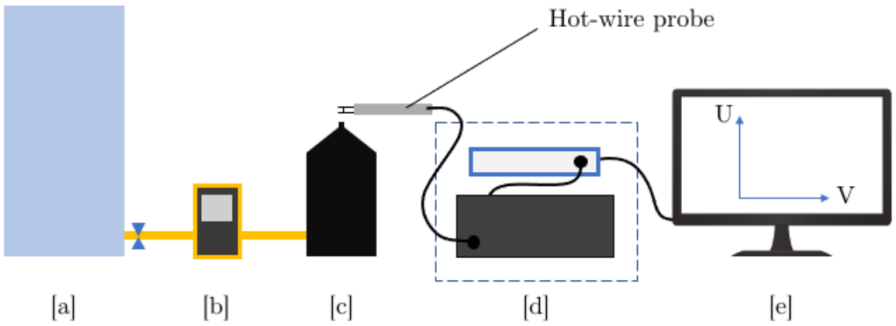

Figure 3.2: Calibration setup consisting of [a] air supply, [b] flow meter, [c] high velocity nozzle, [d] DAS and [e] the StreamWare Pro software.

$$V = \frac{Q}{A * 60000} \tag{3.3}$$

A full calibration is then performed, recording voltage values at 10-20 measurement points distributed linearly from the minimum to maximum flow velocities. The data is exported to Microsoft Excel, where voltage is plotted against flow velocity and a fourth order trend line is fit to the data, allowing

the associated interpolation coefficients to be extracted. Such a calibration curve is shown in Figure 3.3. As it is recommended to perform probe calibration on a regular basis, the probes used in this study were calibrated multiple times over the course of the research, with the calibration range chosen in accordance with the range of velocities to be measured for each experiment.

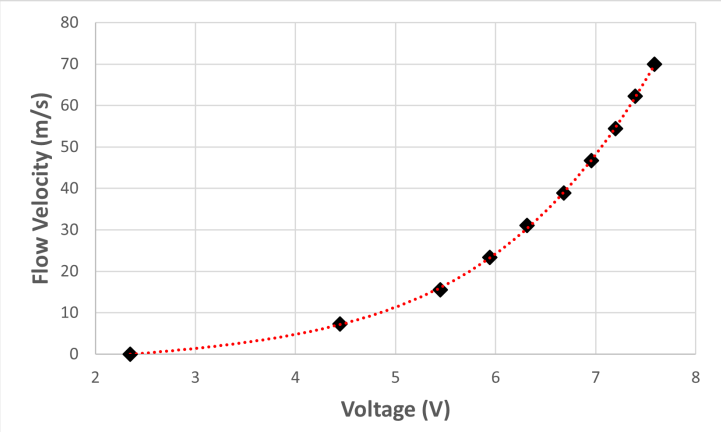

Figure 3.3: Calibration curve up to $70ms^{-1}$ for 55P11 HWA.

Experimental Rig

Many of the HWA experiments discussed in later sections involve the measurement of flow parameters at multiple points on a line or plane. Therefore, in order to enable accurate and reliable movement and positioning of the probe, a traverse with Computer Numerical Control (CNC) was utilised. The traverse, which was developed and used in previous research work [58], was driven by three stepper motors, an Arduino Uno board and controlled by a Matlab script. The probe was connected to the Dantec Dynamics 55H26 right angled probe support, and this was attached to the movable component of the 3D stage by means of a bespoke connector. This permitted the measurement of flow velocity at a series of defined points in 3 dimensional space. Figure 3.4 illustrates the rig setup and its positioning relative to the previously discussed open jet wind tunnel. The Matlab script used to control the traverse and record velocity data is available in Appendix A1.3. The Matlab script shown in Appendix A1.3 was used to perform 400 velocity measurements on a 120x100mm plane.

As the traverse was used in the measurement of flow deflection, it was advantageous to calibrate its movement with distance to enable the accurate calculation of the shielding height of various nozzles. Therefore, a simple calibration was performed in which the distance moved by the traverse, D, with 100 steps of the stepper motors was measured. Hence, the number of steps per mm of desired movement was easily calculated using $\frac{100}{D}$.

Flow Characteristic Measurement

For flow velocity measurement, the sampling rate was set to 1kHz, with a measurement time of 5 seconds. Therefore, 5,000 voltage measurements were saved and converted to velocity values in Matlab, according to the fourth order polynomial as discussed in the calibration section. The mean of these values was used as the flow field velocity at each measurement point.

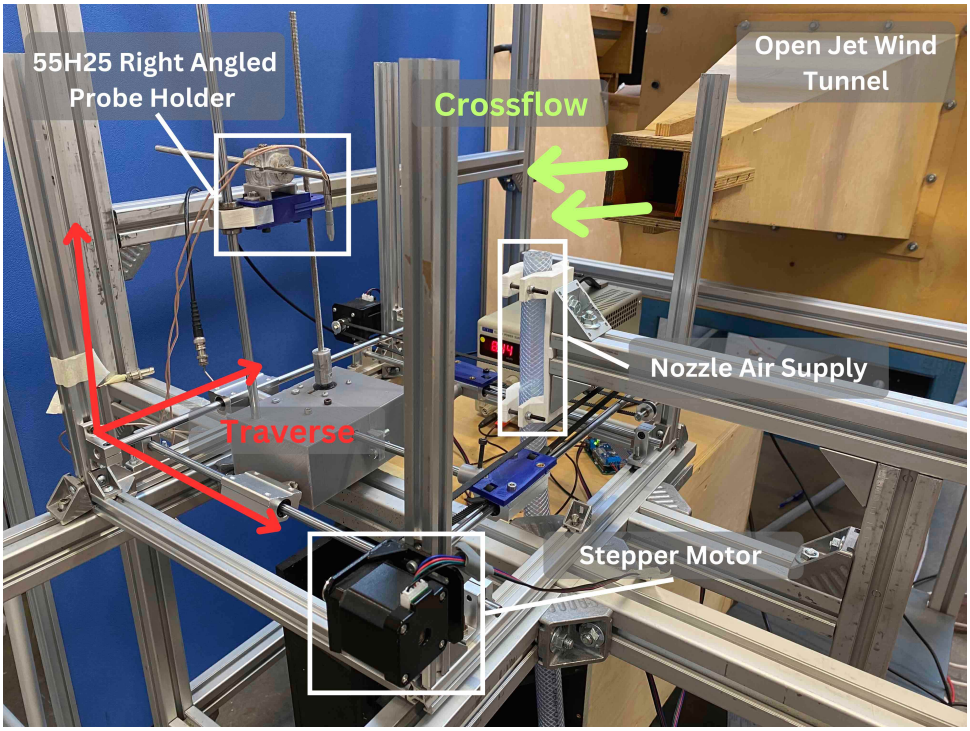

Figure 3.4: Experimental rig consisting of traverse, open jet wind tunnel and nozzle air supply.

The HWA measurement data also permits the calculation of turbulence intensity, which is a potentially useful measure of turbulence. For tests where turbulence intensity was the primary quantity of interest, the sampling rate was increased to 5kHz, which is consistent with sampling rates seen in the literature [59], and the measurement time was also set to 5 seconds, hence the sample size was 25,000 data points. The turbulence intensity, I, was calculated according to Equation 3.4, where σ represents the standard deviation, and M is the mean velocity.

$$I = \frac{\sigma}{M} \tag{3.4}$$

Sampling Error

The sample sizes mentioned in 3.1.2 were chosen such that they were large enough to ensure minimal sampling error. The Standard Error, SE, was calculated according to Equation 3.5, where N is the sample size. Knowledge of SE permitted the calculation of a confidence interval according to Equation 3.6, where $\bar{x}$ is the mean of the data and z is the confidence interval value, which is equal to 1.96 for the calculation of a 95% confidence interval.

$$SE = \frac{\sigma}{\sqrt{N}} \tag{3.5}$$

$$CI = \bar{x} \pm z\frac{\sigma}{\sqrt{N}} \tag{3.6}$$

With these calculations, it was possible to state a 95% confidence interval for each HWA velocity

measurement, which was less than or equal to $\pm 0.3 ms^{-1}$ for all measurements performed at 1kHz and $\pm 0.15 ms^{-1}$ for all 5kHz measurements.

3.1.3 Sound Level Measurement

In order to compare acoustic performance of air nozzles, sound level tests were performed with the SVAN 971 Sound Level Meter (SLM) by Svantek. The SLM was placed on a tripod at a height equal to that of the nozzle being studied. While numerous studies mentioned in the literature have performed similar tests utilising multiple measurement points in order to account for the directionality of the acoustic noise, this was not considered in this study due to the presence of variable quantities of jets and varied nozzle geometry, such as outlet angles, impairing the consistency of such results. Figure 3.5 depicts the inconsistencies which would be experienced with such a test, as jet interference with the SLM was a concern and would not have been consistent across tests. Therefore, consistency was achieved by placing the SLM 1m away from the nozzle outlet and at 90° to the average jet flow direction for one side of the nozzle, as shown in Figure 3.6. This permitted the standardised measurement of nozzle sound level with respect to the direction of the jet flow. While it is recognised that inconsistencies related to directionality and total outlet length (and therefore noise source length) were still present in the system, this experimental setup permitted a sufficiently indicative insight into acoustic performance. Care was also taken to ensure the air jet did not impinge on any surface within reasonable distance, which would cause additional noise. Images of the experimental setup are shown in Appendix A1.5.

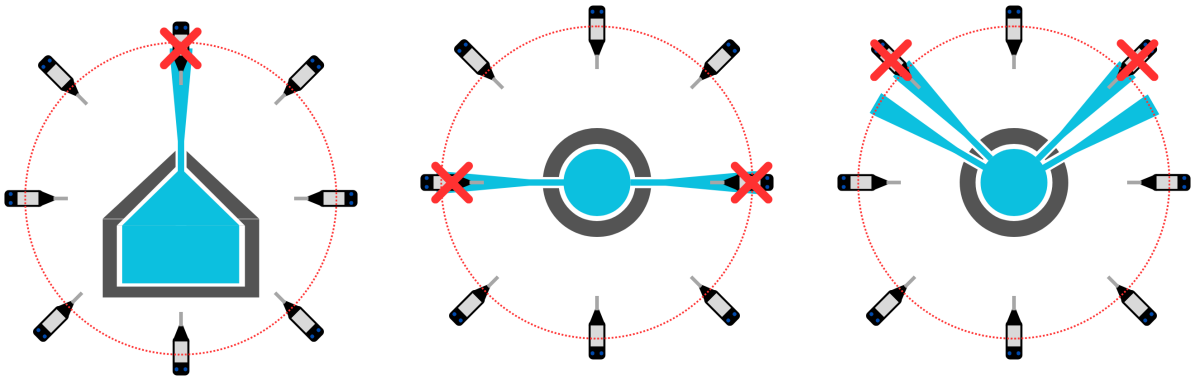

(a) Single outlet jet.

(b) Single outlet jet on each side of nozzle.

(c) Dual jet and oblique blowing on each side of nozzle.

Figure 3.5: Difficulties were experienced in determining the correct SLM placement due to widely varying nozzle designs.

The SLM permitted the measurement of sound levels with various filters, notably A, C and Z weightings. The most widely mentioned weighting in the literature is the A weighting, and so it was decided to perform the sound level tests with this. In particular, the equivalent continuous sound level, LA_{eq}, was recorded over a period of 30 seconds. This is effectively a recording of the average sound pressure level over the measurement period, and is typically deemed useful for the measurement of fluctuating noise. It was considered appropriate to adopt this technique due to the unknowns surrounding the presence of turbulence and vorticity in the nozzles, which could produce transient acoustic performance.

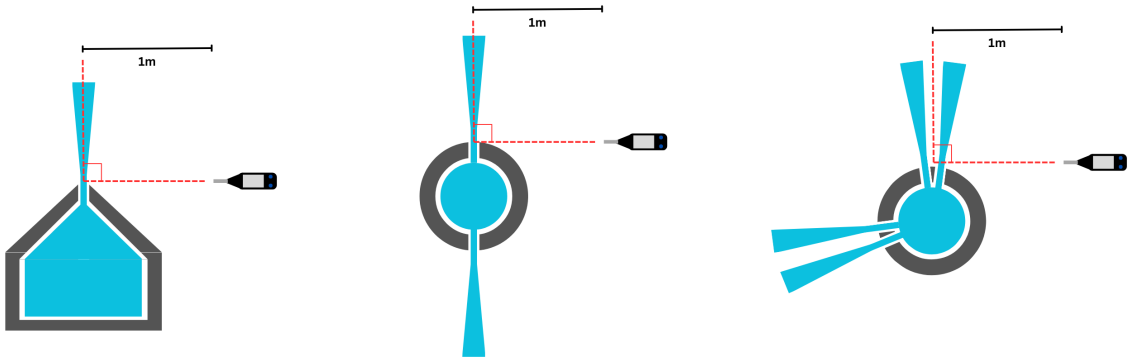

(a) Single outlet jet.

(b) Single outlet jet on each side of nozzle.

(c) Dual jet and oblique blowing on each side of nozzle.

Figure 3.6: Acoustic measurements standardised with respect to the mean direction of outlet flow.

3.2 AWB Wind Tunnel Facility

3.2.1 Anechoic Wind Tunnel Testing

The air curtains developed through this project were tested on a 1:7.65 scale model of the Lagoon NLG in the AWB, which is DLR's small, high quality test facility for aeroacoustic noise measurements. The facility is an open jet, closed circuit tunnel, as shown by the plan view graphic in Figure 3.7a. The test section is located in an anechoic plenum with dimensions $8x8x5m^3$, as shown in Figures 3.7b & 3.7c. The wind tunnel nozzle is 0.8m wide by 1.2m high and can achieve flow velocities up to $65ms^{-1}$ at low turbulence intensities.

The facility was upgraded in 2008 as described by Pott-Pollenske and Delfs [60], whereby a new layout for the flow circuit was adopted utilising an installation of turning veins in every corner. Such veins all feature the Krober profile in order to minimise pressure loss, while porous foam covers the sheet metal core on both the suction and pressure side in order to facilitate sound absorption. Furthermore, this facility upgrade saw the addition of an adaptive collector which could be moved vertically up or down in order to collect the sometimes highly bent down-wash, hence preventing it from impinging on the floor and creating unnecessary noise.

Acoustic Measurement

A number of microphones were positioned at specific locations in the wind tunnel in order to perform acoustic analysis of the various landing gear configurations. A sampling rate of 102kHz was used and sound spectra were generated at each microphone location, and hence the acoustic performance of various nozzle configurations could be measured and compared. Table 3.1 outlines the microphone positions, while Figure 3.8 depicts the arrangement in the wind tunnel with the landing gear installed. The origin of the coordinate system is the centre of the exit plane of the wind tunnel nozzle.

A Fast Fourier Transform (FFT) was used to transform the measurement data to the frequency domain, using 4096 samples per FFT and averaging with 748 samples. This enabled the visualisation of acoustic performance using frequency spectra which plot the sound level, in dB, against the frequency, which was measured from 74Hz to 39,000Hz, although this study focused on frequencies

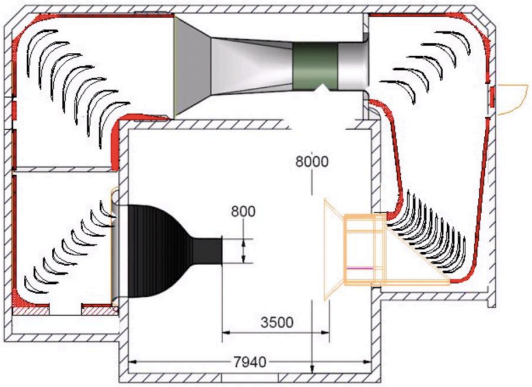

(a) AWB wind tunnel plan.

(b) AWB wind tunnel collector.

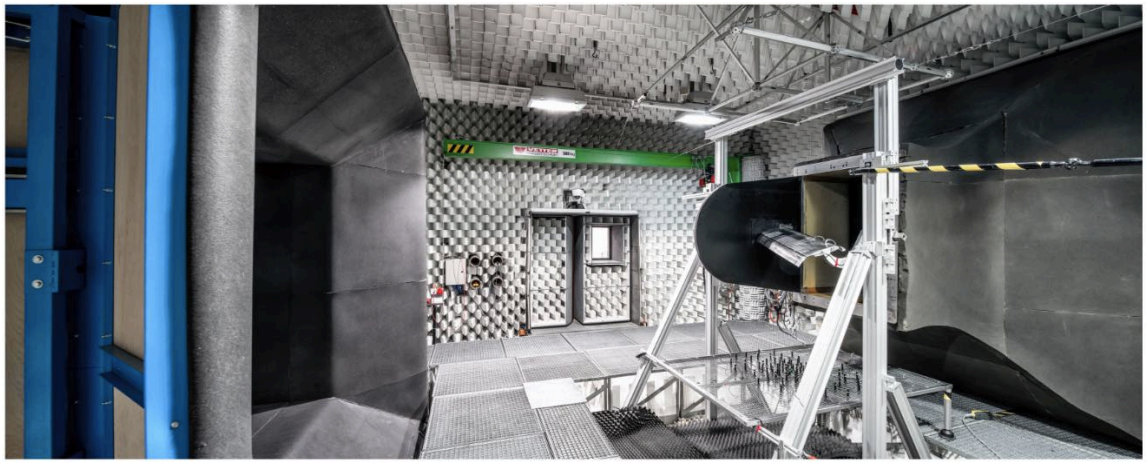

(c) AWB wind tunnel collector (left) and nozzle (right).

Figure 3.7: AWB wind tunnel at DLR Braunschweig.

Microphone	X	Y	Z
M1	-0.166	-0.011	0.975
M2	0.084	-0.011	0.975
M3	0.469	-0.011	0.975
M4	0.469	0.230	0.975
M5	0.475	0.850	0.480
M6	0.714	0.849	-0.488
M7	0.714	0.849	0.012

Table 3.1: Microphone Coordinates

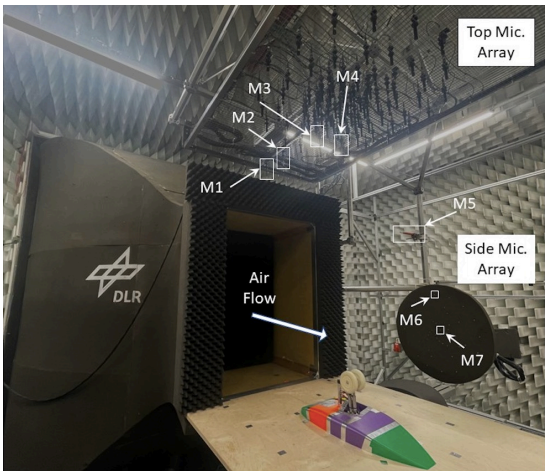

Figure 3.8: Microphone array positions in AWB wind tunnel

below the audible limit for humans which is 20kHz. 1/3 octave bands were also measured with centre frequencies ranging from 100Hz to 31500Hz. Furthermore, it was advantageous to calculate a measure of overall acoustic noise intensity, hence the overall sound pressure level (OASPL) was calculated for each microphone position. The A-weighted sound pressure level was also calculated to

provide a measure of perceived noise levels for human hearing.

Beamforming

While acoustic spectra graphs are valuable for the analysis of air curtain configurations, the arrangement of microphones in arrays permits the use of beamforming to detect the localisation of sound sources. Beamforming enables the localisation of sound sources in a similar way to that of human hearing. Acoustic waves have a well defined propagation speed that depends only on the medium in which they travel. Therefore, sound propagating from a given source will reach a point in space with a phase which is dependant only upon the distance travelled. Furthermore, acoustic waves feature decaying amplitude with distance travelled from the source. Using multiple microphones at different locations, or two ears in the case of human hearing, the sound source position can be calculated using these differences in amplitude and phase. While complex acoustic sources commonly exist in aeroacoustics, featuring dipole and quadropole sources, it is common to assume the distance between the microphone array and source is sufficiently large such that the source can be approximated by a distribution of monopole sources.

Beamforming was therefore utilised in the study in order to determine the predominant noise sources in the system. Horizontal (M1-M4 as shown in Figure 3.8) and Vertical (M5-M7) microphone arrays were installed in the wind tunnel such that sound source localisation could be performed both from a top view of the landing gear, and a side view. It is important to note that no shear layer or distance corrections have been applied to the beamforming data used in this study. Therefore, minor discrepancies are to be expected between measured and actual location and amplitude results.

3.3 Summary of Experimental Methods

The highly controlled and acoustically favourable conditions available in the AWB wind tunnel are necessary to definitively validate the air curtain concept as a noise reduction technology on a scaled model of aircraft landing gear. However, prior to the test campaign in the AWB, experimental facilities in the Trinity College fluids lab will be employed to aid the design of air curtain nozzles. A small open jet wind tunnel will be used in combination with HWA to measure flow deflection capabilities of various nozzles in a cross flow. In addition, sound levels related to the self noise of the nozzles will be measured, in the absence of cross flow, using a SLM. The AWB wind tunnel tests will then consist of the use of an anechoic wind tunnel featuring low turbulence intensity jet flow. Two microphone arrays installed in vertical and horizontal orientations will generate frequency spectra, and a beamforming algorithm will be employed for the localisation of the noise sources in the system.

4 Preliminary Results

While the overarching goal of the research was to perform a series of wind tunnel tests with a view to assessing the validity of the air curtain concept when implemented on a landing gear scale model, the majority of the early focus was aimed at developing a nozzle which would overcome the failings of the nozzles discussed in Section 2.2. As mentioned previously, this involved noise reduction and the improvement of jet flow uniformity. Therefore, this section will discuss the preliminary results obtained in the development of the final low noise air curtain nozzle design philosophy.

4.1 Dual Jet Nozzle

As discussed in the literature review, the concept of a dual jet air curtain has been studied and validated as a viable noise reduction technology, with lower noise levels than that of the single jet air curtain. However, its implementation on a landing gear had not yet been studied. Therefore, as a first point of optimisation, a dual jet nozzle was designed featuring the same geometry and baffle design as the single jet nozzle resulting from prior work, which shall henceforth be referred to as the 'Reference Nozzle'. The dual jet featured the same total inlet area as the reference nozzle, hence the same flow rate could be achieved. 40% of the flow was distributed to the upstream outlet/jet, and the downstream/main jet received 60% of the flow. This was intended to achieve a stronger downstream jet which was shown in the literature to achieve the greatest results. The geometry used is shown in more detail in Appendix A1.4.

The described dual jet nozzle was 3D printed and is shown in Figure 4.1b, alongside the equivalent single jet nozzle in Figure 4.1a. Note that the original connector which was compatible with the nozzle led to some air leakage so this was sealed for consistency. The two nozzles were tested with an inlet air supply of $0.018 m^3 s^{-1}$. The HWA was used to characterise the deflection of cross flow by each nozzle, and sound level tests were performed to compare acoustic performance.

4.1.1 Cross flow Deflection

The respective air curtains were subjected to a cross flow of 28m/s and the HWA was used to characterise the resulting deflection. The measurements were taken with 10mm spacing across a plane parallel to the cross flow, with dimensions equal to 60mm in the span-wise direction, and 90mm in the stream wise direction. An illustration of the test setup is shown in Figure 4.2.

As shown by the HWA velocity measurement results in Figure 4.3, the shielding effect of the two nozzles were comparable. These contour plots represent the change in velocity of the cross flow due

(a) Single jet air nozzle

(b) Dual jet air nozzle

Figure 4.1: Single and Dual Jet air curtain nozzles. Note that the original connector which was compatible with the nozzle led to some air leakage so this was sealed for consistency.

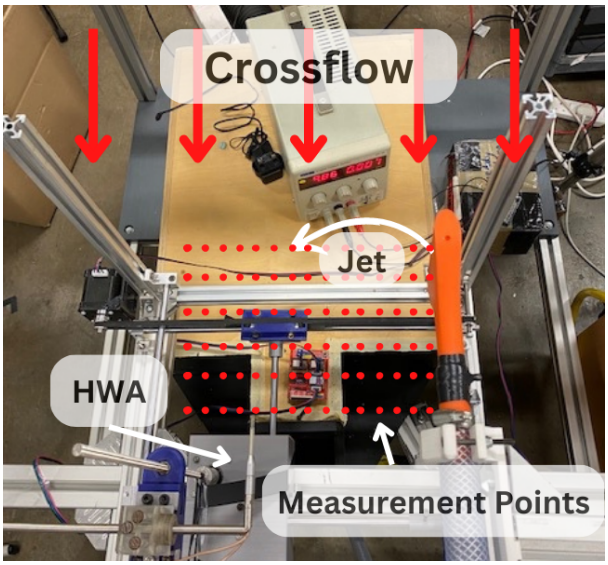

Figure 4.2: HWA test setup with cross flow and measurement plane

to the air jet, with the position (115,70) representing the position of the most upstream outlet (or the position of the only outlet for the single jet). The nozzle outline and approximate jet paths have been illustrated on the contour plots for clarity.

4.1.2 Sound Level Test

Sound level tests were performed in accordance with the procedure outlined in Section 3.1.3. Such tests showed a 3dB reduction with the dual jet compared to the reference nozzle. This was a logical result as the flow rate was constant for each of the nozzles, hence as the dual jet featured double the total outlet area, it was to be expected that the flow velocity at the outlet was lower than that of the reference nozzle, according to Equation 4.1. The noise reduction can be attributed to this outlet velocity reduction as the the lip noise at the outlet is said to scale with the 5^{th} power of velocity, while the impact of increasing the total outlet area, and hence the noise source, can be described by

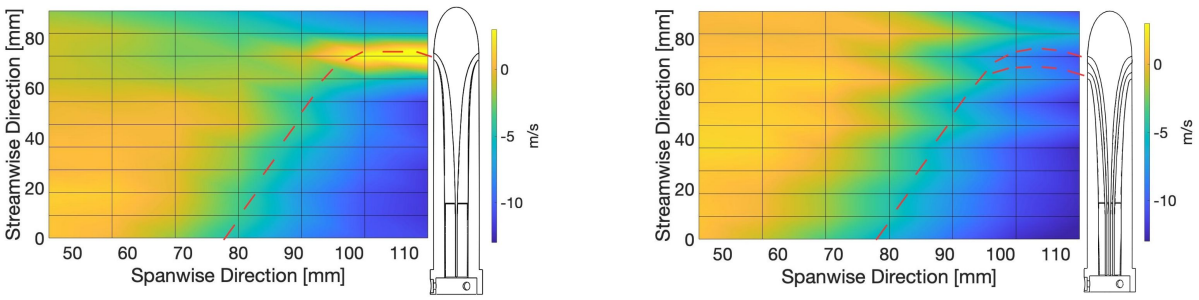

(a) Velocity change due to single jet

(b) Velocity change due to dual jet

Figure 4.3: Contours of the change in velocity, recorded with the HWA.

a logarithmic scale according to Equation 4.2, where I_{total} is equal to the total sound intensity level in W/m^2. Hence the reduction in lip noise is dominant.

$$Q = VA \tag{4.1}$$

$$dB_{total} = 10 \log_{10} \left(\frac{I_{total}}{10^{-12}} \right) \tag{4.2}$$

4.2 Industrial Air Blade

Planar air jets are used in many modern industrial applications, most notably in cleaning and drying on production lines. As workplace noise levels are regulated, it is advantageous for such air blades to produce low acoustic noise emissions. Therefore, a number of air blades exist on the market which claim attractive acoustic performance. One such device is the 150mm Neublade Airstrip, which was purchased for the purpose of assessing its performance and employing a reverse engineering approach to the design of a landing gear air curtain nozzle, if its performance proved impressive. The device which will henceforth be referred to as 'Air blade' is shown in Figure 4.4.

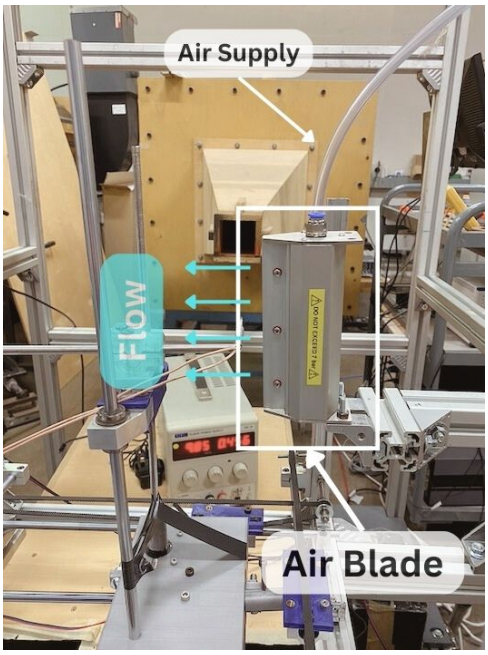

Figure 4.4: Air Blade pictured during a cross flow deflection test.

The Air blade was supplied with $0.047 kgs^{-1}$ of air at a pressure of 6 bar, which represented a choked flow condition, as further opening of the air supply valve did not correspond to a change in volumetric flow rate. Sound level tests revealed the acoustic performance was significantly better than the reference nozzle, at 83.6dB compared to 103.9dB. Furthermore, a consistent outlet flow was observed, with little or no variation in flow across the length of the outlet. This was believed to result from the

occurrence of choked flow and will be discussed in greater detail below.

4.2.1 Flow Deflection

As acoustic performance alone is not a sufficient indicator of effectiveness, the flow deflection performance of the Air Blade was also investigated. For the purpose of this comparison, a one dimensional line of points was measured, as opposed to the two dimensional plane of points measured in the previous flow deflection test. Velocity measurements were taken 120mm downstream of the nozzle outlet and from 0mm to 100mm in the span-wise direction, spaced 5mm apart. The nozzles were subjected to a cross flow of 28m/s and the inlet flow conditions were consistent with what was previously stated, with the Air Blade positioned such that the air curtain was blown in a direction normal to the cross flow. The change of velocity in the span wise direction is shown in Figure 4.5a, clearly indicating a greater velocity reduction by the Air Blade and hence superior performance.

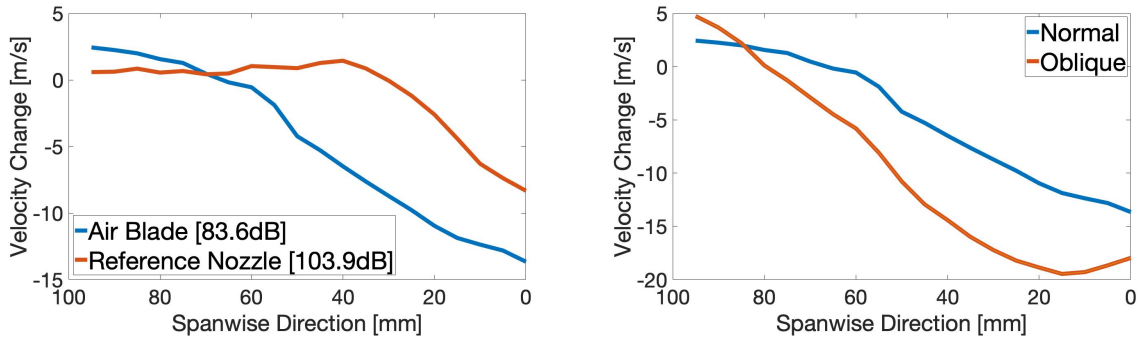

(a) Shielding of Air Blade and reference nozzle, 120mm downstream of outlet.

(b) Shielding effect of Air Blade when blown normal and oblique to the cross flow.

Figure 4.5: Flow deflection test results of Air Blade.

While the above results indicate the superiority of the Air Blade design, previous research has shown that performance improvements are to be expected when the air curtain is blown in a direction oblique to the oncoming cross flow. Hence, in order to gauge the potential of the Air Blade, the flow deflection test was rerun with the nozzle facing 15° in the upstream direction. The results of this study are shown in Figure 4.5b, which is consistent with prior research indicating the superior performance of oblique blowing.

4.2.2 Design Analysis

Due to the favourable performance of the Air Blade, its design was analysed with a view to adopting a similar design philosophy for further nozzle prototypes. It was recognised that the Air Blade consisted of just a hollow chamber with very small outlet openings. It was these outlets which were believed to present the majority of the favourable performance characteristics, and so a Dino-Lite Digital Microscope was used to view and measure the outlet geometry. Figure 4.6 presents the results of this investigation, revealing the 1.7mmx0.14mm outlet hole size, with a slightly elliptical shape.

It was not known if the outlet shape was a contributing factor to the performance, or if it was simply the result of the chosen manufacturing method. However, it was considered likely that the small outlet dimensions were the most significant contributing factor to acoustic performance, due to the

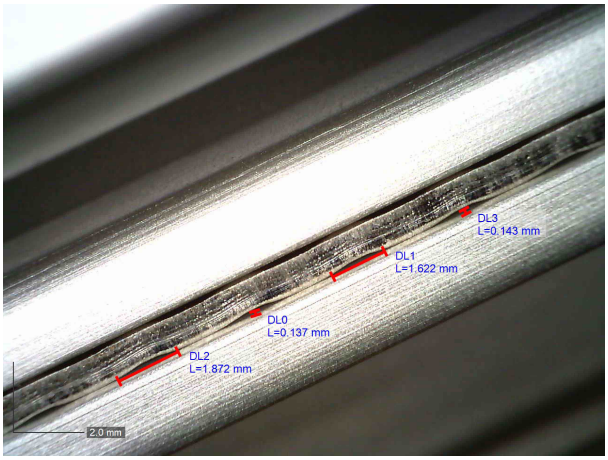

Figure 4.6: Microscopic view of the Air Blade outlet

inverse relationship between frequency of noise produced and characteristic dimension, as discussed in the literature.

Choked Flow

As mentioned, it was believed that the flow at the nozzle outlet was choked, and that this was responsible for the uniform outlet flow observed. In order to achieve choked flow, certain conditions must first be met, most notably the pressure ratio between downstream static and upstream stagnation pressure must lie below that of the critical pressure, P^*. As shown in Equation 4.3, P^* depends only on the ratio of specific heats of the gas in question, γ. For air, $\gamma = 1.4$, and hence $\frac{P^*}{P_o} = 0.528$. Hence, as P^* is equal to normal atmospheric pressure of 101kPa, the minimum required stagnation pressure upstream of the outlet, P_o, is equal to 191kPa or 1.91 bar in order to achieve choked flow.

$$\frac{P^*}{P_o} = \left(\frac{2}{\gamma+1}\right)^{\frac{\gamma}{\gamma-1}} \tag{4.3}$$

Furthermore, sufficient mass flow rate must be provided to the nozzle in order to achieve true choked flow. Fleigners formula may be employed in order to calculate this, which is given in Equation 4.4. The total outlet area was calculated by assuming rectangular outlets of 1.7mm x 0.14mm and spaced 1.7mm apart along the 150mm length. P_o was estimated as 5 bar, accounting for head losses in the pipework, while T_o was estimated as the typical room temperature of 292K. Therefore, $\dot{m} = 0.043 kg/s$, which shows reasonable agreement with the experimentally calculated mass flow rate of 0.047kg/s.

$$\frac{\dot{m}}{A^*}\frac{\sqrt{T_o}}{P_o} = \sqrt{\frac{\gamma}{R}\left(\frac{2}{\gamma+1}\right)^{\frac{\gamma+1}{\gamma-1}}} = 0.04042 Kg^{0.5} K^{0.5} J^{-0.5} \tag{4.4}$$

This simple analysis provides validation to the theory that the flow is choked at the nozzle outlet. As choked flow represents a maximal velocity condition, the outlet flow velocity is therefore constant

and equal to the speed of sound if boundary layer effects are neglected. It is worth noting that the boundary layer is likely to have a non-negligible effect on the actual velocity due to the small dimensions of the outlet, and this is discussed briefly in 4.3.4.

4.3 Design Philosophy

Considering the above findings, a fundamental design philosophy was developed which was based on the following two underlying principles:

- The use of a micro nozzle geometry could enable significant reductions in noise levels in the audible range.
- The correct selection of outlet area and upstream pressure, coupled with sufficient mass flow rate could lead to a choked flow condition at the outlet, and a resulting uniform velocity profile.

The ability to manufacture working prototypes in a timely manner was a primary design constraint. While previous nozzles have almost exclusively been manufactured by means of plastic 3D printing techniques, such nozzles did not utilise pressurised air. Due to the relatively low strength, brittleness and occurrence of manufacturing imperfections, for safety reasons, plastic 3D printing was considered an unsuitable manufacturing technique and hence aluminium was chosen as a more suitable material for its more desirable mechanical properties. Nozzle designs were therefore limited by the resources available in the Trinity College manufacturing workshop. It was proposed to achieve the micro nozzle geometry by drilling holes in an aluminium container to be pressurised with air as shown in Figure 4.7a, hence the outlet size was limited by the minimum drill bit diameter available, which was 0.5mm.

4.3.1 Geometric Considerations

In order to permit easy integration in the landing gear model, a hollow tube was used to act as the pressurised air chamber, hence the design shall henceforth be referred to as 'air tube'. The tube was open at one end and was sized accordingly to permit the direct attachment of a 19mm air hose, as shown in Figure 4.7b. It was worth considering that a thinner tube was favourable from an aerodynamics perspective, as it would cause minimal flow obstruction and hence minimal drag. However, as the goal of the air tube geometry was to achieve choked flow at the outlets, the cross sectional area of the internal chamber of the tube had to be considered, as choked flow would only occur at the point in the system of minimum cross sectional area. Therefore, treating the outlet holes as a single outlet with cross sectional area equal to A_{outlet}, as calculated by Equation 4.5, the cross sectional area of the tube chamber was required to be larger than this with a sufficient factor of safety.

$$A_{outlet} = N\pi \left(\frac{d}{2}\right)^2 \tag{4.5}$$

where N is the total number of outlet holes, and d is the hole diameter.

Hence, applying an arbitrary factor of safety of 1.5, the minimum tube internal diameter, d_T was calculated as follows:

$$d_T > 1.5A_{outlet} \tag{4.6}$$

Conversely, this analysis limited the number of holes that could be drilled in the tube, once the tube was manufactured. Hence a conclusive model was established, limiting the number of holes in the tube, and is as follows:

$$N < \frac{8d_T}{3\pi d^2} \tag{4.7}$$

4.3.2 Choked Flow and Uniformity

In an attempt to further understand the effects of choked flow, the HWA was used to measure the flow velocity at the outlets for a range of upstream pressure values. The probe was positioned at a distance of 5mm from the most upstream hole of the air tube, as shown in Figure 4.7c and the velocity and flow rates were measured with an air supply of 2 bar to 6 bar, in 0.5 bar increments. The experiment was then performed again with the probe positioned at the most downstream hole. For each measurement, the flow valve on the air supply was fully open.

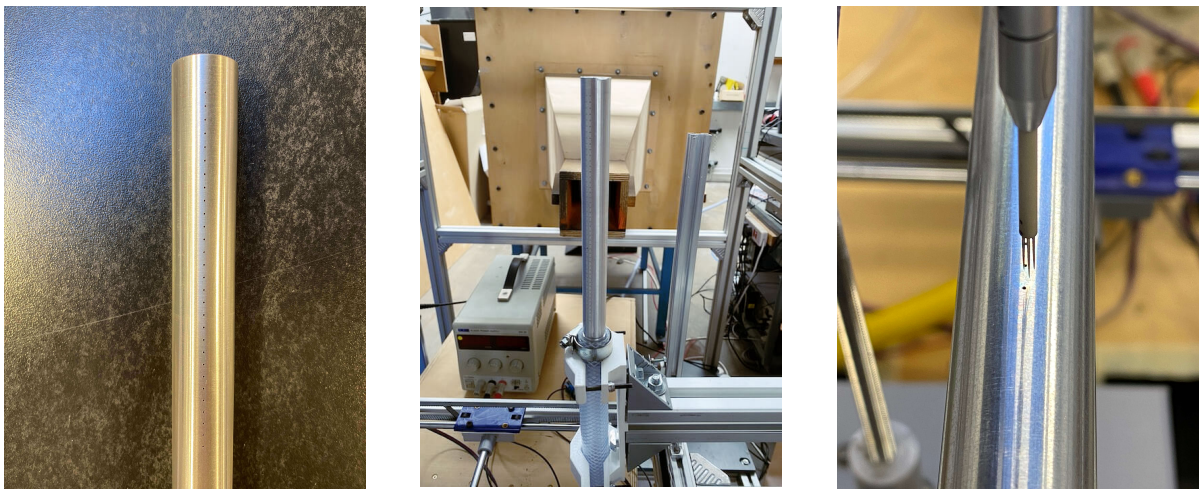

(a) Air Tube outlet holes (b) Air Tube with hose attached (c) Flow velocity measurement

Figure 4.7: Design philosophy prototype and analysis

The results of the experiment are presented with a visual representation in Figure 4.8. Clearly, the flow velocity reached a limit between 4 and 4.5 bar, with a plateau developing above 4.5 bar. Therefore, it was clear that the flow at the outlet was indeed choked, and importantly, this corresponded to a uniform flow velocity across the outlet holes. It is similarly important to note that the non choked condition corresponded to a variation in the outlet velocity between upstream and downstream holes, hence highlighting the importance of achieving choked flow.

While the variation in velocity between the upstream and downstream outlets is challenging to definitively explain due to the complexity of compressible flow, some basic explanation can be offered. The

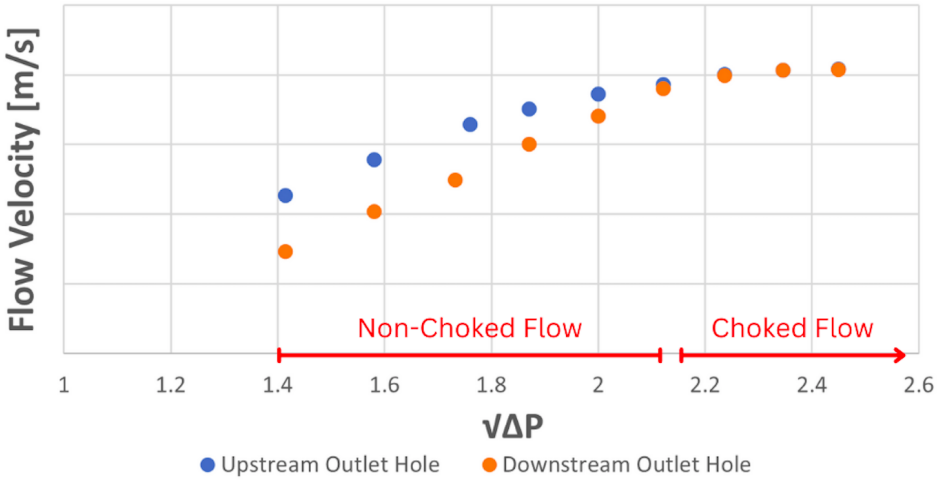

Figure 4.8: Flow velocity measurements at most upstream and most downstream outlet holes for a range of air pressures.

variation in outlet velocity is indicative of a pressure differential within the tube which corresponds to a pressure drop in the downstream direction. This is due to multiple reasons such as head losses at each outlet, which accumulate in the downstream direction. There is also a likely increase in turbulent flow downstream as effects of exiting air become more influential, and such an increase in turbulence significantly increases the head loss in the tube. Furthermore, pressure is lost along the length of the tube as air exits through the outlets, and this too is a cumulative effect in the downstream direction. For example, the problem can be simplified to the case of a diverging nozzle by treating the the cross sectional area, A, at any point as the sum of the tube internal cross sectional area, and the area of all outlet holes upstream of that point. Eulers equation, can be used to describe the pressure drop as a function of the gradient of cross sectional area, and is given by Equation 4.8.

$$\frac{\partial p}{\partial x} = -\rho v^2 \frac{\partial A}{\partial x} \tag{4.8}$$

When calculated, the values for $\frac{\partial p}{\partial x}$ are found to be rather small, however this basic analysis provides some insight and explanation for the flow behaviour observed at upstream and downstream holes when the air pressure was insufficient to achieve choked flow.

It was considered constructive to accept the pressure at which the velocity plateau begins as the minimum required air supply pressure to achieve choked flow. It was previously calculated that the critical upstream pressure would be 192kPa or 1.92 bar, however this velocity plateau only began to develop at a pressure of 4.5 bar, which indicated large pressure losses of 2.5 bar in the system. A large contributor to this pressure loss was likely the flow meter which was used, while a number of kinks and flow contractions were also present.

4.3.3 Acoustic Performance

Sound level tests were performed to assess the acoustic performance of the newly developed air tube with a view to comparing its performance against that of the air blade and reference nozzle. The

tests showed the air tube to exhibit superior performance, over both the reference and air blade. The air tube achieved noise reductions of 23dB from that of the reference nozzle, and 1.9dB from the air blade. However, it was noted that to the human ear, the air tube produced a harsher sound than that of the air blade. A frequency analysis was considered, however it was ultimately deemed unnecessary as the underlying goal of the research was focused on sound level rather than frequencies.

4.3.4 Flow deflection

The three nozzles were subjected to a crossflow of 28 ms^{-1} and a HWA was used to measure flow deflection accross a line of 20 points spaced 5mm apart and 120mm downstream of the nozzle outlet, as was performed in the initial analysis of the air blade. In each case, the nozzle was supplied with maximum flow rate from the available air supply at 6 bar pressure.

It was considered relevant to compare the Mass Flow and Flow Momentum of each nozzle as prior studies have drawn relations between jet flow momentum and cross flow deflection, and the results of this comparison are shown in Table 4.1. While the air tube outlet spacing was designed such that it would be consistent with that of the air blade, it was found that the actual mass flow rate, normalised to per meter of outlet length, was significantly lower at 0.21 $kgm^{-1}s^{-1}$ compared to 0.31 $kgm^{-1}s^{-1}$. The mass flow rate of the reference nozzle was highest at 0.67 $kgm^{-1}s^{-1}$, which is logical as it featured a significantly larger outlet area per unit length. However, the momentum of the reference nozzle was affected by the substantially lower outlet flow velocity, which was measured by the HWA as 73.88 ms^{-1} compared to a velocity of 200 ms^{-1} measured 5mm from the outlet of the Air Tube. While the flow was said to be choked in the Air Tube outlets, and hence the flow velocity would be expected to be 340 ms^{-1}, the actual flow velocity was in fact lower due to jet spreading in the 5mm between the outlet and measurement point. In addition, due to the small scale, boundary layer effects were expected to contribute to the reduction of actual outlet velocity, causing a sort of flow blockage, and hence the value of 200 ms^{-1} was conservatively utilised as the actual outlet velocity, and is consistent with the outlet choked flow velocity measurements taken previously in 4.3.2.

The results of this analysis are presented in Figure 4.9. Despite the lower momentum per unit outlet length, the air tube showed comparable performance with that of the air blade, which was far superior to that of the reference nozzle. Furthermore, consistent with previous findings, oblique blowing was shown to improve shielding ability.

Nozzle	Outlet Velocity [ms^{-1}]	Mass Flow [$kgm^{-1}s^{-1}$]	Momentum [kgs^{-2}]
Reference	73.88	0.667	49.254
Air Blade	200	0.3136	62.7232
Air Tube	200	0.2145	42.8916

Table 4.1: Mass flow and momentum, for all nozzles tested, normalised to per unit outlet.

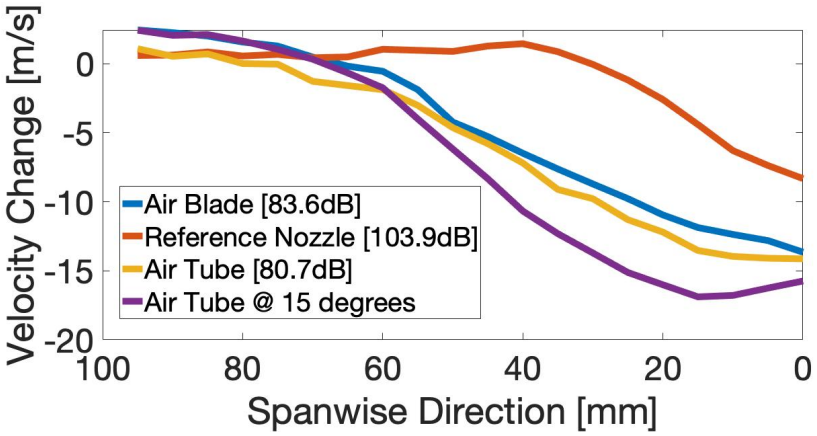

Figure 4.9: Flow deflection of 28 ms^{-1} cross flow, 120mm downstream of outlet

Version	Downstream Outlet Angle [α]	Upstream Outlet Angle [β]
1	15^o	30^o
2	30^o	45^o
3	45^o	60^o

Table 4.2: Oblique blowing optimisation test configurations

4.3.5 Further Optimisation

Oblique Blowing Angle

While the results presented above were highly encouraging, it was important to recognise that the flow deflection tests were performed for the rather low cross flow velocity of 28 ms^{-1} compared to the 60-65 ms^{-1} which would be tested in the final wind tunnel tests. Such higher velocities would likely see a significant reduction in shielding and hence further optimisation was sought.

As previously mentioned, a dual jet design produces superior shielding to that of a single jet. Therefore, a second row of holes was drilled, aligned with the original row and offset by 15^o with respect to the central axis of the tube. This setup was then subjected to a cross flow and the optimum oblique blowing angle was sought. Three different oblique blowing configurations were tested, and are described in Table 4.2, with an illustration of the geometric configuration shown in Figure 4.10.

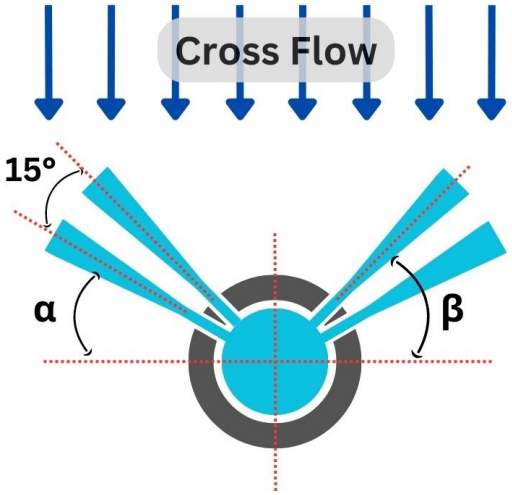

Figure 4.10: Dual jet geometric configuration

The results of this analysis revealed that the test configuration 3 produced the greatest shielding effect. Contour plots of the shielding of configurations 1 and 3 in a 2D plane downstream of the inlet are shown in Figure 4.11.

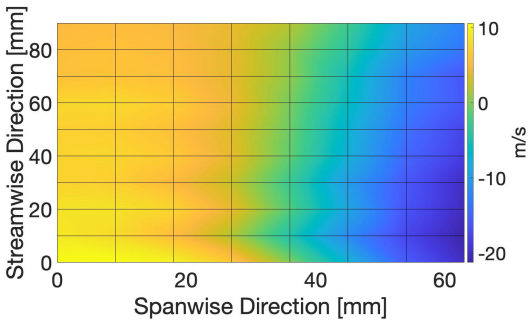

(a) Configuration 1.

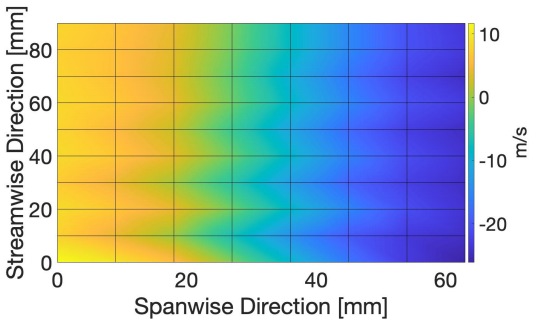

(b) Configuration 3.

Figure 4.11: Velocity change due to shielding in a 34 ms^{-1} cross flow.

Mass Flow Increase

While configuration 3 showed impressive shielding, there existed the possibility to utilise a higher volumetric flow rate if the particular dimensions of the air tube permitted. For example, for the prototype air tube with internal diameter 12mm and total outlet length of 190mm, Equation 4.7 would suggest a notable rise in volumetric flow rate could be exploited before issues would arise relating to choked flow. Therefore two further optimisations were prototyped and tested.

Firstly, while the literature suggests that reducing the distance between outlet holes may lead to higher audible noise levels, it is also suggested that this may only take effect when holes are placed within 2 diameters of each other. Therefore, with a view to increasing mass flow rate per unit length, an air tube was developed with hole spacing of 2.5mm rather than the originally chosen 3.5mm, as shown in Figure 4.12. The orientation of the rows of holes was unchanged. This air tube shall henceforth be referred to as the High Density Air Tube.

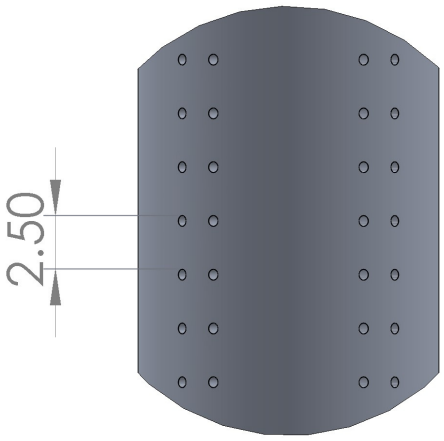

(a) High density air tube featuring 2.5mm hole spacing.

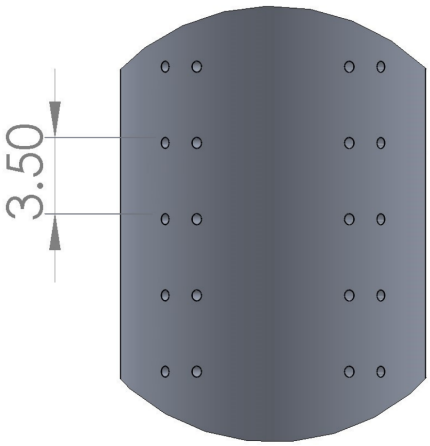

(b) Reference tube featuring 3.5mm hole spacing.

Figure 4.12: High density air tube and reference air tube compared.

In addition, the shielding improvement seen by the dual jet in Section 4.1 indicated that the additional jet improved shielding not only through increased mass flow rate, but also due to the dynamics of the shielding effect on the downstream jet. Therefore, another air tube, referred to as Triple Jet,

was developed with a third row of holes, positioned at an oblique blowing angle of 30°, and with the other two rows of holes positioned as in configuration 3. A hole spacing of 3.5mm was maintained. A comparison between the dual and triple jet configurations is shown in Figure 4.13.

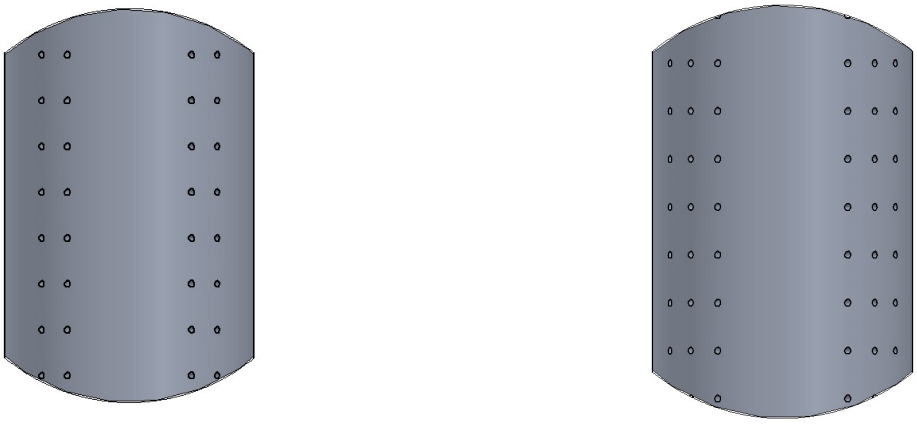

(a) Dual Jet

(b) Triple Jet

Figure 4.13: Air tube configuration variations with constant hole spacing of 3.5mm.

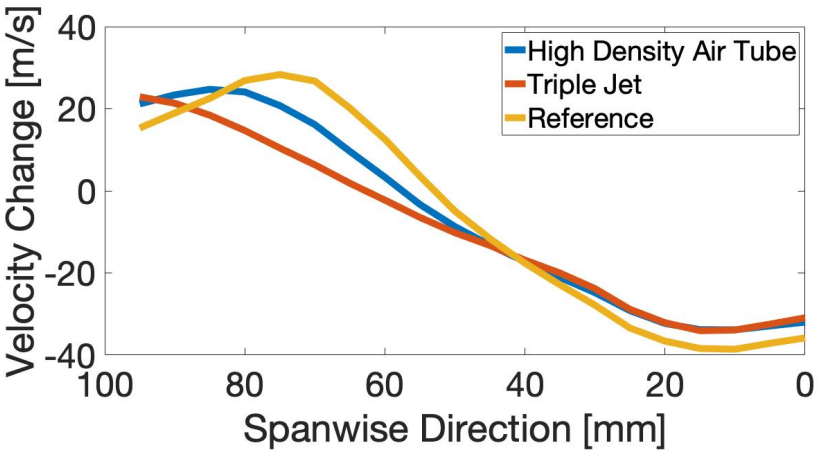

Figure 4.14: Comparison of flow deflection 120mm downstream of outlet in 38 ms^{-1} cross flow, for three Air Tube concepts

Figure 4.14 illustrates the velocity change 120mm downstream of the outlet for each of the air tube concepts. Clearly, the higher mass flow rate per unit length of the High Density Air Tube and Triple Jet has led to an increased shielding effect, while the increased jet shielding of the Triple Jet is likely the cause for its superiority compared to the High Density Air Tube. It is also worth noting that the High Density Air Tube features 40% more holes per 100mm outlet length than the reference, while the Triple Jet features 50% more, and this is also a likely cause for its superior shielding over the High Density Air Tube.

Acoustically, the High Density Air Tube showed no significant increase in noise production, with 77.6dB(A) recorded with a pressure of 5 bar, compared to 77.2dB(A) recorded for a comparable nozzle featuring the reference geometry. While a similar result was observed with the Triple Jet, it should be noted that the flow rate available in the Trinity College fluids lab was insufficient to achieve

choked flow due to the high mass flow rate requirement which was a result of the large number of holes. Therefore this test was somewhat inconclusive.

Internal Mesh Insert

While the aforementioned designs showed promising performance, further reductions in acoustic noise were still sought to maximise potential. While much of the sound energy was thought to be of high frequency, above the audible hearing range, the total acoustic noise at the nozzle outlet could still be reduced further by reduction of the outlet velocity. However this was challenging as the choked flow condition was critical in enabling the uniformity of outlet flow. Therefore, it was proposed to line the interior of the tube with a fine mesh such that the flow rate would be reduced, and a resulting reduction in outlet velocity was expected. While this concept was aimed at reducing acoustic noise, its effect on shielding was of primary concern.

A mesh lining consisting of layered fine mesh and a less fine mesh was constructed and inserted into the tube, as shown in Figure 4.15a. The fine mesh used was size 400 according to ASTM - E11, which features openings of size $37\mu m$. The larger mesh was a size 60 mesh with openings of size $250\mu m$ and was primarily intended to act as a supporting structure for the fine mesh. While every effort was made to prevent leakage of air around the mesh, a less uniform outlet flow was observed and this was attributed to air leakage around the ends and along the seam of the mesh.

(a) Mesh lining inserted into the inside of the air tube, consisting of a layer of very fine mesh and a supporting layer of mesh with larger apertures.

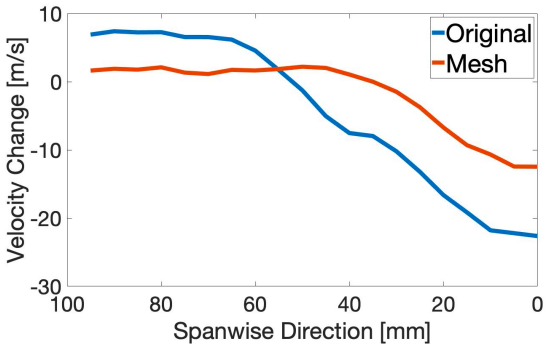

(b) Shielding achieved with and without mesh 120mm downstream of outlet.

Figure 4.15: Air tube mesh insert tests.

Despite the flow leakage, a 5dB reduction in sound level was observed due to the addition of the mesh. This also corresponded to a 49% reduction in volumetric flow rate, and so its effect on shielding was studied, consistent with previously mentioned cross flow deflection studies. The nozzle was subjected to a cross flow of $35ms^{-1}$ and shielding was measured 120mm downstream of the outlet. The results of this test are shown in Figure 4.15b, which clearly depict the significant decline in shielding when the mesh insert was used.

The conclusion was drawn that the negative effects of reduced shielding was too great to proceed with further development of this concept. However, future work could focus on experimentation with different mesh densities such that an optimum balance of noise reduction and shielding could be

achieved.

4.3.6 Tube End Treatment

It was noted that while the air tubes discussed above show considerable acoustic performance improvements over the previously designed single and dual jet 3D printed nozzles, the sound level tests were conducted in the absence of a cross flow. While the sound level delta between the two design philosophies was large enough to assume the Air Tube approach would retain its superiority when subjected to a cross flow, it was theorised that the 10-20mm region at the end of the tube where no outlet holes were drilled could act as a particularly noisy region. This region was necessary to facilitate the threads into which the the end stopper was screwed onto the tube, however it was assumed this region would act as a cylinder in a cross flow and hence lead to noisy vortex shedding.

Based on a range of tests with cross flow velocities ranging from 30-65ms^{-1}, and tube outer diameters ranging from 14-19mm, the range of Reynolds numbers expected was 30,000 - 88,000. This lies within the $300 < Re < 3.5x10^5$ range in which a fully turbulent vortex street is typically observed. Such a flow regime was expected to affect the acoustic efficiency of the nozzles, and hence the addition of an airfoil shaped end cap was investigated. A range of end cap designs were 3D printed, and their associated CAD drawings are shown in Figure 4.16. While it was not possible to directly measure the effect of the end cap on acoustic performance in the Trinity College Fluids Lab, the turbulence intensity in the wake of the Air Tube end was considered a suitable indicator of acoustic performance. Hence the goal was to reduce the turbulence intensity in the wake region.

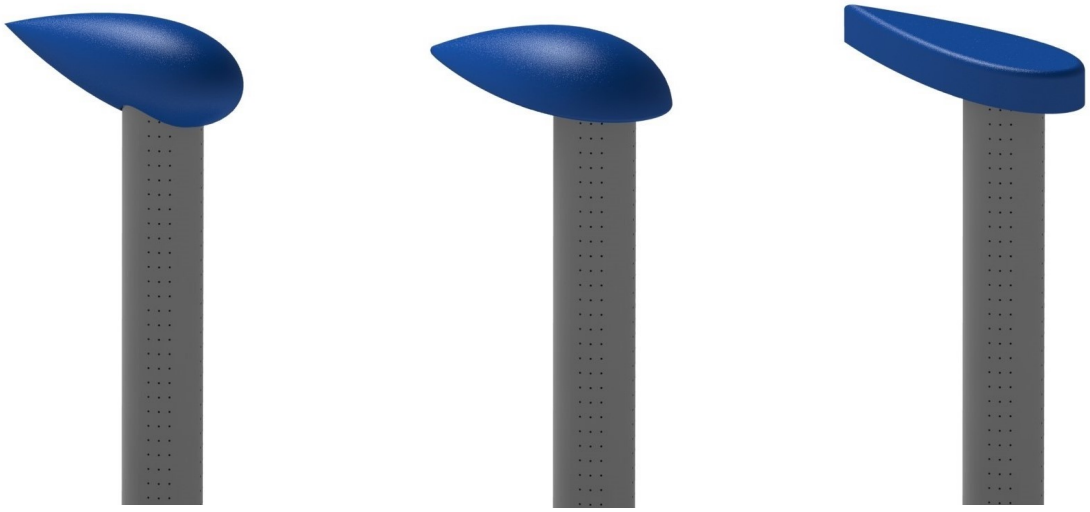

(a) Teardrop Cap 1 - NACA 0030 airfoil.

(b) Teardrop Cap 2 - NACA 0040 airfoil, flat bottom.

(c) Teardrop Cap 3 - NACA 0030 airfoil, flat top and bottom.

Figure 4.16: Various nozzle placement configurations.

Probe placement was considered highly relevant in the measurement of a turbulent wake. While the optimal downstream placement in the x direction has typically been found to be 2-5 diameters

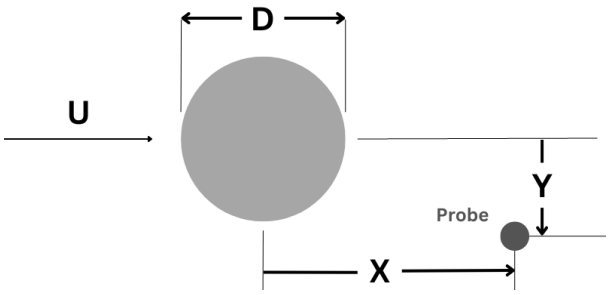

Figure 4.17: Probe placement for cylinder wake turbulence intensity tests.

downstream [61], the exact position for optimal measurement of vorticity is dependant on the Reynolds number of the specific flow. Therefore, some studies have used empirical data gathered from various points to determine an optimum position for downstream placement [62]. In addition, placement of the probe in the centre of the wake has been shown to give a poorer measure of vorticity than placement to the outside [63], such as 0.25-0.5 diameters in the y direction. Therefore optimal placement is estimated to lie within $(X/D, Y/D) = (2-5, 0.25-0.5)$, with X and Y defined according to Figure 4.17. Hence, a probe placement of $(X/D, Y/D) = (5, 0.25)$ was chosen in accordance with these findings. Further images of the testing procedure are available in Appendix A1.6.

As the goal of the end caps was to reduce noise of the tube ends during operation, each of the tests were conducted with the nozzle turned on and in a state of choked flow, with 5 bar of air pressure supplied. The air tube was placed in a cross flow of 50 ms^{-1} with a turbulence intensity of 12%. A reference test performed with no end cap provided validation for the presence of a highly turbulent wake downstream of the air tube end, with a turbulence intensity value of 40% recorded. Each of the end caps were found to reduce the turbulence intensity, with Cap 2 providing the greatest reduction of 53.9% to a value of 18% turbulence intensity. The full results of the analysis are provided in Table 4.3. Cap 1 features the smoothest profile with no edges, hence it was expected to produce the greatest results, however it in fact produced the poorest results. This was partly attributed to the poor quality of connection between the cap and the tube, as the flat surface of the other caps permitted a smoother connection to be achieved.

Test	Reference	Cap1	Cap2	Cap 3
Turbulence Intensity (%)	39.83	32.21	18.35	25.56
Reduction from Reference (%)	-	19.13	53.93	35.83

Table 4.3: End cap effect on wake turbulent intensity

5 Results

With a clear design philosophy established from the previous section, a series of air nozzles were designed and manufactured for integration in a scaled model of the Lagoon NLG. Such nozzles were tested with various configurations and experimental conditions in the AWB wind tunnel, the results of which will be discussed in detail in the following section.

5.1 Nozzle Designs and Configurations

Nozzles were designed in accordance with the findings of Section 4.3, with some variations relating to the outlet hole spacing and the number of rows of holes used. Such variations are described in Table 5.1, and were chosen with the intention of testing nozzles with varying deflection capabilities in the final test campaign. Note that the AT nozzle consisted of two rows of holes in the region that would shield the landing gear leg, and a third row in the region intended to shield the wheels to account for the extra span wise deflection required in this region. Images of the nozzles are shown in Figure 5.1, while further details are available in Appendix A2.1.

Nozzle	Hole Spacing [mm]	Number of Rows of Holes	Hole Angles [^{o}]
Air Tube (AT)	3.5	2 (3 in wheel region)	(30)-45-60
Local Low Density (LLD)	3.5	2	45-60
Local High Density (LHD)	2.5	2	45-60

Table 5.1: Final Nozzle Designs

Nozzle Integration

The AT nozzle was positioned in a consistent position upstream of the landing gear, as shown in Figure 5.3a and by the fuselage mounted vertical air curtain in Figure 2.5 in the Literature Review. Various configurations existed utilising the local nozzles (LLD and LHD) and were comparable with the landing gear mounted air curtains in Figure 2.5. Therefore, a variety of brackets were designed and manufactured which permitted the mounting of the local nozzles in various orientations on the landing gear. The brackets were designed to aid the ease of assembly in an attempt to minimise time spent re-configuring the setup between tests during the wind tunnel test campaign, which was expected to be time limiting. Furthermore, reducing the protrusion of the bracket into the cross flow was of primary interest during the design, as this would potentially lead to additional noise and aerodynamic drag. The upright bracket designed to shield the main leg, as shown in Figure 5.3b, was manufactured from aluminium, as its orientation in the cross flow was expected to lead to high

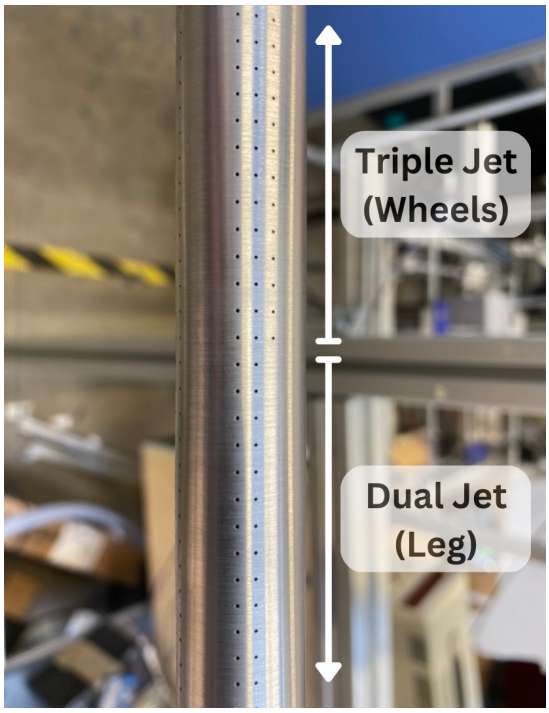

(a) Air tube with a combination of dual jet and triple jet outlet

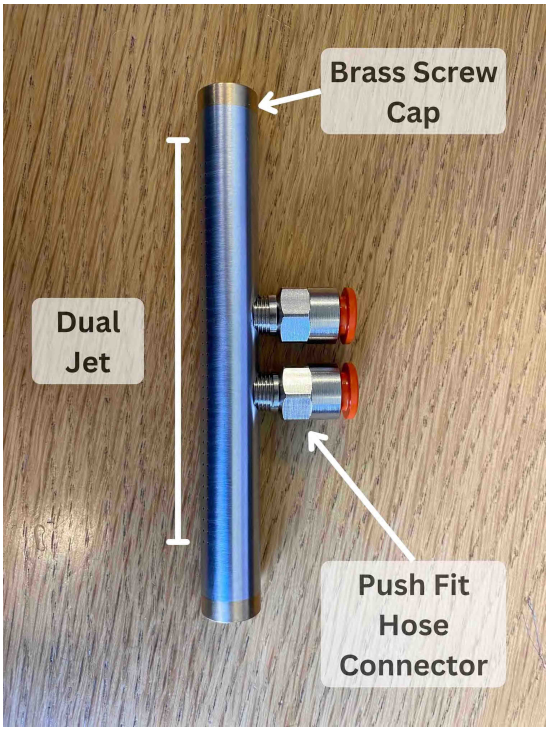

(b) Local nozzle featuring two push fit hose connections with tapered threads for an air tight seal.

Figure 5.1: The final manufactured air tube and local nozzle.

bending stresses from the aerodynamic loads. It was attached directly to the bay via a series of bolts. The bracket designed to shield the wheel region, as shown in Figure 5.3c, was 3D printed using ABS plastic with 100% infill, as it featured more complex geometry which would be difficult to manufacture from steel or aluminium. The wheel bracket was screwed into existing threaded holes on the landing gear. Both configurations could be utilised simultaneously, as shown in Figure 5.3d. CAD drawings of the brackets are shown in Figure 5.2, while images of the brackets are available in Appendix A2.1.2.

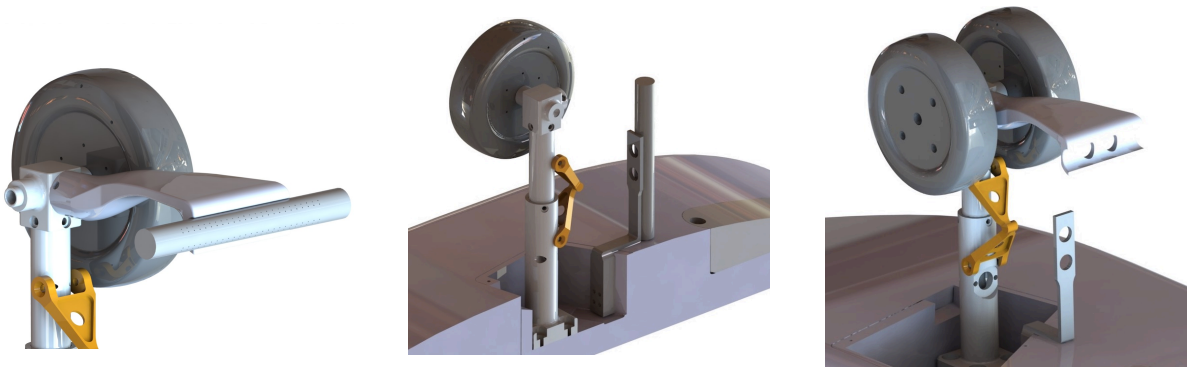

Figure 5.2: Local nozzle brackets.

Furthermore, the industrially available Air Blade which was discussed in Section 4.2 was integrated into the landing gear base such that it could be tested in the final test campaign. The landing gear bay was 3D printed with a cavity into which the Air Blade could be inserted such that it could act as a fuselage mounted horizontal air curtain as described by Figure 2.5 in the Literature Review

section. The Air Blade was integrated at an angle of 30° to the vertical, in the upstream direction, in order to avail of the increased deflection performance of oblique blowing, as previously discussed. Its integration is shown in Figure 5.3e and could also be combined with the use of the local nozzles in the wheel region as shown in Figure 5.3f. Further images of the integration in the 3D printed bay are shown in Appendix A2.1.3.

(a) AT nozzle configuration

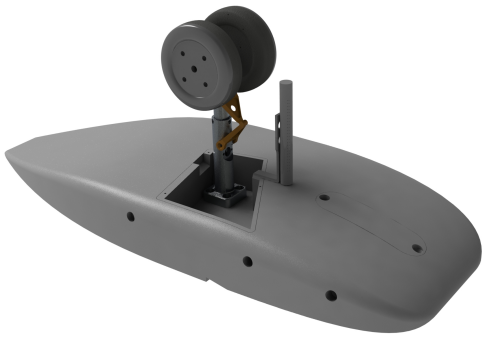

(b) Local nozzle main leg (ML) placement

(c) Local nozzle (LLD or LHD) Wheel placement.

(d) Local nozzles with wheel and leg (Wheel & ML) placement

(e) AB integrated into landing gear base

(f) AB with local wheel nozzle (AB & Wheel)

Figure 5.3: Various nozzle placement configurations and their associated abbreviations.

5.2 AWB Wind Tunnel Tests

5.2.1 Smoke Test

While acoustic performance was the main result of interest, a smoke generator and probe were used to achieve a flow visualisation in the initial stages of the wind tunnel test campaign. The purpose of this test was to establish if the air curtain was sufficiently deflecting cross flow around the landing gear. The AT and AB nozzles were used for this test, with air pressures of 2 and 7 bar respectively, in a $30ms^{-1}$ cross flow. The smoke probe was positioned at various points upstream of the nozzles and the smoke trail was observed.

While the white smoke was difficult to visualise on the background, it offered an insight into the level of flow deflection achieved. Figure 5.4a shows a significant degree of flow deflection around the upper half of the AT, which features three rows of outlet holes to maximise flow deflection around the wheels. While some vortices were observed over the top of the air curtain, the general consensus was that the nozzle was functioning as intended and a sufficient level of shielding was achieved at this cross flow velocity and nozzle air pressure. Figure 5.4b shows a good level of deflection was also achieved with the AB for the given conditions.

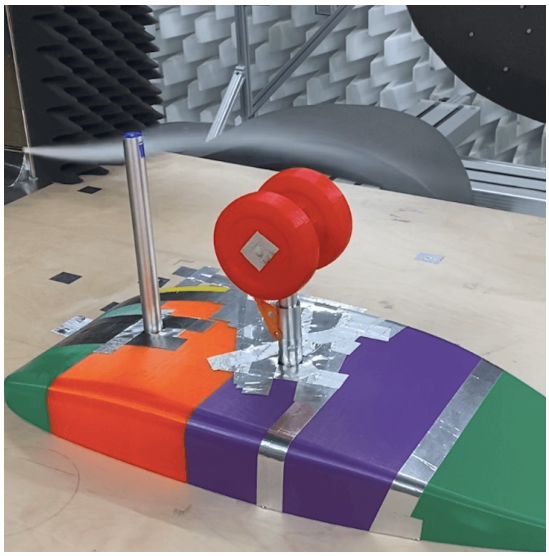

(a) AT with 2 bar pressure.

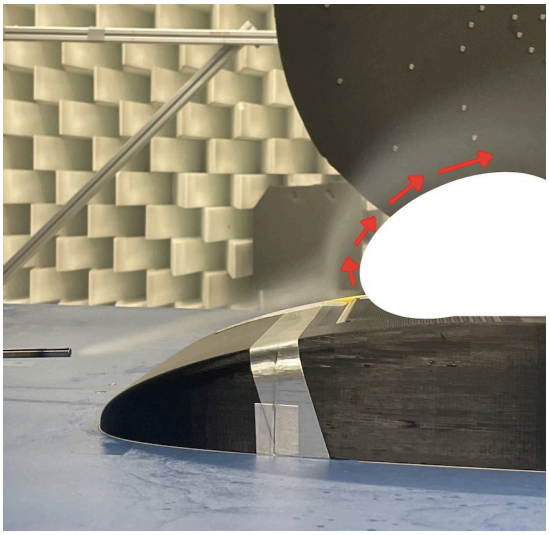

(b) AB with 7 bar pressure.

Figure 5.4: Smoke tests with $30ms^{-1}$ cross flow.

5.2.2 Tube End Caps

As discussed in 4.3.6, the presence of turbulent vortex shedding in the wake of the tube ends was a likely source of noise when the tube end, which features a small section with no outlet holes, was exposed to a cross flow. Therefore, prior to execution of a full test matrix, the developed end caps were tested in the AWB wind tunnel in order to assess their ability to reduce such noise. Hence the lowest noise configuration could be used for the remaining tests.

For the purpose of this simple assessment, the LHD nozzle in the wheel configuration on the Lagoon landing gear was tested with and without the use of end caps. The microphone arrays recorded

acoustic performance with cross flow velocities of 30, 45 and 63 ms^{-1} respectively, with a mass flow rate of 31.6 gs^{-1} from the LHD nozzle.

With 30 ms^{-1} cross flow, reduction in various peaks in the acoustic spectrum were observed, particularly at M5 and M6, as shown in Figure 5.5. Overall dB(A) sound level reductions were observed at all microphones ranging from 0.15dB(A) to 0.26dB(A). This represents a rather insignificant sound level reduction, and tests performed at higher cross flow velocities showed no reduction in sound levels due to the use of the end caps, however no increases were observed. Due to the slight improvements seen at 30 ms^{-1}, and the lack of adverse effects, it was decided to adopt the end caps for the remaining analysis.

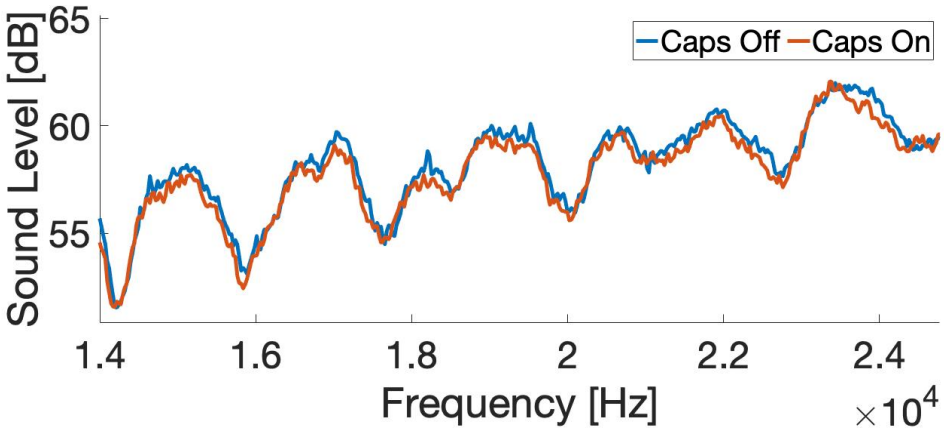

Figure 5.5: M5 frequency spectrum for cap test at 30 ms^{-1} cross flow

5.2.3 Test Matrix

Due to equipment constraints in the DLR, it was not possible to perform a wide range of tests while varying nozzle air pressures. Therefore, the testing was primarily performed in two segments, one with a low pressure air supply of 2 bar, and another with a high pressure air supply of 7 bar. While various landing gear nozzle configurations were tested, the bay cavity configuration was also varied between open, as in the drawings in Figure 5.3, and closed with aluminium foil tape, as in Figure 5.4a. The test matrix is shown in Table 5.2. Each test was performed with cross flow velocities ranging from 0 ms^{-1} to 63 ms^{-1}, which will be described in the following sections.

5.2.4 Nozzle Performance Comparison

While frequency spectra, sound level and beam forming results were generated for all tests, the data will be presented in a manner which allows for clear and simple comparisons. Therefore, the data from tests 3, 4, 5 and 6 will first be analysed. These tests represent a closed cavity with nozzle air pressure of 7 bar. 1/3 octave bands measured at the M6 location from the 30 ms^{-1}, 45 ms^{-1} and 63 ms^{-1} cross flow conditions are presented in Figures 5.6, 5.7 and 5.8 respectively.

It is clear from these results that the self noise of the nozzles was dominant over the aerodynamic noise of the landing gear across the full frequency spectrum at the lowest cross flow velocity of 30 ms^{-1}, due to the minimal noise of the landing gear. Noise reductions were observed with the AT at

Test	Configuration	Mass Flow [gs^{-1}]	Cavity	Pressure [bar]
1	Ref	-	Open	-
2	Ref	-	Closed	-
3	AT	47.5	Closed	7
4	AB	21.6	Closed	7
5	LHD Wheel	31.2	Closed	7
6	LHD Wheel & AB	44.3	Closed	7
7	AT	28.2	Closed	2
8	LLD ML	29	Closed	7
9	LHD ML	33	Closed	7
10	LHD Wheel, LLD ML	48	Closed	7
11	AB	21.6	Open	7
12	AB	Variable	Open	Variable
13	AB, LHD Wheel	Variable	Open	Variable

Table 5.2: Test matrix for AWB wind tunnel tests

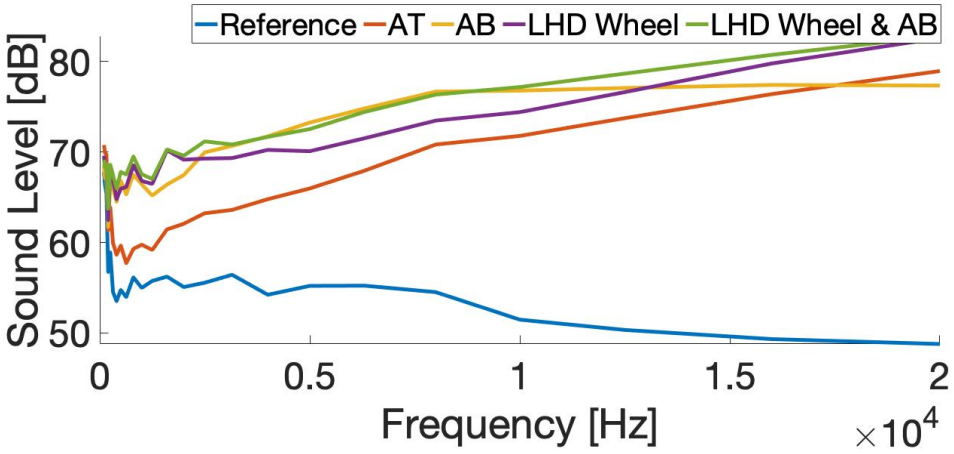

Figure 5.6: 1/3 octave bands for 30 ms^{-1} cross flow with closed cavity and 7 bar nozzle air pressure.

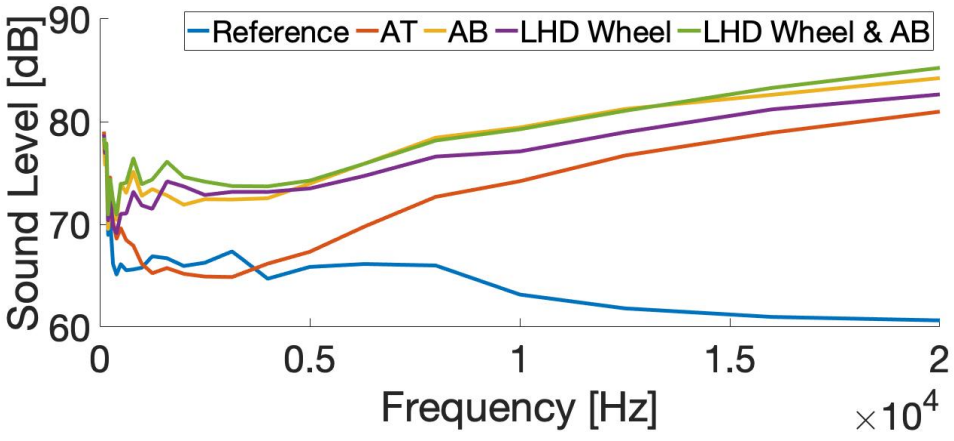

Figure 5.7: 1/3 octave bands for 45 ms^{-1} cross flow with closed cavity and 7 bar nozzle air pressure.

higher cross flow velocities, with the greatest reduction observed at the highest cross flow velocity of 63 ms^{-1}. At this condition, the AT configuration showed meaningful reductions in the 1/3 octave

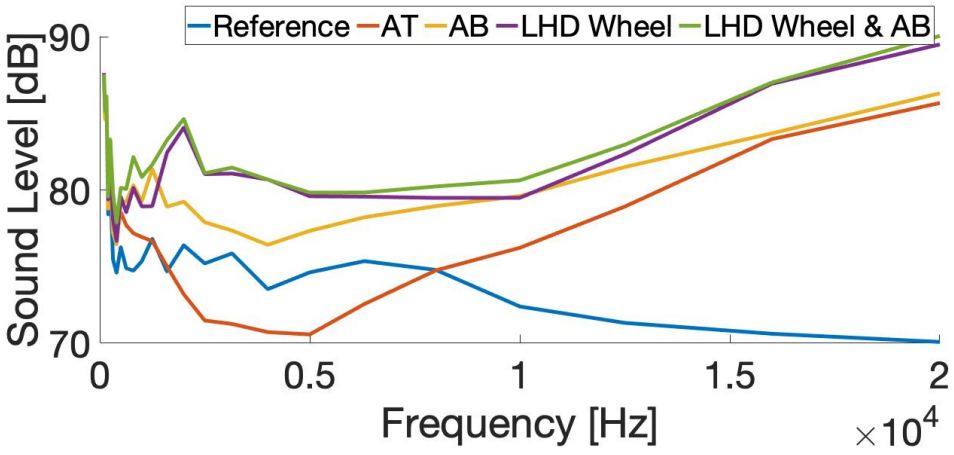

Figure 5.8: 1/3 octave bands for 63 ms^{-1} cross flow with closed cavity and 7 bar nozzle air pressure.

bands within the 1kHz to 8kHz range at all microphone locations. This is also evident in the narrow band, as shown by the reduction in sound level from the reference at the M5 location in Figure 5.9. It is important to note however, that this noise reduction was coupled with increases in noise levels above 10kHz. The other nozzle configurations showed no noise reduction effect, and led to an increase in the sound levels in all octave bands.

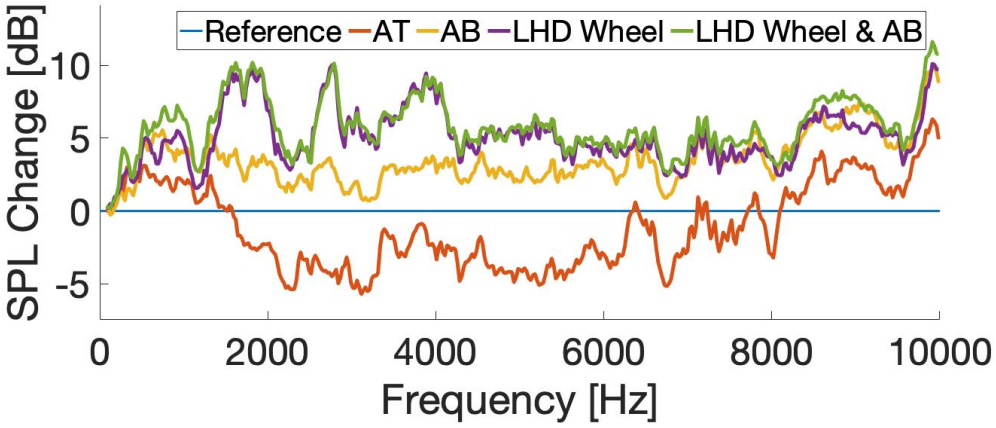

Figure 5.9: Noise reduction in the narrow band from 0Hz to 10kHz at the M5 location for 63 ms^{-1} cross flow velocity.

5.2.5 Air Tube

Beam forming results of the AT test with 63 ms^{-1} cross flow show large sound level reductions up to 10kHz, with a maximum reduction of 12 dB observed from the horizontal array at 5kHz. Beam forming permitted the visualisation of the noise source and hence the cause of the acoustic changes was studied. A redistribution of the noise source was evident, with the landing gear generating lower levels of noise at all frequencies. Below 10kHz, while the AT did contribute to noise levels, overall noise levels were reduced. Above 10kHz, the AT became the dominant source of noise and was responsible for an increase in overall levels. This analysis is shown for various frequency bands with a side view of the landing gear using the vertical microphone array in Figures 5.10 & 5.11, while results from a top view of the landing gear using the horizontal microphone array are shown in Figures 5.12

& 5.13.

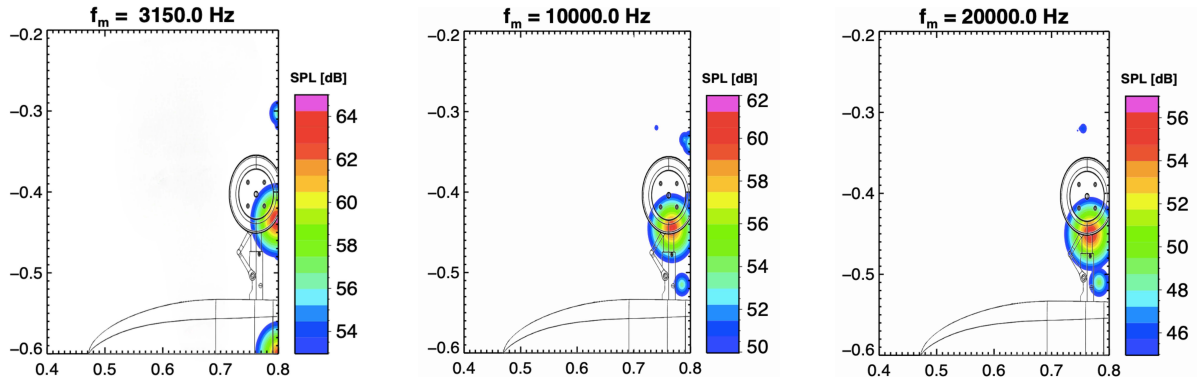

Figure 5.10: Reference landing gear configuration beam forming results for vertical array with 63 ms^{-1} cross flow.

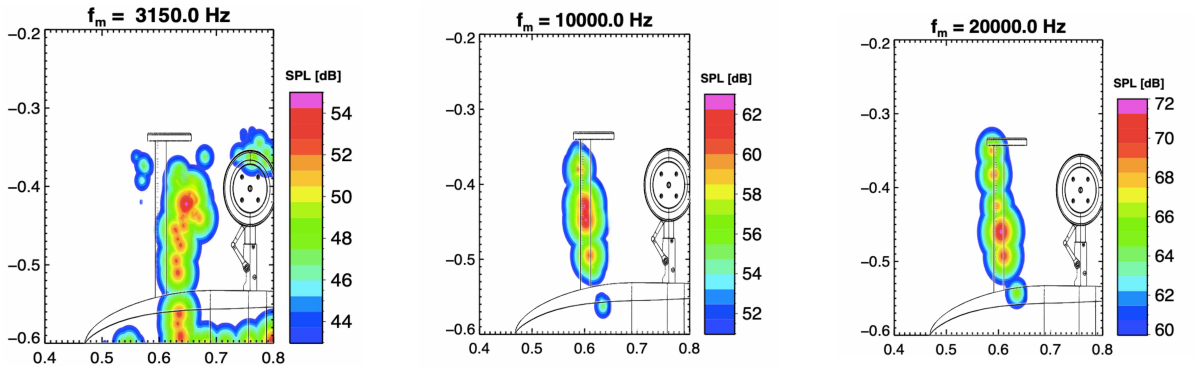

Figure 5.11: AT landing gear configuration beam forming results for vertical array with 63 ms^{-1} cross flow.

Further analysis of the AT configuration was performed in which the nozzle pressure was varied. This corresponded to tests 3 and 7 from the test matrix outlined in Table 5.2. The AT was supplied with pressures of 2 bar and 7 bar, and was subjected to cross flows of 30 ms^{-1} and 63 ms^{-1}. The change in the 1/3 octave bands from the reference tests are shown in Figure 5.14. As previously mentioned, the nozzle supplied with 7 bar did not achieve noise reductions in 30 ms^{-1} cross flow due to the high self noise of the nozzle. Interestingly, the AT achieved noise reductions at this cross flow velocity when supplied with 2 bar, as shown in Figure 5.14a. However, with 63 ms^{-1} cross flow, a far more significant the noise reduction was achieved with 7 bar pressure. Figure 5.15 provides insight into this, as the horizontal array beam forming results indicate that at the 5kHz frequency, adequate shielding was not achieved by the AT pressurised at 2 bar. Therefore, the dominant noise source in the system was aerodynamic noise of the landing gear, as indicated by 5.15a. When supplied with 7 bar pressure, adequate shielding was achieved such that the landing gear was not a dominant source of noise but rather the nozzle, albeit at lower levels as shown by the scale in 5.15b.

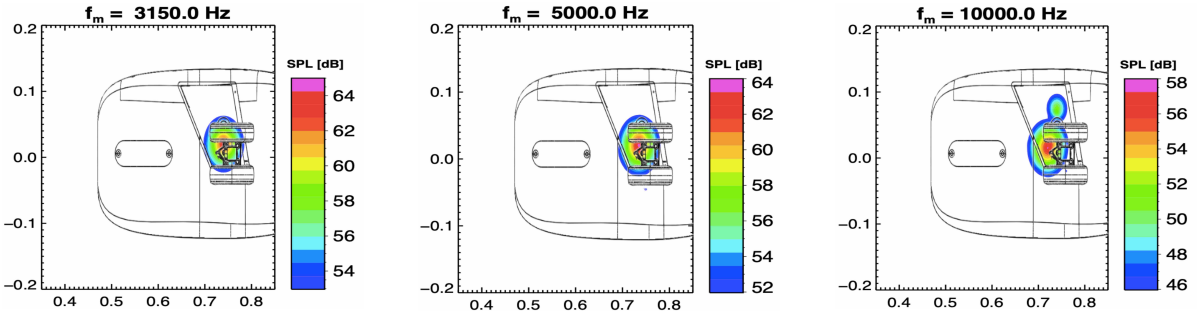

Figure 5.12: Reference landing gear configuration beam forming results for horizontal array with 63 ms^{-1} cross flow.

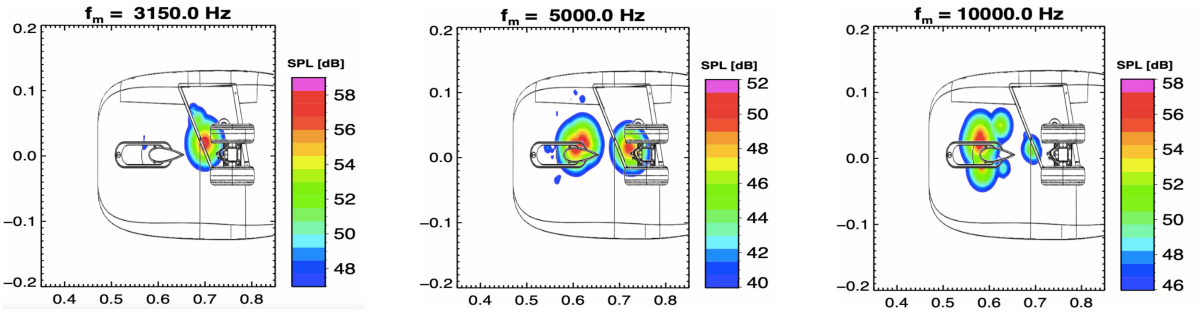

Figure 5.13: AT landing gear configuration beam forming results for horizontal array with 63 ms^{-1} cross flow.

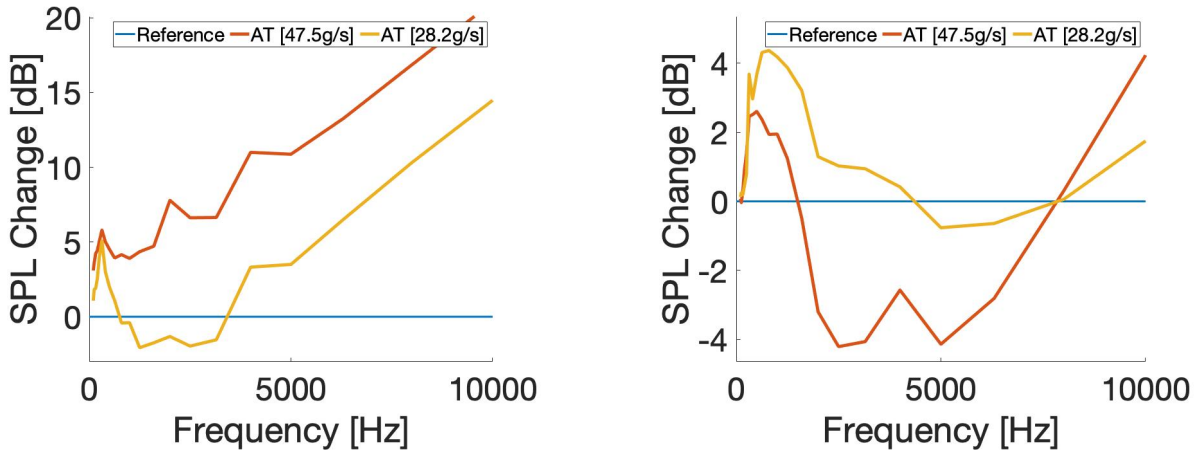

(a) 30 ms^{-1} cross flow.

(b) 63 ms^{-1} cross flow.

Figure 5.14: 1/3 octave bands at M5 for AT with varying nozzle pressures and cross flow velocities.

5.2.6 Local Nozzles

Tests were conducted with the local nozzles, LHD and LLD, in various configurations. Initially, a test was conducted to assess the impact of the geometry variation of the two nozzles. For this test the nozzles were individually tested in the LLD ML and LHD ML configurations, with no cross flow and 7 bar air pressure, as described by tests 8 and 9 in the test matrix. The results of this analysis are presented in Figure 5.16, with Figure 5.16a displaying the narrow band frequency spectra at the

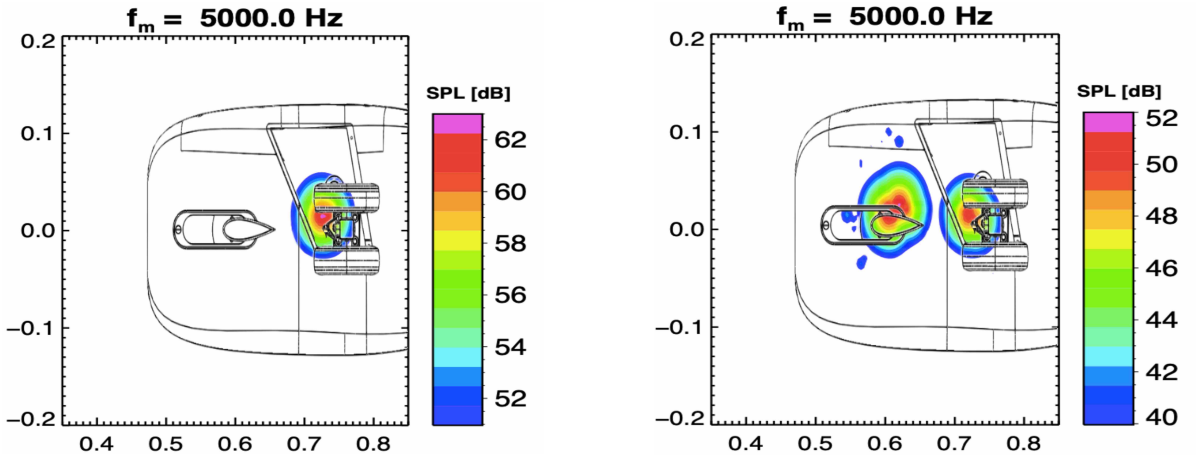

(a) 2 bar.

(b) 7 bar.

Figure 5.15: AT landing gear configuration beam forming results for horizontal array with 63 ms^{-1} cross flow.

M7 location, and Figure 5.16b illustrating the difference between the two frequency spectra. While a detailed analysis will be presented in the Discussion section, it is clear that the LHD nozzle produced more low frequency noise while producing similar levels of high frequency noise.

Furthermore, the noise reduction potential was tested for the various configurations corresponding to tests 8, 9 and 10 from the test matrix. Such tests showed noise increases with the use of all configurations, with the least amount of extra noise added for the 63 ms^{-1} cross flow condition. The 1/3 octave bands for this test are shown in Figure 5.17.

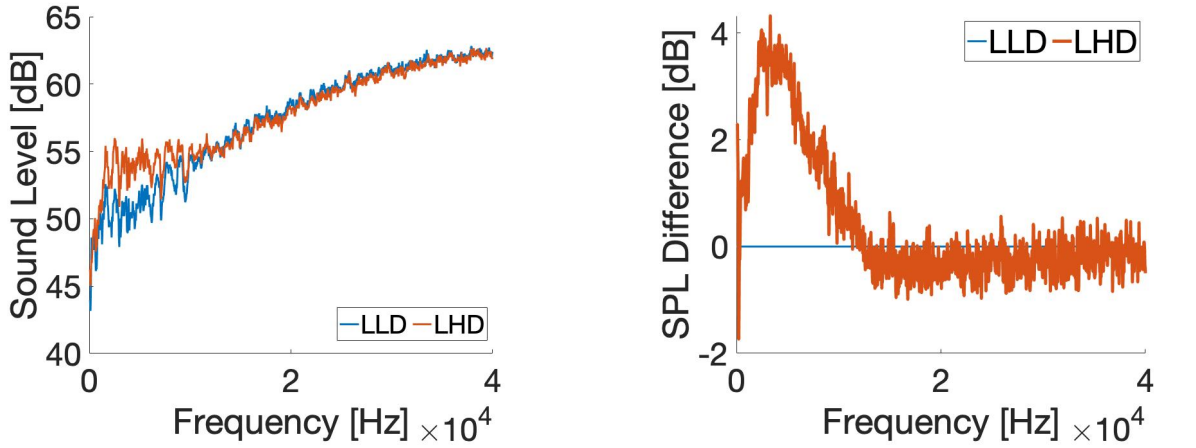

(a) Narrow band frequency spectra for LLD and LHD in the absence of cross flow.

(b) Change in SPL between LLD and LHD with no cross flow.

Figure 5.16: Acoustic performance of LLD versus LHD nozzles at M7.

However, beamforming results indicated that sufficient shielding could be achieved such that the noise source at the landing gear leg was suppressed. This is illustrated in Figure 5.18. In this test, 2 bar pressure was supplied to the nozzles, resulting in a total mass flow rate of 20 gs^{-1}, and the landing gear was subjected to a 30 ms^{-1} cross flow. It is evident from these results that the 41dB noise source on the leg in the reference test was successfully suppressed. The total noise did increase

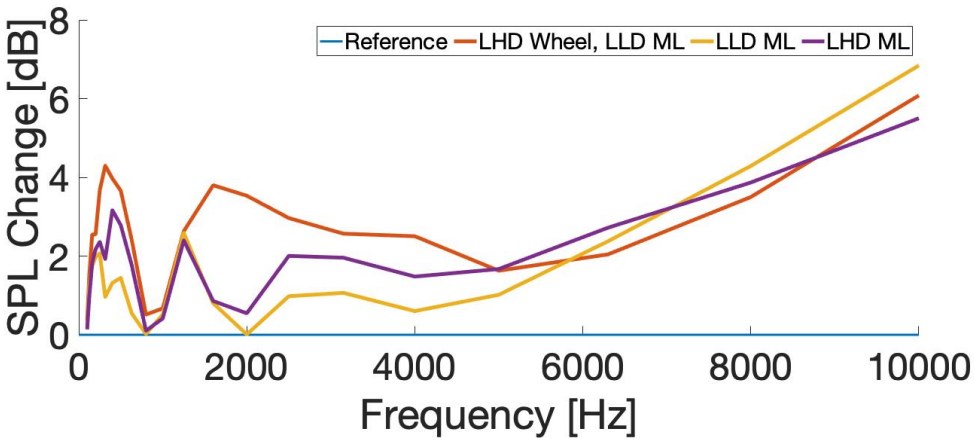

Figure 5.17: Acoustic performance of local nozzle configurations in 63 ms^{-1} cross flow

with the addition of the nozzles, however this was due to the self noise of the nozzles which was greater than that of the landing gear aerodynamic noise.

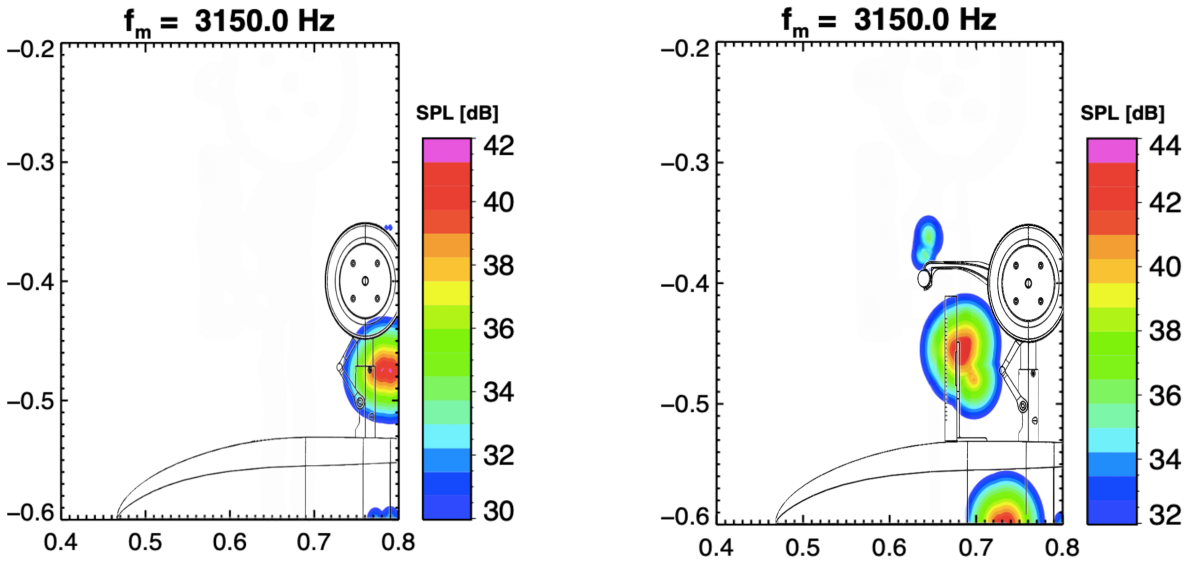

(a) Reference.

(b) LHD Wheel & LLD ML.

Figure 5.18: Beamforming results in the 3150Hz frequency band for LHD Wheel & LLD ML with 30 ms^{-1} cross flow.

5.2.7 Air Blade

While the AB showed little potential for sound reduction in the tests discussed above, such tests involved closure of the bay cavity with aluminium foil tape. Test 11 in the test matrix investigated the impact of the AB on noise levels with and without cavity closure. Figure 5.19 illustrates the impact of the AB on noise levels with each of the two bay cavity configurations. The AB showed greater potential for noise reduction with the open cavity configuration, and achieved reductions at multiple frequencies.

Further analysis of this observation using beam forming suggest the AB was successful in suppressing

cavity noise rather than landing gear noise, at some frequencies. Figure 5.20 illustrates this effect at 8kHz. In the reference test, a noise source existed on the lower right corner of the illustration, which corresponded to the location of the bay cavity. When the AB was installed, this noise source was no longer present.

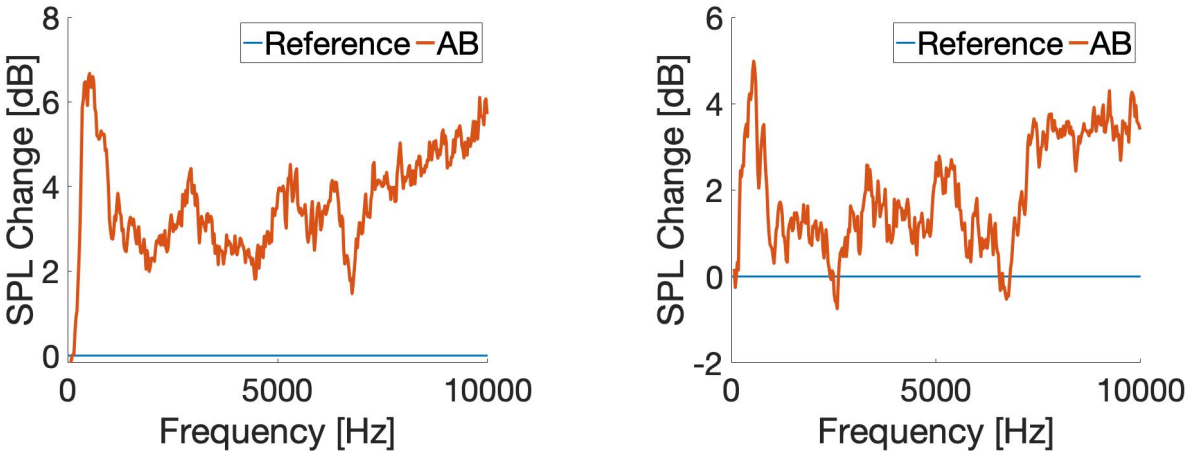

(a) Cavity closed

(b) Cavity open.

Figure 5.19: Narrow band frequency spectra reduction at M2 for AB with cavity closed and cavity open with 63 ms^{-1} cross flow.

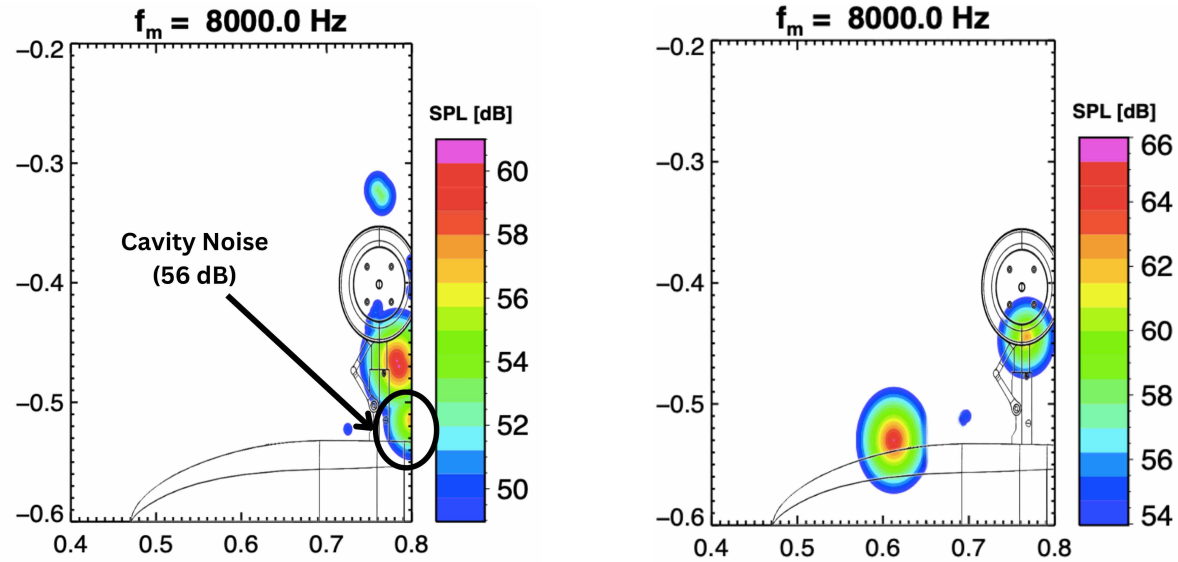

(a) Reference

(b) AB with 21.6gs^{-1} flow rate.

Figure 5.20: 63 ms^{-1} cross flow with cavity open

5.2.8 Mass Flow Rate Influence

As mentioned previously, the deflection of cross flow using a planar jet of air is proportional to the momentum of the planar jet. Therefore, greater mass flow is believed to be advantageous in achieving improved shielding. As the outlet flow was choked for all nozzles, the only method by which mass flow could be increased was by increasing the upstream air pressure, and hence the air density. However, it was theorised that such increases in mass flow rate would present an acoustic penalty, as the self

noise of the nozzle would be increased. While it was not possible to test these influences throughout the test campaign due to equipment limitations, a small scale study was performed to asses the relationship between mass flow rate, shielding and nozzle self noise.

The AB configuration was tested in the absence of cross flow, and with cross flow of 30, 45 and 63 ms^{-1}. Acoustic measurements were taken at each cross flow condition, with nozzle air pressures of 3, 4 and 5 bar corresponding to mass flow rates of 11, 14 and 17.4 gs^{-1} respectively. What was clearly evident was the increase in self noise with higher mass flow rates, as shown in Figure 5.21a, where no cross flow was present. A similar phenomenon was observed in the presence of cross flow, with Figure 5.21b illustrating the sound level increase at the M7 microphone for a cross flow of 30 ms^{-1}. This sound level increase was observed for all three of the tested cross flow conditions for the AB configuration.

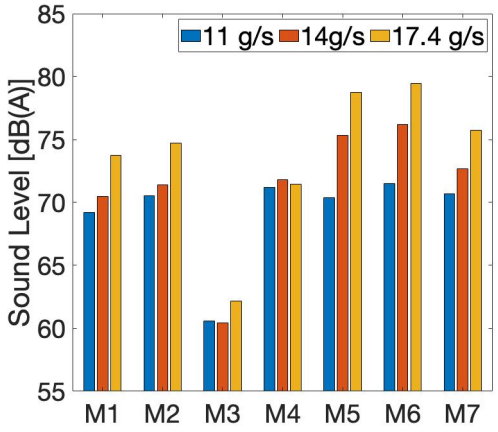

(a) Self noise of AB recorded at each microphone location with varying mass flow rate.

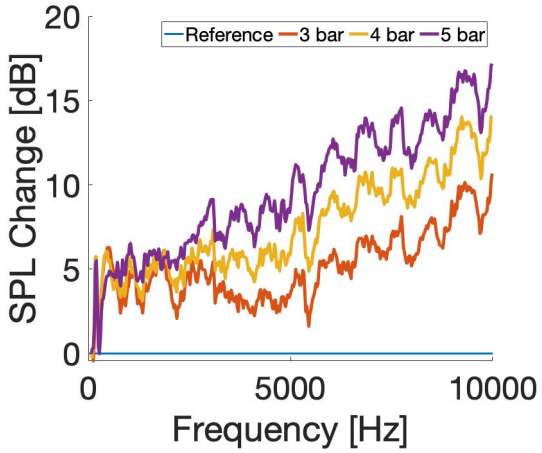

(b) Frequency spectrum at M7 with varying nozzle pressures and 30 ms^{-1} cross flow.

Figure 5.21: Impact of nozzle pressure on sound levels.

While this test showed negative effects associated with increasing pressure, the AB showed little potential for noise reduction in the general tests and so further analysis of mass flow variations with other configurations was considered appropriate. Therefore, the LHD Wheel configuration was added to the system, such that the AB & LHD Wheel configuration was used. For this test, nozzle air pressures of 2.7, 3.8 and 6.9 bar were used, yielding mass flow rates of 22.3, 28.7 and 44.4 gs^{-1} respectively.

Consistent with the previous test, in the absence of cross flow, increases in mass flow rate corresponded to increases in self noise levels, as shown in Figure 5.22a. When subjected to a cross flow of 63 ms^{-1}, higher sound levels were recorded for all microphones compared to the reference, again highlighting the failure of this configuration to effectively reduce noise levels. However, as shown in Figure 5.22b, reductions in sound levels were observed across all microphones when the flow rate was increased from 22.3gs^{-1} to 28.7 gs^{-1}. This would suggest greater shielding was achieved which yielded acoustic performance gains that dominated over the associated increase in self noise. Furthermore, with the exception of the M2 microphone location, further increasing the mass flow rate to 44.4 gs^{-1} resulted in an increase in the sound levels. Suggesting increases in self noise dominated over corresponding

noise reductions due to the increased shielding effect at this higher flow rate.

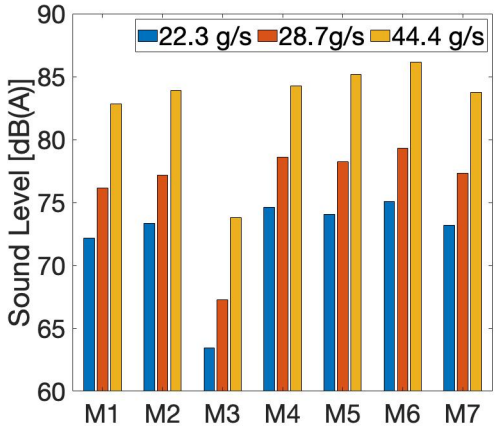

(a) Sound levels with varying mass flow rate and no cross flow.

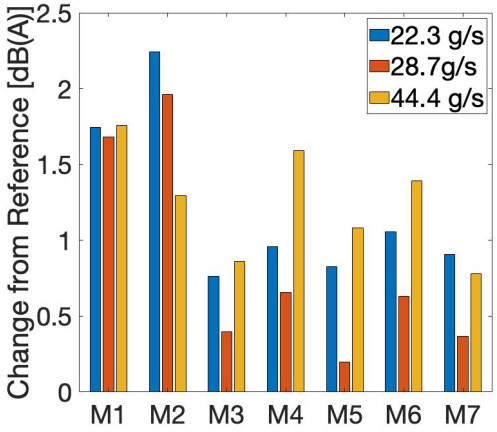

(b) Sound level change with respect to the reference in a 63 ms^{-1} cross flow.

Figure 5.22: Impact of nozzle pressure on sound levels for AB & LHD Wheel configuration.

6 Discussion

Summary of Results

The results show that aerodynamic noise reduction of the Lagoon NLG was achieved in some frequency ranges through the implementation of air curtains. Such noise reductions were highly sensitive to nozzle design, cross flow velocities, and the mass flow rate supplied to the nozzle. The AT nozzle was the most effective nozzle for noise reduction, by a substantial margin, achieving meaningful noise reductions in the 1-8kHz range in 63 ms^{-1} cross flow. Beamforming results presented in Figures 5.10 & 5.11 indicate it successfully shielded the landing gear from high velocity cross flow, and achieved up to a 12 dB reduction for the 5kHz frequency band, based on the results from the horizontal microphone array. Further reductions were achieved throughout the 1-10kHz frequency range. At frequencies above 10kHz, as was the case with all nozzles, the self noise of the nozzle dominated over that of the landing gear, and hence led to an increase in noise levels in this range. The LLD and LHD local nozzles showed little potential for noise reduction, with all tested configurations leading to increases in noise levels for the full frequency range. Comparison of the self noise of the LLD and LHD nozzles revealed the LHD nozzle produced more low frequency noise. The AB also showed poor noise reduction performance, however closer analysis revealed its reduction of landing gear bay cavity noise in the tests conducted with the bay cavity open. Finally, the impact of nozzle pressure on noise was analysed and found to be consistent with the literature. Increases in pressure increased the mass flow rate and led to increases in nozzle self noise. However, in some cross flow conditions, increases in mass flow rate led to net noise reductions, due to the corresponding increase in shielding.

Air Tube

In line with the underlying hypothesis of the air curtain proposal, the working principle of air curtain noise reduction has been validated, primarily through the tests conducted with the AT configuration. That is that the air curtain deflected cross flow around the landing gear, as shown by the smoke tests, and that this deflection led to a reduction in noise levels, as shown by the beamforming results of the AT tests. While previous studies have examined the suppression of tonal noise using air curtains, this is the first successful validation of the hypothesis when applied to a landing gear scale model, and hence this is a significant finding. While increases in high frequency noise were substantial, high frequency noise is known to experience greater attenuation in the atmosphere than low frequency, and therefore it is possible that the AT configuration would yield reductions in overall perceived noise levels if implemented in a flight test or if the appropriate corrections for atmospheric attenuation were applied.

Local Nozzles

Beamforming results indicate that the local nozzles were capable of achieving sufficient shielding such that the noise source at the landing gear was suppressed. Therefore, their lack of noise reduction can be attributed to the self noise of the nozzles. The LLD nozzle featured the same hole spacing as the AT, while the LHD nozzle featured denser hole spacing. Consistent with the literature which discusses the impact of micro nozzle hole spacing on acoustics, the denser hole spacing of the LHD nozzle produced more low frequency noise, and hence showed poorer performance. The extent of this effect was somewhat surprising, as the literature suggested the effects of increasing hole spacing would be negligible for hole spacing greater than 2-3 diameters. The LLD nozzle featured 7 hole diameters between hole centres, while the LHD featured 5. The notable reduction in acoustic performance was not expected, and highlights the sensitivity of nozzle self noise to geometry. Regardless of the increased noise of the LHD nozzle, even the self noise of the LLD nozzle was higher than required to achieve a noise reduction. Therefore, the nozzle connection design was likely also a cause of excess noise production. While the AT consisted of a simple tube which connected directly to the air supply pipe, the local nozzles featured two push to fit hose connectors in addition to a Y tube connector downstream which split the 3/4" air supply hose into two 8mm tubes. This increased complexity likely led to more turbulence within the internal components of the nozzle and hence more self noise.

Air Blade

The AB showed a good level of deflection in the smoke test, and this deflection was responsible for the suppression of bay cavity noise, However, the deflection was not sufficient to shield the whole landing gear and the beamforming results showed it did not succeed in suppressing the noise source on the landing gear. While a higher flow rate and an improved nozzle design could almost certainly achieve sufficient shielding, this bay integrated configuration is unlikely to yield an effective and efficient air curtain, as it requires significantly larger cross flow deflection than the other configurations. Furthermore, while the AB outlet geometry inspired the micro nozzle AT concept, it did feature different outlet hole philosophies due to the available manufacturing facilities. The AT outlet holes were shown in both Trinity College and AWB tests to produce less noise than the AB, and the reason for this could be the focus of future work.

Mass Flow Rate

The mass flow rate tests provided an interesting, although limited, insight into the sensitivities within the system. The tests performed with the AT showed that as cross flow velocity changed, so too did the mass flow rate which yields the greatest performance. Tests conducted with three mass flow rates showed that a low mass flow rate did not yield sufficient shielding to reduce noise, while a very high mass flow rate caused excessive nozzle self noise. Therefore, it can be concluded that for each cross flow velocity, an optimum mass flow rate exists, and hence the system can be tuned to achieve an optimum balance of shielding and self noise. This conclusion highlights a weakness in the AWB test campaign, as a thorough analysis of this effect was not performed. Hence, while the AT was successful in achieving noise reductions, it is likely that more impressive reductions could have been achieved with more focus on tuning the flow rate to cross flow conditions.

7 Conclusions and Recommendations

7.1 Conclusions

This research project sought to achieve validation for the use of air curtains as an aircraft landing gear low noise technology (LNT). While the flow deflection capabilities of a planar jet in cross flow have been well reported, the self noise of air curtain nozzles used in previous work has inhibited any acoustic benefit. Therefore, this project involved an iterative approach to the development of a series of low noise air curtain nozzles which were tested in the AWB wind tunnel to assess their impact on landing gear noise levels. Using HWA, acoustic spectral analysis and beamforming techniques, the following conclusions were drawn:

- The use of a pressurised nozzle featuring choked flow at the outlets achieved a uniform planar jet of air, which was found to be difficult to achieve with the previously developed low pressure nozzles.
- Noise reductions were achieved with the use of an Air Tube (AT) nozzle at various cross flow velocities and mass flow rates, with the most substantial noise reduction observed in a 63 ms^{-1} cross flow and with a mass flow rate of 47.5 gs^{-1}. With this setup, noise reductions were evident between 1kHz and 8kHz, with beamforming indicating a 10-12dB reduction at the 5kHz frequency band, although this was not shear layer or distance corrected. Hence, this affirms the hypothesis and serves as initial validation for employing air curtains as an aircraft landing gear LNT.
- While beamforming indicated a large reduction in landing gear source noise across all frequencies, the self noise of the nozzle was dominant above 10kHz and led to substantial increases in noise levels above this frequency.
- Three other nozzle designs, which were implemented in various configurations, did not yield notable noise reductions. Beamforming results indicated that cross flow deflection was achieved in all configurations, however nozzle self noise was higher than seen for the AT, and hence acoustic benefits were impaired. From this it was concluded that acoustic performance is highly sensitive to nozzle design, and the impact of nozzle outlet geometry, such as outlet hole spacing, has an impact on the production of noise. In this study, the LLD nozzle showed superior acoustic performance to that of the LHD nozzle, which had more closely spaced outlet holes.
- An optimum mass flow rate exists for each nozzle and is a function of cross flow velocity. At

this optimum mass flow rate, sufficient shielding is achieved to suppress landing gear noise, while excess shielding is avoided which would lead to excessive nozzle self noise. This optimum was likely not reached in the AT tests as only two different mass flow rates were used.

In summary, while landing gear noise was successfully reduced in the 1-10kHz range, increased high frequency noise and the failure of multiple nozzles to achieve acoustic benefits have highlighted the complexity of successful implementation. However, optimisation of AT flow rates and outlet geometry may yield further noise reductions. As a successful concept validation for air curtain technology has been achieved, this work merits the publication of the findings discussed above, and hence a paper titled "Aerodynamic noise reduction of aircraft landing gear using air curtain technology" is currently being drafted with the intent to publish in the Aerospace Science and Technology journal.

7.2 Recommendations

Nozzle Outlet Optimisation

While noise reductions were successfully achieved with the AT nozzle configuration, the AWB test campaign highlighted the sensitivity of acoustic performance to nozzle geometry. While the AT nozzle outlet hole geometry was designed based on preliminary test results and information available in the literature, this study lacked a thorough parametric analysis of the outlet geometry and its impact on landing gear noise reductions. Therefore, future work should investigate the impacts of hole size, spacing and perhaps the use of a meshed outlet on noise reduction performance. This study's preliminary tests conducted in the Trinity College fluids lab utilised A-weighted SPL readings from a SLM to assess acoustic performance. It is recommended that a more thorough analysis of the acoustic spectrum be performed in the 1-20kHz range. This will permit the closer analysis of the impact of hole spacing on low frequency noise production.

Optimum Mass Flow Rate Analysis

As mentioned, a thorough analysis of the relationship between mass flow rate and noise reduction should be performed, in order to determine optimum input parameters for the nozzle. Future work should aim to devise a model which can calculate the required mass flow rate for a given cross flow velocity, such that performance is maximised.

High Frequency Noise Correction

The production of high frequency noise by the nozzle has been discussed and presents the only barrier to total validation of the AT configuration. As the significance of the high frequency noise was not a focus of this research, future work may seek to apply or develop a correction factor such that atmospheric attenuation is accounted for in the calculation of perceived noise levels.

Bibliography

[1] Q Cui, Y Hu, and L Yu. Can the aviation industry achieve carbon emission reduction and revenue growth simultaneously under the cng2020 strategy? an empirical study with 25 benchmarking airlines. *Energy*, 245, 2022.

[2] D Hummels. Transportation costs and international trade in the second era of globalization. *Journal of Economic Perspectives*, 21(3):131–154, 2007.

[3] B Lenaerts, F Allroggen, and R Malina. The economic impact of aviation: A review on the role of market access. *Journal of Air Transport Management*, 91(102000), 2021.

[4] R Sordello, O Ratel, F F. de Lachapelle, C Leger, A Dambry, and S. Vanpeene. Evidence of the impact of noise pollution on biodiversity: A systematic map. environmental evidence. *Environmental Evidence*, 9(1), 2020.

[5] B Lenaerts, F Allroggen, and R Malina. The economic impact of aviation: A review on the role of market access. *Journal of Air Transport Management*, 91(102000), 2021.

[6] D.S Lee, D.W Fahey, P.M Forster, P.J Newton, R.C.N Wit, L.L Lim, B Owen, and R Sausen. Aviation and global climate change in the 21st century. *Atmospheric Environment*, 43(22-23): 3520–3537, 2009.

[7] T Munzel, M Sørensen, and A Daibe. Transportation noise pollution and cardiovascular disease. *Nature Reviews Cardiology*, 18(9):619–636, 2021.

[8] K Zhao, P Okolo, E Neri, P Chen, J Kennedy, and G. J Bennett. Noise reduction technologies for aircraft landing gear-a bibliographic review. *Progress in Aerospace Sciences*, 112, 2020.

[9] A Marsh and A McPike. Noise levels of turbojet- and turbofan-powered aircraft. *Sound: Its Uses and Control*, 2(5):8–13, 1963.

[10] J Piet, N Molin, and C Sandu. Aircraft landing gear provided with at least one noise reducing means. *US Patent 20100108805*, 2010.

[11] P. N Okolo, K Zhao, J Kennedy, and G. J Bennett. Mesh screen application for noise reduction of landing gear strut. In *22nd AIAA/CEAS Aeroacoustics Conference*, 2016.

[12] M Murayama, Y Yokokawa, K Yamamoto, and T Hirai. Computational study of low-noise fairings around tire-axle region of a two-wheel main landing gear. *Computers & Fluids*, 85: 114–124, 2013.

[13] Gareth J. Bennett and Kun Zhao. Air Curtain Flow Control for Aerodynamic Noise Reduction. In Rolf Radespiel and Richard Semaan, editors, *Fundamentals of High Lift for Future Civil Aircraft*, volume 145, pages 279–295. Springer International Publishing, Cham, 2021. ISBN 978-3-030-52428-9 978-3-030-52429-6. doi: 10.1007/978-3-030-52429-6_18. URL http://link.springer.com/10.1007/978-3-030-52429-6_18. Series Title: Notes on Numerical Fluid Mechanics and Multidisciplinary Design.

[14] Inventor innovative design of installed airframe components for aircraft noise reduction. home | inventor., 2021. URL https://w3.onera.fr/inventor/home. Accessed: 20-02-2023.

[15] Gareth J. Bennett, Jiang Lai, Gordon O'Brien, Daniele Ragni, Francesco Avallone, and Michael Pott-Pollenske. Flow Control and Passive Low Noise Technologies for Landing Gear Noise Reduction. In *28th AIAA/CEAS Aeroacoustics 2022 Conference*, Southampton, UK, June 2022. American Institute of Aeronautics and Astronautics. ISBN 978-1-62410-664-4. doi: 10.2514/6.2022-2848. URL https://arc.aiaa.org/doi/10.2514/6.2022-2848.

[16] C Meuly. The implementation of air curtains on realistic aircraft nose and main landing gear. *Unpublished master's thesis*, 2022.

[17] G. J Bennett, J Lai, G O'Brien, D Ragni, F Avallone, and M Pott-Pollenske. Flow control and passive low noise technologies for landing gear noise reduction. In *28th AIAA/CEAS Aeroacoustics 2022 Conference*, 2022.

[18] K Zhao, Y Liang, P Okolo, Y Wang, Z Wu, and G.J Bennett. Suppression of aerodynamic noise using dual-jet air curtains combined with perforated fairings. *Applied Acoustics*, 158, 2020.

[19] Erick Burgueño Salas. Airline industry worldwide - number of flights 2004-2022, 2022. URL https://www.statista.com/statistics/564769/airline-industry-number-of-flights/.

[20] Clémence Baudin. Self-rated health status in relation to aircraft noise exposure, noise annoyance or noise sensitivity: The results of a cross-sectional study in france. *BMC Public Health*, 21(1), 2021.

[21] M Basner, C Clark, A Hansell, J Hileman, S Janssen, K Shepherd, and V Sparrow. Aviation noise impacts: State of the science. *Noise and Health*, 19(87):41–50, 2017.

[22] Mathias Basner and Sarah McGuire. Who environmental noise guidelines for the european region: A systematic review on environmental noise and effects on sleep. *International Journal of Environmental Research and Public Health*, 15(3):519, 2018.

[23] P. O Davies, Fisher M.J, and M.J Barratt. The characteristics of the turbulence in the mixing region of a round jet. *Journal of Fluid Mechanics*, 15(3):337–367, 1963.

[24] D. L Huff. Noise reduction technologies for turbofan engines. In *35th International Congress and Exposition on Noise Control Engineering*, 2007.

[25] X Liu, D Zhao, D Guan, S Becker, D Sun, and X Sun. Development and progress in aeroacoustic noise reduction on turbofan aeroengines. *Progress in Aerospace Sciences*, 130, 2022.

[26] W Dobrzynski. *Airframe Noise-Landing Gear Noise*. John Wiley & Sons, Ltd, 2010.

[27] W Dobrzynski, L Chow, S Malcom, A Boillot, O Dereure, and N Molin. Experimental assessment of low noise landing gear component design. *International Journal of Aeroacoustics*, 9(6): 763–786, 2010.

[28] W Dobrzynski, B Schöning, L. C Chow, C Wood, M Smith, and C Seror. Design and testing of low noise landing gears. *International Journal of Aeroacoustics*, 5(3):233–262, 2006.

[29] R Merino-Martínez, J Kennedy, and G. J. Bennett. Experimental study of realistic low–noise technologies applied to a full–scale nose landing gear. *Aerospace Science and Technology*, 113, 2021.

[30] N Molin, J.-F Piet, L. C Chow, M Smith, W Dobrzynski, and C. Seror. Prediction of low noise aircraft landing gears and comparison with test results. In *12th AIAA/CEAS Aeroacoustics Conference*, 2006.

[31] R Elkoby, L Brusniak, R Stoker, M Khorrami, A Abeysinghe, and J. Moe. Airframe noise test results from the qtd ii flight test program. In *13th AIAA/CEAS Aeroacoustics Conference*, 2007.

[32] Y Li, X Wang, and D. Zhang. Control strategies for aircraft airframe noise reduction. *Chinese Journal of Aeronautics*, 26(2):249–260, 2013.

[33] K Boorsma, X Zhang, and N. Molin. Landing gear noise control using perforated fairings. *Acta Mechanica Sinica*, 26(2):159–174, 2009.

[34] J Kennedy, E Neri, and G. J. Bennett. The reduction of main landing gear noise. In *22nd AIAA/CEAS Aeroacoustics Conference*, 2016.

[35] G. J Bennett, P. N Okolo, K Zhao, J Philo, Y Guan, and S. C. Morris. Cavity resonance suppression using fluidic spoilers. *AIAA Journal*, 57(2):706–719, 2019.

[36] T Sijpkes and J Wickerhoff. Aeroplane provided with noise-reducing means, as well as a landing gear and blowing means, US Patent US20040104301 A1, 2004.

[37] S Oerlemans and A. De Bruin. Reduction of landing gear noise using an air curtain. In *15th AIAA/CEAS Aeroacoustics Conference*, 2009.

[38] K Zhao, X Yang, P. N Okolo, and W. Zhang. Use of a plane jet for flow-induced noise reduction of tandem rods. *Chinese Physics B*, 25(6), 2016.

[39] J. E Williams and C. G. Gordon. Noise of highly turbulent jets at low exhaust speeds. *AIAA Journal*, 3(4):791–793, 1965.

[40] B.R Ramaprian and H. Haniu. *Turbulence measurements in plane jets and plumes in Crossflow*. Iowa Institute of of Hydraulic Research, University of Iowa, 1983.

[41] G. J Bennett, K Zhao, J Philo, Y Guan, and S. C Morris. Cavity noise suppression using fluidic spoilers. In *22nd AIAA/CEAS Aeroacoustics Conference*, 2016.

[42] K Zhao, X Yang, P. N Okolo, Z Wu, W Zhang, and G. J. Bennett. A novel method for defining the leeward edge of the planar jet in crossflow. *Journal of Applied Fluid Mechanics*, 10(5): 1475–1486, 2017.

[43] Kun Zhao, Eleonora Neri, Patrick Okolo, John Kennedy, and G.J. Bennett. Landing gear noise reduction by double jet air curtain configuration. In *22nd International Congress on Sound and Vibration*, 2015.

[44] K Zhao, S Alimohammadi, P. N Okolo, J Kennedy, and G. J. Bennett. Aerodynamic noise reduction using dual-jet planar air curtains. *Journal of Sound and Vibration*, 432:192–212, 2018.

[45] S Sheen. Noise generated by multiple-jet nozzles with conical profiles. *International Journal of Occupational Safety and Ergonomics*, 17(3):287–299, 2011.

[46] D Moyano, D Paraiso, and R González-Lezcano. Possible effects on health of ultrasound exposure, risk factors in the work environment and occupational safety review. *Healthcare*, 10(3): 423, 2022.

[47] S Sheen. Effect of exit spacing in a multiple-jet nozzle on noise levels at audible frequencies. *Journal of Occupational and Environmental Hygiene*, 8(6):349–356, 2011.

[48] A Safari Variani, A Dastamoz, S Zare, A Nikpey, and S. Ahmadi. The acoustic performance of 3d printed multiple jet nozzles with different configurations. *Sound & Vibration*, 54(1):43–55, 2020.

[49] H Coanda. Device for deflecting a stream of elastic fluid projected into an elastic fluid, US Patent US2052869 A, 1936.

[50] M Trancossi and A Dumas. Coanda synthetic jet deflection apparatus and control. *SAE Technical Paper Series*, 2011.

[51] P Li and N Halliwell. Industrial jet noise: Coanda nozzles. *Journal of Sound and Vibration*, 99 (4):475–491, 1985.

[52] D Simons, M Snellen, R Merino Martinez, and A. Malgoezar. Noise breakdown of landing aircraft using a microphone array and an airframe noise model. In *In 46th International Congress and Exposition on Noise Control Engineering*, pages 4361–4372, 2017.

[53] Federal Aviation Administration. Guidelines for adjustment of aircraft noise levels for the effects of background noise., 2003. URL `https://www.faa.gov/documentLibrary/media/Advisory_Circular/Appendix3.pdf`. Accessed: 06-04-2023.

[54] K. Attenborough. Sound propagation in the atmosphere. *Springer Handbook of Acoustics*, page 117–155, 2014.

[55] H. E Bass, L. C Sutherland, and A. J. Zuckerwar. Atmospheric absorption of sound: Update. *The Journal of the Acoustical Society of America*, 88(4):2019–2021, 1990.

[56] S. Moreno. Landing gear noise reduction using air curtains., 2014. Unpublished thesis.

[57] H Bruun. *Hot-wire anemometry: Principles and Signal Analysis*. Oxford University Press, 2002.

[58] P. Bathla and J. Kennedy. 3d printed structured porous treatments for flow control around a circular cylinder. *Fluids*, 5(3):136, 2020.

[59] L Shi, Z Yu, and A. J Jaworski. Investigation into the strouhal numbers associated with vortex shedding from parallel-plate thermoacoustic stacks in oscillatory flow conditions. *European Journal of Mechanics - B/Fluids*, 30(2):206–217, 2011.

[60] M Pott-Pollenske and J. Delfs. Turbulence measurements in plane jets and plumes in crossflow. In *14th AIAA/CEAS Aeroacoustics Conference (29th AIAA Aeroacoustics Conference)*, 2008.

[61] C Clark. Measuring the vortex-shedding frequency behind staggered cylinders in cross-flow. *Mechanical Engineering Master's Theses*, 2018.

[62] J Silva-Leon and A. Cioncolini. Effect of inclination on vortex shedding frequency behind a bent cylinder: An experimental study. *Fluids*, 4(2):100, 2019.

[63] L Kovásznay. Hot-wire investigation of the wake behind cylinders at low reynolds numbers. *Proceedings of the Royal Society of London. Series A. Mathematical and Physical Sciences*, 198 (1053):174–190, 1949.

A1 Trinity College Testing

A1.1 Experimental Rig Data Acquisition System

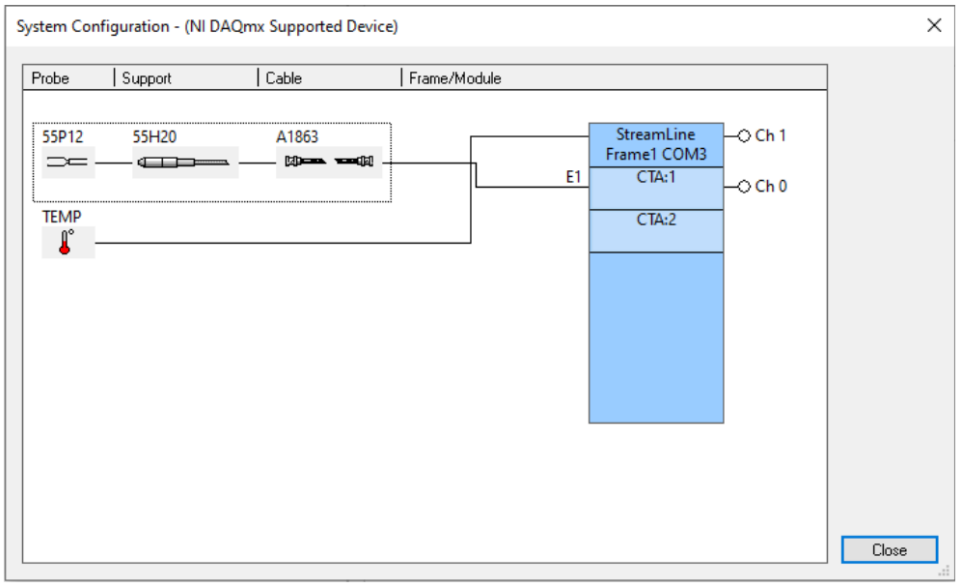

Figure A1.1: System configuration in the Streamware Pro software

(a) PXI controller with hot wire probe connected to Ch0 and temperature probe connected to CH1

(b) Front view of StreamLine 90N10 frame with thermometer connected

Figure A1.2: Data acquisition setup.

Figure A1.3: Rear view of StreamLine 90N10 frame with thermometer connection, probe connection to Analog Out 1, connection to PXI controller (silver) and power supply (black).

A1.2 Hot Wire Calibration

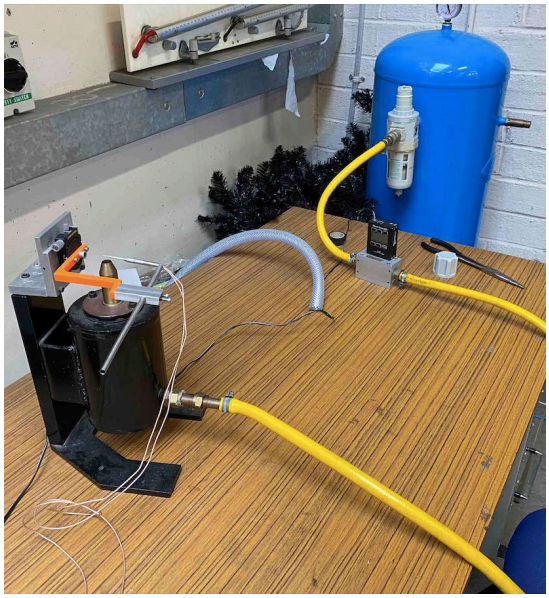

(a) HWA calibration setup. Note that the flow meter used was replaced by the one shown in A1.5 as it had a higher measurement range

(b) The hot wire probe was placed at the outlet of the high velocity nozzle. It is important to note that it must be positioned with the same orientation as it will have for future velocity measurement tests.

Figure A1.4: HWA calibration

Figure A1.5: The flow meter which was used for the majority of calibrations and tests featured a measurement range up to 850 SLPM

A1.3 Matlab Code for Traverse Control and Velocity Measurement

```
close all;
clear all;

%% Verification of connection
daq.getVendors;
daq.getDevices;

%% Verification of probe operation
tic % start timer
daq.getDevices;
s=daq.createSession('ni'); %create national instrument session
addAnalogInputChannel(s,'PXI2Slot2',0,'Voltage');
s.Rate=1000; % measurement frequency (Hz)
s.NumberOfScans=5000; % number of measurement points
mesureU=s.startForeground();
average=mean(mesureU); %to calculate mean values at each point
toc % end timer

%% Defining Motor Control
a = arduino('COM4','Uno','Libraries','Adafruit/MotorShieldV2');
shield = addon(a,'Adafruit/MotorShieldV2');
smX = stepper(shield,1,200,'RPM',75);
smY = stepper(shield,2,200,'RPM',75);

%% Probe Calibration Test %%%
%movement in Y direction of 100 results in how much mm movement??
test_increment = 100; %number of steps used for callibration
y_dist = 20;%20mm per 100 steps
y_size = test_increment/y_dist; %steps per mm
x_dist = 20;%20mm per 100 steps
x_size = test_increment/x_dist; %steps per mm

%% Test Setup %%%
% change number of measure points if needed (m and n)
tic % start timer
m=20;  %number of measurement points Y axis
n=20;  % number of measurement points X axis
x_tot=100; %x dimension of measurement plane (mm)
y_tot=120; %y dimension of measurement plane (mm)
```

```
x_step=x_tot/n; %step size in mm
y_step=y_tot/m; %step size in mm
Y=-round(y_size*y_step); %Y-INCREMENT
X=-round(x_size*x_step); %X-INCREMENT

% calibration coefficients from streamware
C0=0.1777;
C1=-3.5006;
C2=2.4583;
C3=-0.5691;
C4=0.0613;
P=[C4 C3 C2 C1 C0]; %defining polynomial of coefficients

resultat1=zeros([m,n]);
voltage1=zeros([m,n]);
RMS=zeros([m,n]);
mesureU=[];
Tot=m*n;
daq.getDevices;
s=daq.createSession('ni');
addAnalogInputChannel(s,'PXI2Slot2',0,'Voltage');
s.Rate=1000; % measurement frequency (Hz)
s.NumberOfScans=5000; % number of measurement points
disp('Starting movement')
pause(1)

%% Begin Probe Movement %%
for i=1:1:max(m,n)   %line by line filling
    if mod(i,2)==0   %if even line i.e. L2 or L4 --> move in
       negative X direction - signs depend on the motor setup and
       starting point of probe
        for j=1:1:m
            lig=m-j+1;   %filling by the end of the line
            mesureU=abs(s.startForeground());
            mesureVelocity=polyval(P,mesureU); % y = polyval(p,x)
               evaluates the polynomial p at each point in x.
            Avg_Voltage=mean(mesureU);
            Avg_Vel=mean(mesureVelocity); %taking avg of all
               readings taken at that point
            R=mesureVelocity-Avg_Vel;
            val=sqrt(mean(R.^2)); %finding rms value
            voltage1(lig,i)=Avg_Voltage;
```

```
            resultat1(lig,i)=Avg_Vel
            RMS(lig,i)=val;
            Tot=Tot-1 % number of measurements remaining
            move(smX,-X); % move by calculated X increment
        end
        pause(1);
        move(smY,-Y) % move by Y increment in negative Y direction
        release(smX);
        release(smY);
    else %if n is odd i.e. L1 or L3 --> move in positive X
       direction
        for j=1:1:m
            mesureU=s.startForeground();
            mesureVelocity=polyval(P,mesureU);
            Avg_Voltage=mean(mesureU);
            Avg_Vel=mean(mesureVelocity);
            R=mesureVelocity-Avg_Vel;
            val=sqrt(mean(R.^2))
            voltage1(j,i)=Avg_Voltage;
            resultat1(j,i)=Avg_Vel
            RMS(j,i)=val;
            Tot=Tot-1
            move(smX,X);
        end
        pause(1);
        move(smY,-Y);
        release(smX);
        release(smY);
    end
    disp('Axis Changing')
    pause(1)
end
```

A1.4 Dual Jet Geometry

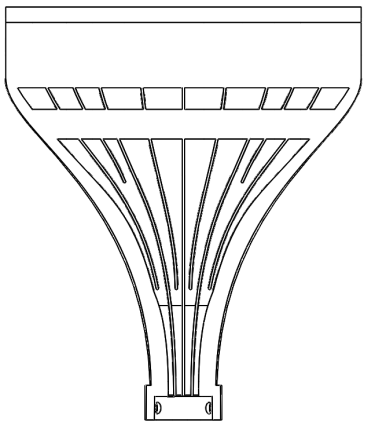

(a) Cross sectional view showing baffle geometry

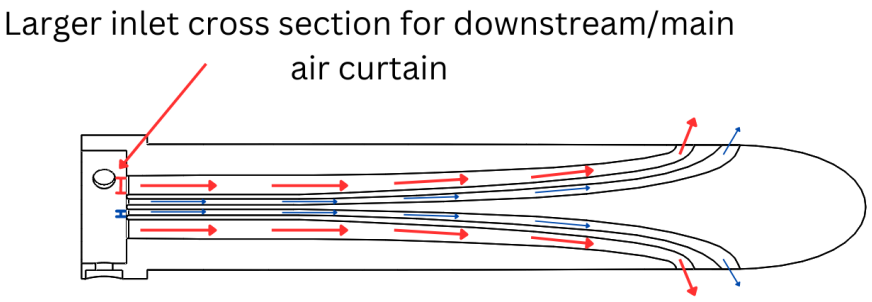

(b) Cross sectional view showing distribution of flow to jets.

Figure A1.6: Dual jet nozzle baffle geometry design for flow distribution.

A1.5 Sound Level Tests

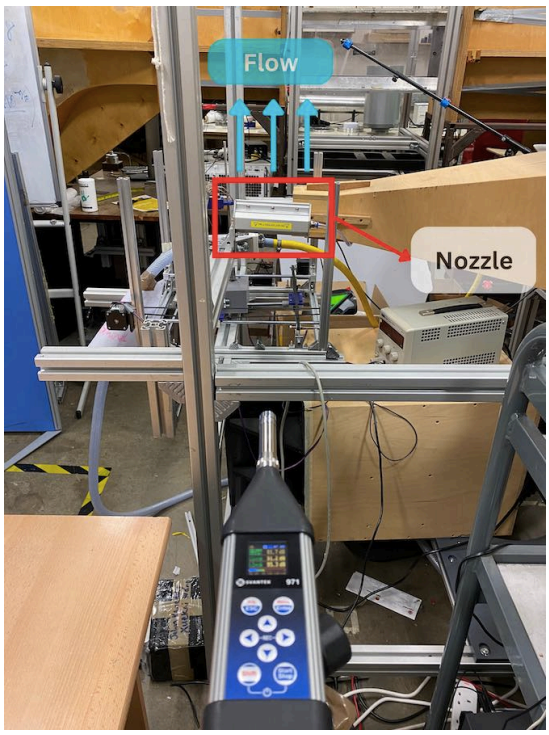

(a) Air Blade

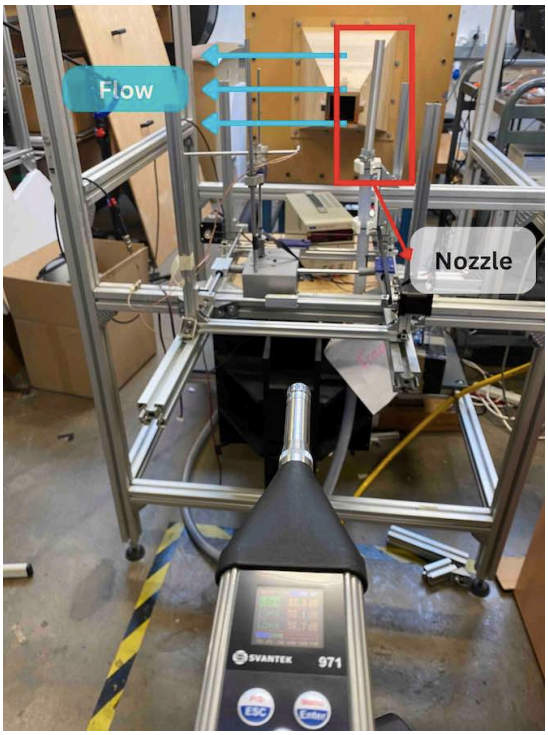

(b) Early Air Tube prototype.

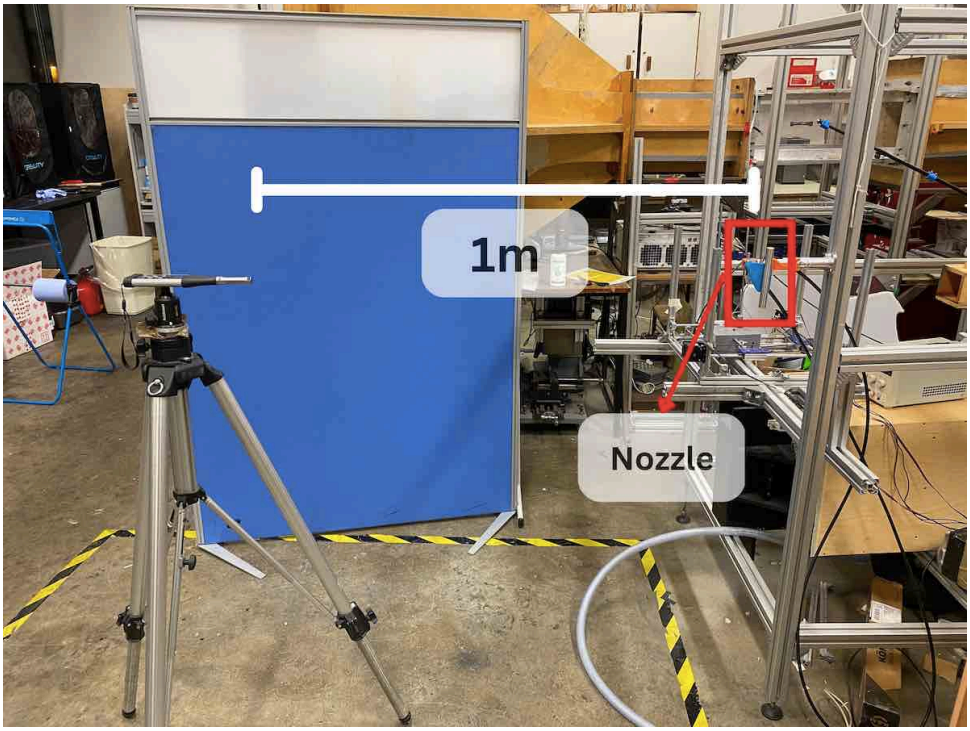

(c) Local nozzle.

Figure A1.7: SLM positioning relative to various nozzles for acoustic tests.

A1.6 End Cap Testing

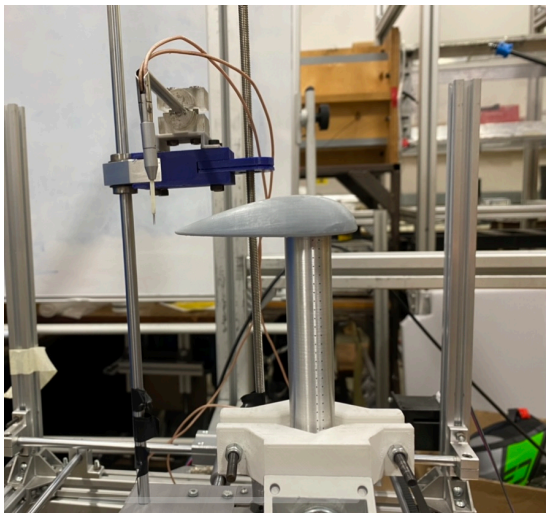

(a) Side view of Cap2 test.

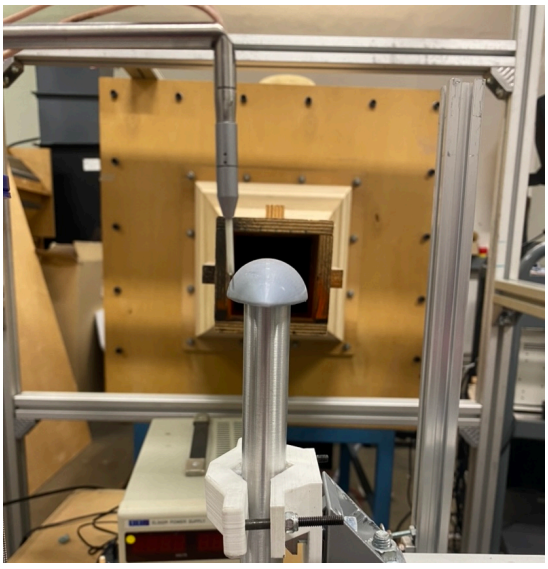

(b) Rear view of Cap2 test.

Figure A1.8: Turbulent intensity measurement of end cap 2, with the intention of reducing vortex shedding at the tube end.

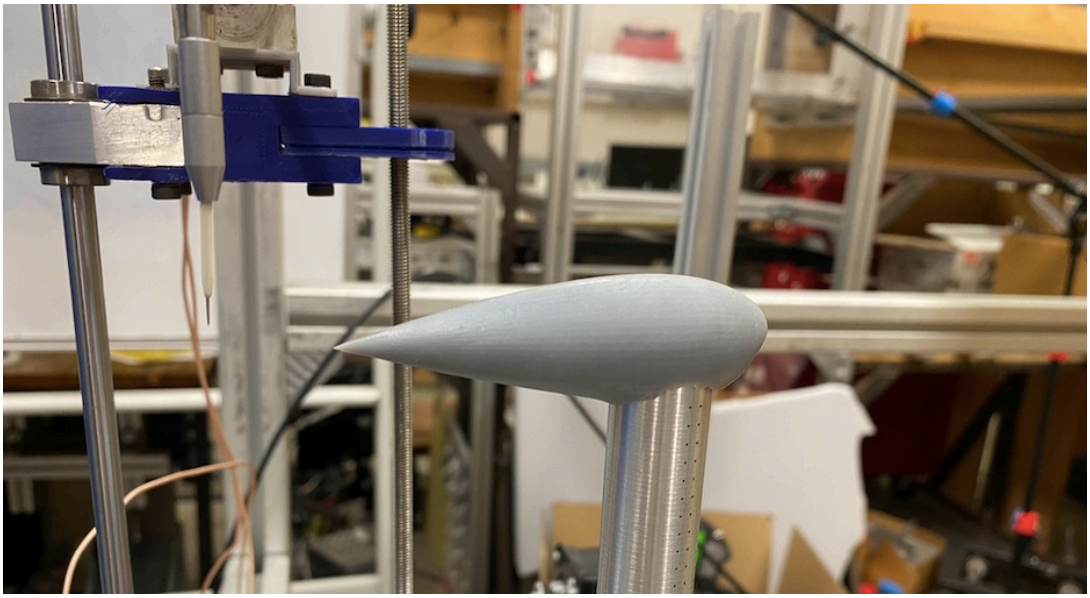

Figure A1.9: Cap 1 test

A2 AWB Wind Tunnel Tests

A2.1 Final Nozzle Designs

A2.1.1 Air Tube

(a) Air tube design, featuring grooves on the open end to facilitate clamping of the air hose.

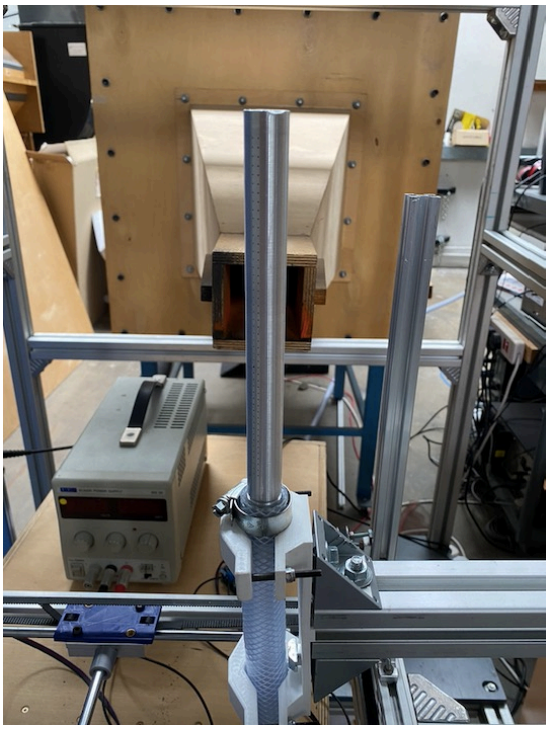

(b) Air tube with hose attached and clamped using a jubilee clip.

Figure A2.1: Air tube design.

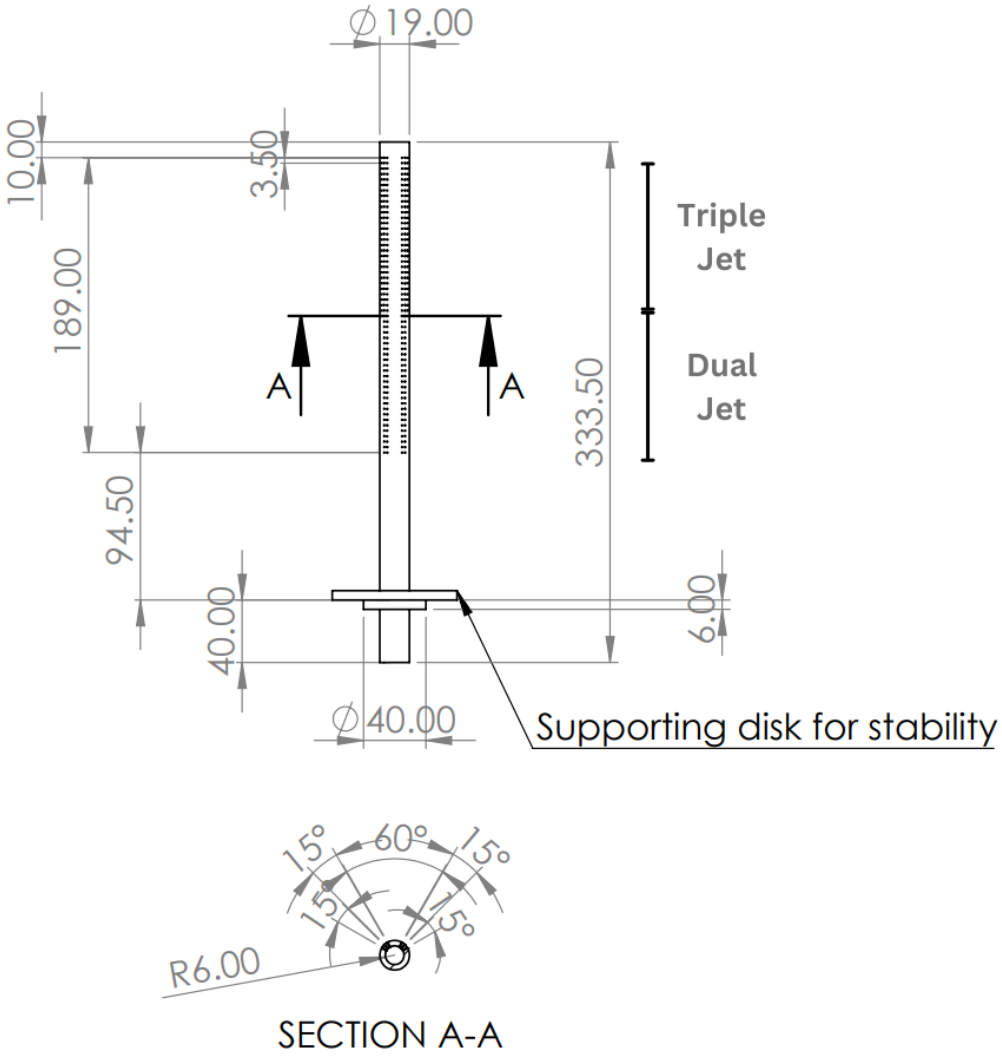

Figure A2.2: AT technical drawing. While this is not a complete drawing, some details have been removed to promote clarity and focus on the outlet hole configuration.

A2.1.2 Local Nozzles

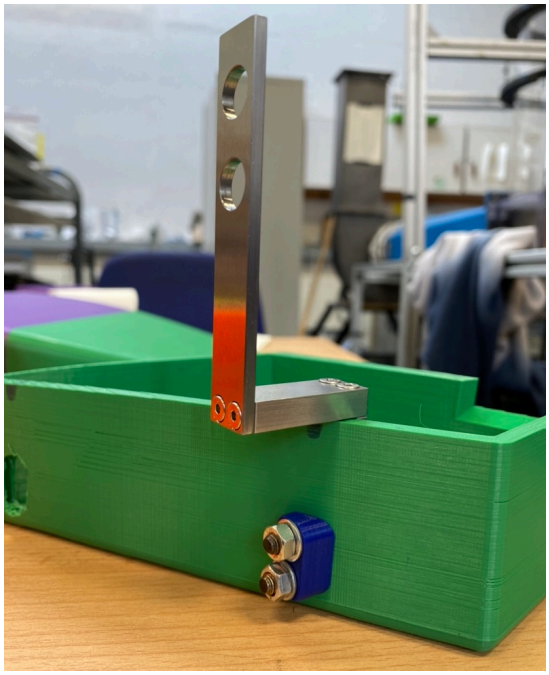

(a) The main leg (ML) bracket for the local nozzle is bolted on to the landing gear bay (green).

(b) The wheel bracket for local nozzles screws directly onto the landing gear.

Figure A2.3: Each of the brackets feature two holes through which the hose connectors screw through into the nozzle, hence acting as the securing mechanism.

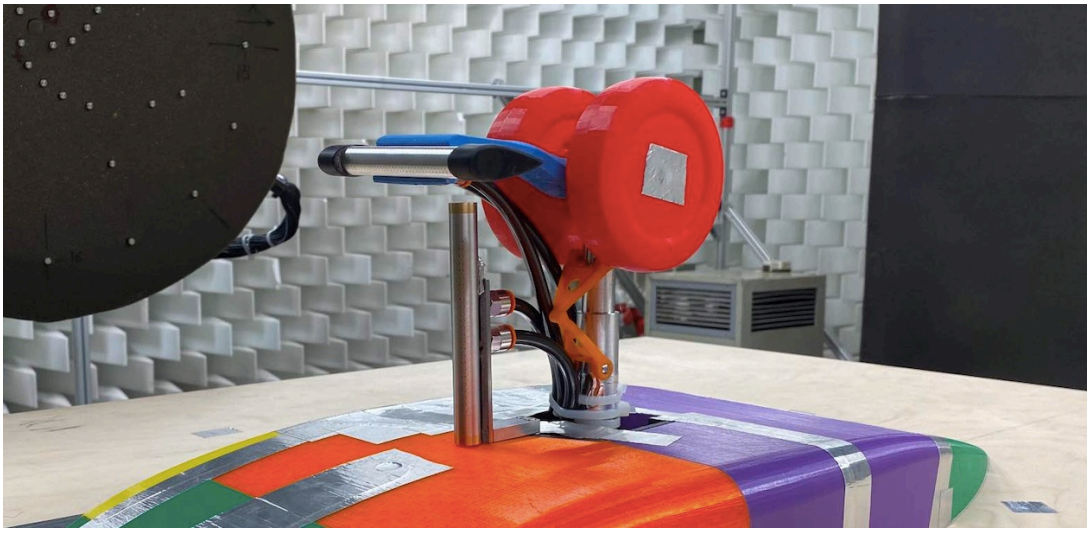

(a) Wheel & ML local nozzle configuration

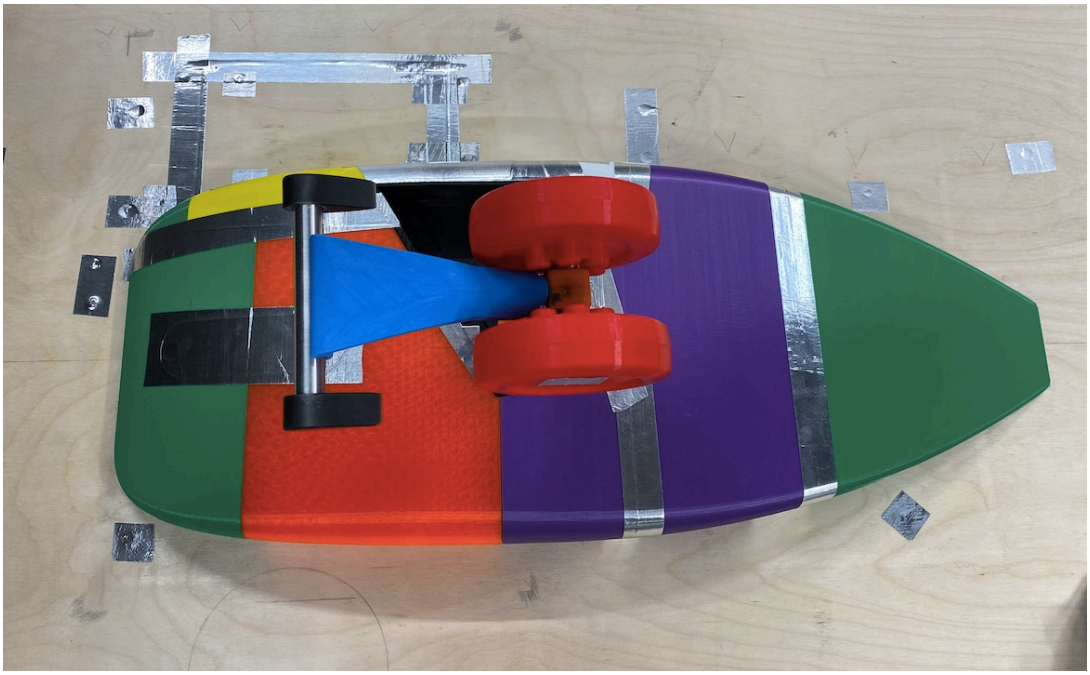

(b) Top view of local wheel nozzle

Figure A2.4: Local nozzles mounted on Lagoon NLG in ML & Wheel configuration.

A2.1.3 Air Blade

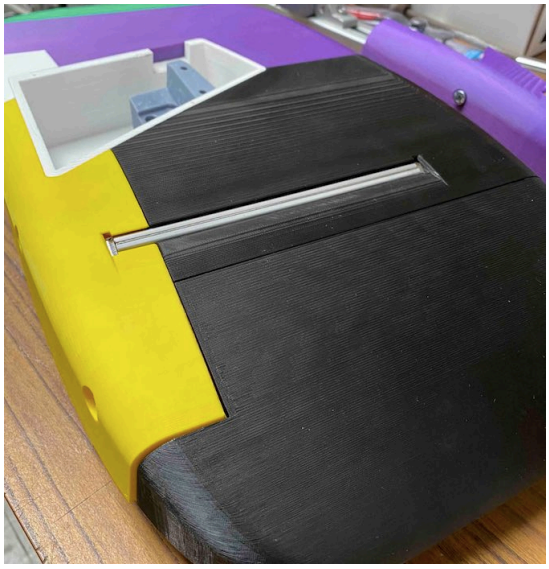

(a) The final Air Blade bay integration

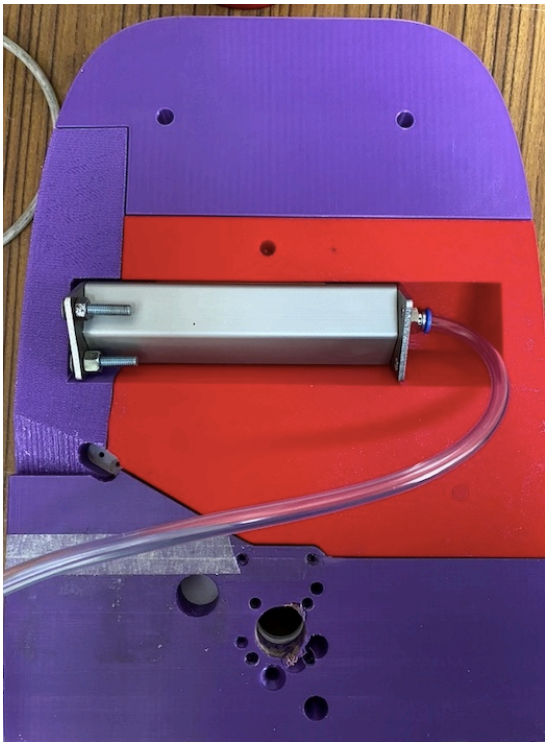

(b) The bottom view of the Air Blade in an first prototype of the bay.

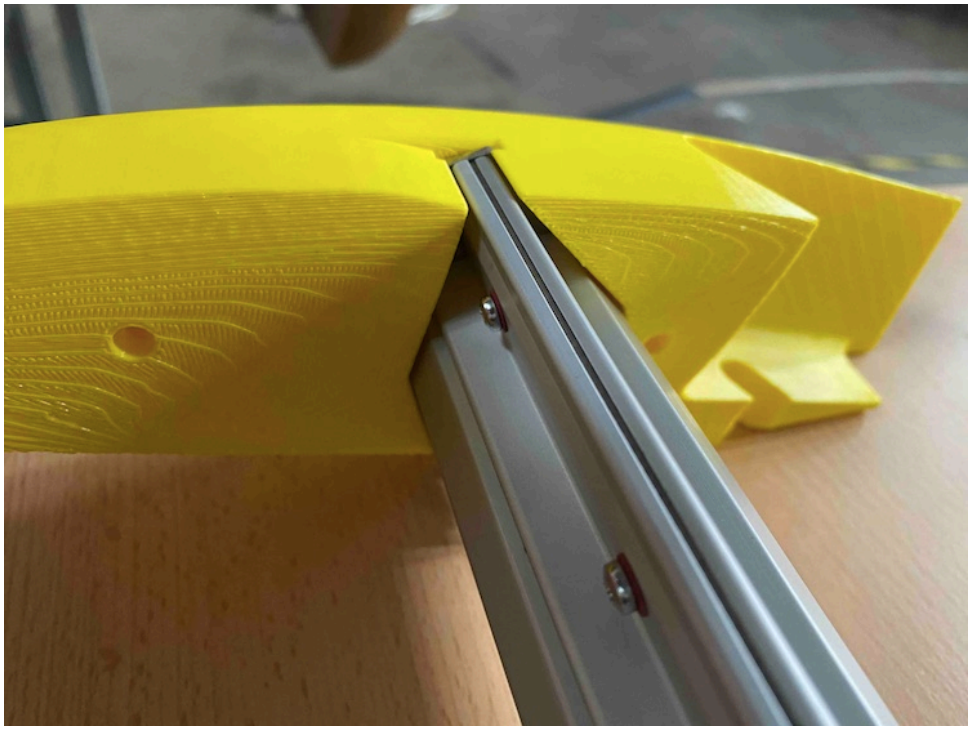

(c) A cavity in the landing gear bay permitted the insertion of the Air Blade.

Figure A2.5: Air Blade.